©Copyright 2015
Aman Ved Kalia

Comparison of Sooting behavior amongst various Liquid fuels

Aman Ved Kalia

A thesis submitted in partial fulfillment of the requirements for the degree of

Master of Science in Mechanical Engineering

University of Washington
2015

Thesis Committee:

Philip C. Malte, Chair

John C. Kramlich

Igor V. Novosselov

Program Authorized to Offer Degree:
Department of Mechanical Engineering

Abstract

Comparison of Sooting behavior amongst various Liquid fuels

Aman Ved Kalia

Supervisory Committee Chairperson: Professor Philip C. Malte
Department of Mechanical Engineering

Hydrocarbon combustion at fuel – air equivalence ratio (ϕ) greater than 1 results in incomplete combustion and formation of black flaky substance, soot. Soot is found responsible for health ailments, global warming and degradation of combustor performance in aircrafts. The study aims at determining the sooting threshold for various fuel samples and correlation of fuel chemical composition with sooting threshold.

Premixed laminar combustion of fuel samples is observed on the Meker burner setup for varying fuel – air equivalence ratio (ϕ). The air flow rate and pressure are kept constant while the flow rate of liquid fuel through the plane jet atomizer assembly is varied with a flow control in – line rotameter and a constant feed pressure. By varying the fuel flow rate, ϕ is varied which causes changes in the flame. At rich ϕ , a bright yellow streak of soot is observed which vanishes when the fuel supply is reduced. This allows in determining the exact value of ϕ at which the sooting begins, called incipient sooting or sooting threshold.

Aromatic compounds show a lower soot threshold due to their ease of forming poly – aromatic hydrocarbons which are the base constituent of soot particulate matter. In succession to aromatic compounds, dicyclic paraffins also lead to lower sooting thresholds. Iso – paraffins, cyclo – paraffins and n – paraffins have a comparatively higher sooting threshold. Experimental results show HRJ – tallow to have the highest sooting threshold with a ϕ of ~ 1.61 and Gevo jet blend a close second with $\phi \sim 1.53$.

Acknowledgments

The task I took at hand has come to fruition and it wouldn't have been possible without the support and guidance of a number of people.

I am thankful to my advisor Professor Philip C. Malte, for giving me an opportunity to learn and work under his guidance and especially for being supportive in my choices and decisions. I am also thankful to my co – advisors Professor John C. Kramlich and Professor Igor V. Novosselov for being an integral part of my work and guiding me to attain the best results. I am thankful to my lab mates especially Anamol Pundle, Arshiya Chime, Garrett Allawatt and Stefan Björnsson in Laboratory for Energy and Environmental Combustion, Mechanical Engineering for their help and advice during my research work.

This work would not have been possible without the fuel samples provided by the Air Force Research Laboratory at Wright – Patterson Air Force base in Dayton, Ohio. The financial support through scholarship and teaching assistantship from Mechanical Engineering department is acknowledged.

Finally, I am most thankful to my parents for motivating and supporting me during my studies and my friends for being like a family away from home.

Table of Contents

List of Figures

List of Tables

List of Nomenclature

General Symbols

Symbol	*Section first used in*	*Description*
$PM_{2.5}$	1.1	Fine particulate matter
LAX	1.1	Los Angeles International Airport
C – C	1.2.1	Carbon – carbon single bond
C – H	1.2.1	Carbon – hydrogen single bond
R	1.2.1	Alkyl group
m_{fuel}	1.2.1	Mass of fuel
m_{air}	1.2.1	Mass of air
FAR	1.2.1	Mass ratio of fuel to air
q	1.2.1	Heat
ΔH_f	1.2.1	Change in enthalpy of formation
T_P	1.2.1	Temperature of products
U_1	1.2.2	Unburnt gas velocity
U_2	1.2.2	Burnt gas velocity
Re	1.2.2	Reynolds number
S_L	1.2.2	Laminar flame speed
T_f	1.2.2	Flame temperature
$T_{adiabatic}$	1.2.2	Adiabatic Flame temperature
H_P	1.2.2	Enthalpy of products
H_R	1.2.2	Enthalpy of reactants
TSI	1.3	Threshold sooting index
JP	1.3	Jet propellant
CtL	1.3	Coal – to – Liquid
GtL	1.3	Gas – to – Liquid
HRJ	1.3	Hydro processed renewable jet
FT	2.1	Fischer Tropsch
AFRL	2.2	Air Force Research Laboratory

vol./vol.	2.3	volume by volume ratio
PJAA		plane jet atomizer assembly
OD	3.1.1	outer diameter
ID	3.1.1	inner diameter
SS	3.1.1	stainless steel
PID	3.1.1	proportional – integral – derivative
SCR	3.1.1	silicon controlled rectifier
$\dot{m}_{fuel}$	3.2.3	mass flow rate of fuel
$\dot{m}_{air}$	3.2.3	mass flow rate of air
RM	4.1.1	rotameter
$n_{A,}\, n_B$	4.1.5	kmoles of A and B
MW	4.1.5	molecular weight in kg/kmoles
V	4.1.5	volume
x	4.1.5	mole fraction
T_b	4.3	black body radiated temperature
P_{loss}	4.3	energy lost as radiation from burner surface
A	4.3	surface area
LHV	4.3	lower heating value
wt.	5.1	weight

Unit Symbols

Symbol	*Section first used in*	*Description*
W	1.1	watts
m	1.1	meter
km	1.1	kilometer
K	1.2.1	kelvin
kcal	1.2.3	kilocalories
mol	1.2.3	moles
^{o}C	1.2.3	degree Celsius
^{o}F	2.1	degree Fahrenheit
kJ	2,2	kilojoules
psig	3.1.1	pound square inch gauge pressure
kPa	3.1.1	kilopascals
kg	3.1.1	kilograms
mm	3.1.2	millimeter
cu.ft.	3.2.2	cubic feet
SLPM	3.2.2	standard liters per minute
s	3.1.1	second

Greek Symbols

Symbol	*Section first used in*	*Description*
ϕ, ϕ_{FAR}	1.2.1	fuel – air equivalence ratio
θ	1.2.2	flame cone angle
Σ	1.2.2	summation
ϕ_C, $\phi_{incipient}$	1.3	critical fuel – air equivalence ratio
Å	1.3	1×10^{-10} meters
ρ	4.1.5	density of fuel
ε	4.1.5	emissivity
σ	4.1.5	Stefan – Boltzmann constant ($5.67 \text{ E-8 W m}^{-2} \text{ K}^{-4}$)

1. INTRODUCTION

A study on the sooting behavior of premixed flames from liquid aviation fuels obtained from different sources is conducted using the Meker burner setup. This thesis serves to document the experimental setup, procedures, observations, results and conclusions made from the study. The first chapter provides the motivation for conducting this research and a review of the basics required for understanding the concepts related to the study.

1.1. Motivation

Fuel is an indispensable commodity for transportation as well as for heavy and small machinery. Today, the term *Fuel* includes any material – solid, liquid or gaseous – that stores the energy to provide kinetic, potential or thermal energy to the system when released. Hydrocarbon based liquid fuels obtained from petroleum are the most widely used fuel type in transportation industry due to their high heating values and high energy density. A bit over 50% of a barrel of oil is refined to be used for propelling automobiles and aircrafts. Alternative sources of energy such as battery – electric, solar – electric and bio – fuels to propel land based vehicles have been implemented and brought into mainstream production to counter fossil fuel depletion, greenhouse gas emissions and particulate matter pollution. These alternative power sources are generally not suitable for aircraft due to problems with weight, size and power density. The exception is bio – derived fuels. Research efforts have been focused on developing renewable sources for aircraft propulsion. At present there are jet propellants derived from bio – feedstock, synthetic processes and by blending different hydrocarbon compounds in varying proportions. The hydrocarbon based fuels release their energy upon combustion which can result in emission of harmful pollutants like Carbon monoxide (CO), oxides of nitrogen (NO_x), oxides of sulphur (SO_x) and soot. These pollutants are the primary cause of degradation of the environment. The constant evolution in the combustion techniques and fuel quality have helped overcome these emissions to a certain extent.

Soot formation during fuel combustion in aircraft engines is of primary concern due to its potential to *a)* degrade the performance of the combustor due to soot coating on the wall liner which impacts cooling and soot coating on the fuel injectors which can cause fuel starvation, *b)* increase carbon particulate in the atmosphere, especially near airports and *c)* assist in nucleation of environmental moisture causing formation of ice crystals on soot particles which affects radiative forcing.

Black carbon serves as a major component of soot along with a few other organic carbon compounds. A report formulated by U.S. Environmental Protection Agency (EPA) titled *"Report to Congress on Black Carbon"* discusses the effect of black carbon emissions on climate and health. It states that black carbon emitted in the atmosphere as $PM_{2.5}$ shows high absorption of solar radiation at all wavelengths. The presence of such particulate matter can result in increase of atmosphere temperature and simultaneously lower the surface temperature. It also results in accelerated melting of the snow due to its deposition. Alterations in the properties of clouds leading to issues with reflectivity, stability and precipitation have also been noticed. [1] The Intergovernmental Policy on Climate Change (IPCC) report of 2013 shows an agreement with the contents of the EPA report mentioned above. The section on *Drivers of Climate Change* in the report suggests positive radiative forcing of nearly 0.55 Wm^{-2} due to black carbon. [2] *Aviation Turbine Fuels: An Assessment of Alternatives* mentions black carbon being responsible for degradation of the combustor wall in gas turbine engines. It descriptively mentions such a problem in conjunction with heavier fuels having higher aromatic and low hydrogen content. [3] As per International Agency on Research for Cancer (IARC), black carbon is found to be carcinogenic in nature with susceptibility to pulmonary cancer and other associated ailments. A recent study conducted near LAX report on particle number concentrations has shown 4 – fold increase during aircraft take – off with wind spreading the particulate upto 10km east of the airport. [4]

Based on the reported issues and concerns which are supported by experimental research data, a much thorough understanding of soot formation is a necessity. This

has motivated the work reported here, entitled *Comparison of Sooting behavior amongst various Liquid Fuels* with the prime objectives of determining the following:

1. Soot thresholds for the various fuels. This is measured as the fuel – air ratio just at the moment before which a yellow – orange luminosity is observed just near the tip of the flame, also called as incipient sooting.
2. Correlation between the different hydrocarbon components of the test fuel and the fuel – air ratio corresponding to incipient sooting to understand how composition influences sooting behavior.
3. In continuation to the previous point, effect of blending two fuels with different fuel – air ratio at incipient sooting.

The previously cited reports also provide sufficient justification for the conducting this study to achieve a better understanding of soot and develop solutions to mitigate this problem in the near future.

1.2. Fundamental Theory

To understand the outcomes of the combustion experiments conducted in the research study for the different fuels, a quick review of the important concepts and theories related to the combustion process, flame structure and chemiluminescence as well as particulate formation is presented here.

1.2.1. Combustion Process

The process of combustion involves reduction and oxidation of a fuel like compound i.e. a chemical that upon dissociation produces radical species along with a large amount of heat that results in the rise of temperature of the reactant gases. This rise in temperature accelerates the production of radical species which establishes a flame front i.e. a luminous thin sheet of high temperature region between the unburnt gas mixture and the product gases.

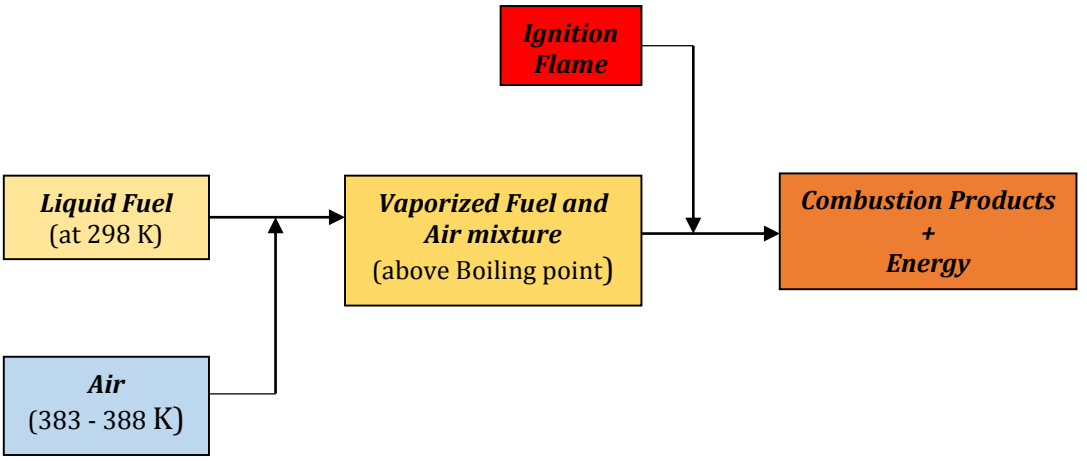

Figure 1.1: Flow diagram depicting combustion process for liquid fuels in the experimental setup.

In reference to the Meker burner study, the liquid hydrocarbon fuels are of prime interest. At a macroscopic level, the process of combustion comprises of two major steps as shown in **Figure 1.1** i.e.

1. *Vaporization of fuel*: Some of the heat supplied for combustion is used to provide the latent heat of vaporization needed for the fuel to undergo a phase change.
2. *Decomposition of fuel*: After vaporization, the C – C bonds and C – H bonds tend to be weakened causing a release of carbon and hydrogen radicals which interact with oxygen radicals and undergo oxidation while simultaneously releasing a high amount of energy and combustion products.

At the microscopic level, as mentioned earlier, the hydrocarbon fuel molecules undergo rapid dissociation by forming hydrogen radicals ($\dot{H}$) and hydrocarbon radicals ($R - H_2\dot{C}$) along with oxygen radicals ($\dot{O}$) from the oxygen in the air which interact with other fuel molecules to produce more radicals or undergo recombination reactions to form the product gases. The highly energetic radicals form a region of high temperature and rapid reaction zone which appears as a thin

luminous sheet called a flame or flame front. The properties of the flame are presented in more detail in the next section.

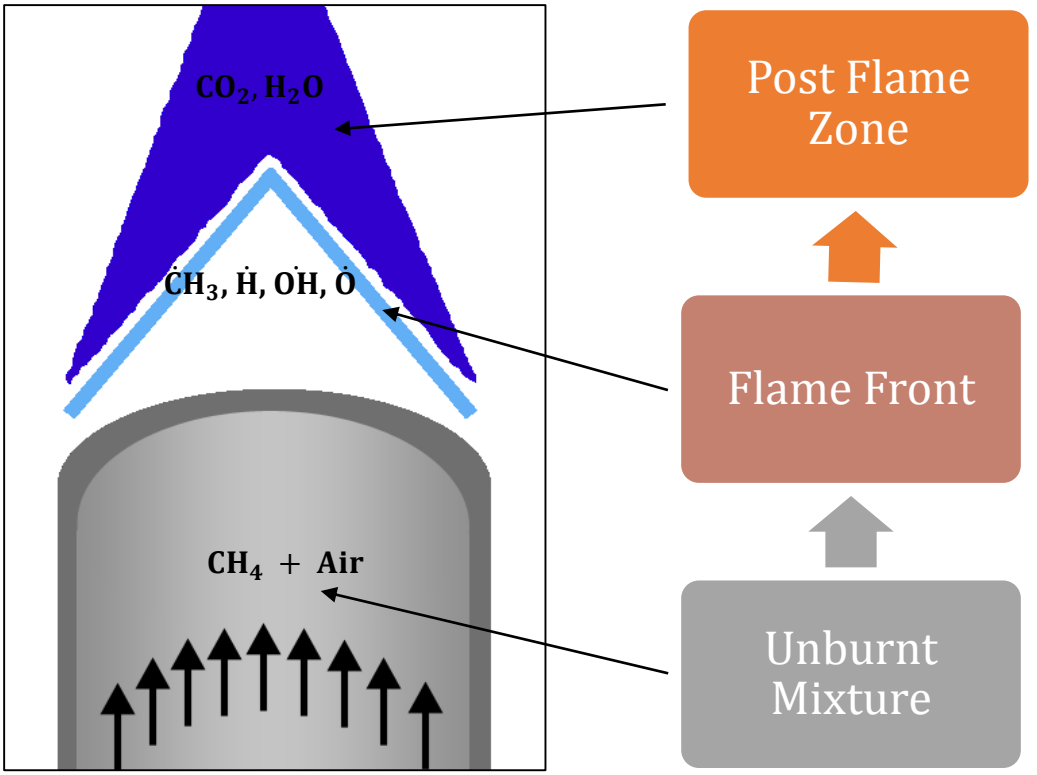

Figure 1.2: Cross – sectional view of a Bunsen flame with different flame zones and chemical species present with methane as the example fuel.

A simple hydrocarbon (C_xH_y) comprises of carbon and hydrogen in a certain ratio on the basis of carbon to hydrogen atom ratio in a single molecule. Methane (CH_4) has a C: H atom ratio of 0.25, which implies that for every single H atom there is a $\frac{1}{4}$ C atom. The fuels used in the Meker burner study are all pure hydrocarbons, implying that they have no other element than carbon and hydrogen in their molecules. These fuels are described in more detail in Chapter 2. The hydrocarbon based fuels undergo decomposition during the combustion process due to high energy and high reactivity of the fuel and oxidizer. As the reacting mixture moves past the reaction zone or the region of flame into the post flame zone the radical species produced in the flame undergo recombination to produce stable compounds of carbon dioxide (CO_2) and water vapor (H_2O). This process is presented in a graphical manner in **Figure 1.2** for

reference by considering methane (CH_4) as the example fuel for simplicity. Methane combustion is usually represented by nearly 300 reactions and involves 50 species.

The ratio of mass of fuel (m_{fuel}) to the mass of air (m_{air}) is termed as the fuel – to – air ratio (FAR) and a variation in this value results in different products of combustion and in extreme cases can push the reaction beyond the flammability limits. For any given fuel, there exists an FAR value which is described for just enough air to attain complete combustion with no excess air or unburnt fuel in the product mixture. This FAR value corresponds to a condition of Stoichiometric combustion. Another term designated by the symbol ϕ_{FAR} or just ϕ called the fuel – air equivalence ratio, is described as the ratio of FAR computed for a given condition to the FAR computed at stoichiometric conditions and is more frequently used in combustion studies. Mathematically, it is defined as following,

$$\phi = \frac{\text{FAR for the desired combustion}}{\text{FAR for stoichiometric combustion}} \qquad 1.1$$

The value of ϕ can be any positive real number, with $\phi < 1$ implying a fuel – lean combustion, $\phi = 1$ referring to stoichiometric combustion and $\phi > 1$ referring to fuel – rich combustion. The stoichiometric combustion of pure hydrocarbon fuels can be represented using the chemical reaction as given below,

$$C_xH_y + \left(x + \frac{y}{4}\right)(O_2 + 3.76N_2) \rightarrow xCO_2 + \left(\frac{y}{2}\right)H_2O + \left(x + \frac{y}{4}\right)(3.76N_2) \qquad 1.2$$

where,

x = number of carbon atoms,

y = number of hydrogen atoms.

The occurrence of combustion for a given fuel and air mixture is bound within an upper and lower values of ϕ, beyond which it is difficult to sustain combustion due to a decrease in generation of radical species along with variation in temperature within the permissible limits of flammability which together are responsible for a self – sustaining combustion. On the lean side ($\phi < 1$) it is termed as lean blowout and on the rich side ($\phi > 1$) it is termed as the rich blowout.

Combustion of fuel results in a large amount of energy release which is useful in sustaining the combustion process and acts as a source of heat energy for various purposes. The thermodynamics involved in the process of combustion can be understood with the first law of thermodynamics applied to a control volume surrounding the flame and heat transfer basics. The major source of heat (q) is from the change in enthalpy of formation (ΔH_f) for the combustion products which results in the increase of temperature in the flame and heating of unburnt fuel air mixture upstream of the flame from convection and radiation.

The products of hydrocarbon combustion depend on the value of ϕ i.e. lean burn or rich burn and the temperature in the post flame zone or product temperature (T_P). For $T_P < 1200K$, in the fuel lean combustion regime ($\phi < 1$) the products of combustion include O_2, H_2O (vap.), CO_2 and N_2 whereas for $T_P > 1200K$ and the same regime additional products such as oxides of nitrogen (NO_x), CO, OH, H and O are also observed. Likewise in the fuel rich combustion regime ($\phi > 1$) the combustion products for $T_P < 1200K$ include CO_2, H_2O, CO, unburnt hydrocarbon and N_2 while for $T_P > 1200K$ additional products as mentioned in the previous case can be observed. Among these products of combustion, unburnt hydrocarbon (HC), carbon monoxide (CO) and oxides of nitrogen (NO_x) are prime sources of emissions.

The unburnt hydrocarbons produced in the fuel rich regime undergo pyrolysis due to the high temperature near the flame and interact with other unburnt hydrocarbon species to result in an agglomeration of carbon rich structure termed as soot. Hence, fuel rich combustion is of key importance in the Meker burner study to understand the sooting behavior of different fuel samples.

1.2.2. Flames

At the initiation of fuel - air combustion in presence of an ignition source, a large number of radical species are produced which carry a large amount of energy which can be percieved as both thermal and luminous energy. This source of energy is termed as a flame or flame front which exists between the reactants and the

combustion products where $\phi = 1$, or the combustion is stoichiometric in nature. (see **Figure 1.3**).

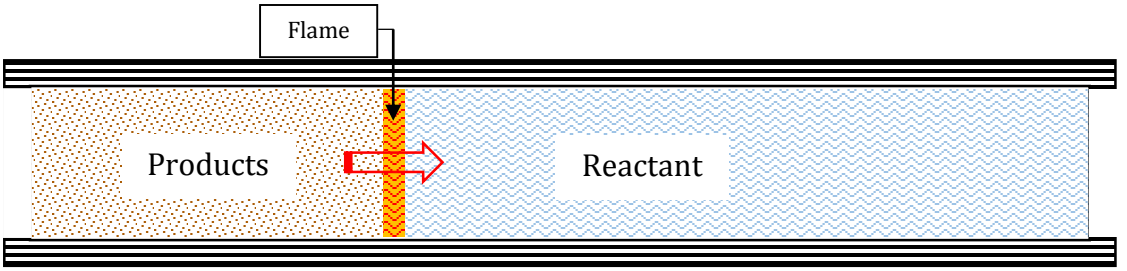

Figure 1.3: One – Dimensional representation of Flame front in a long open ended tube.

In **Figure 1.3**, the flame is shown to propagate through the medium in the direction of unburnt mixture or reactants which are assumed to be stationary. Considering a control volume around the flame and on applying momentum conservation it is found that if the unburnt mixture has an axial velocity U_1 and the product gases have an axial velocity U_2, both opposite in the direction of flame propagation then there will be condition when the flame a can be stabilized at a particular location for observation purposes. This concept is observed in Bunsen burner flames and Meker burner flames used in stationary flame studies.

As the flame is constituted within a fluid medium (vapor or gas phase) the flow properties of fluids determine the flame type which is broadly classified on the basis of flow Reynolds number as *Laminar* or *Turbulent* and on the basis of fuel and air interaction as *Premixed* or *Diffusion* flame. **Figure 1.4** depicts these flames in case of a Bunsen burner setup. Laminar flames are associated with flows having $\mathrm{Re} < 2000$ and turbulent flames are associated with flows having $\mathrm{Re} > 4000$ based on the tube velocity and diameter. A premixed combustion flame implies that a relatively homogenous fuel and air mixture is subjected to combustion with the sustenance of flame independent of air entrainment from the environment, whereas a diffusion

flame as the name suggests is sustained due to the diffusion between the fuel vapor and air in the environment with the flame located close to the diffusing interface.

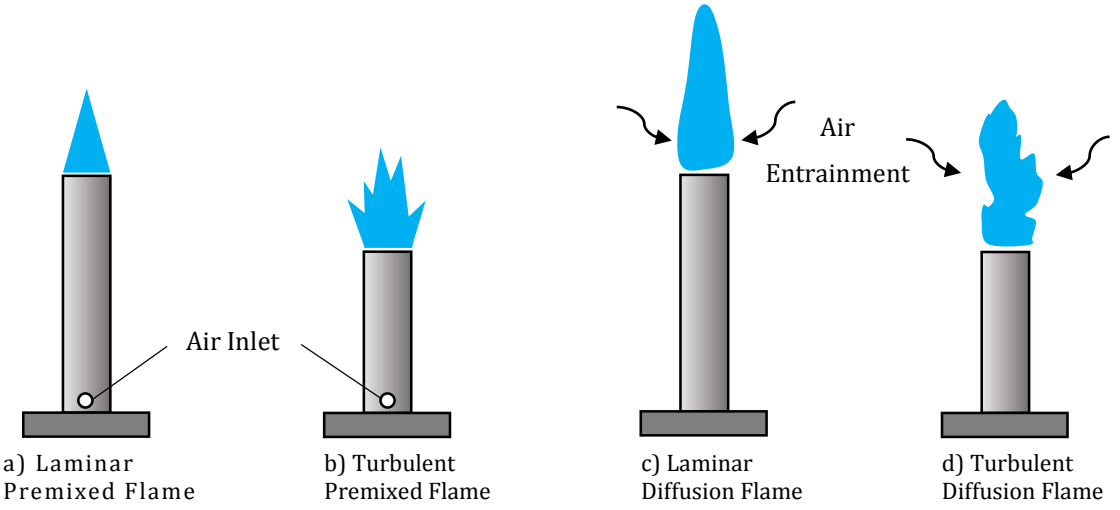

Figure 1.4: Different types of flames as observed in a Bunsen burner.

The choice of flame type preferred for conducting a study on the properties of fuel depend on the objective of the study or the physical component being modelled with a simple combustion setup such as a Bunsen burner or a Meker burner. In the Meker burner study a premixed flame is studied due to the following advantages:

1. A fully developed laminar flow of the reactant mixture provides a consistent and well – defined cone like structure to the flame at the burner exit. The flame has minimal or no instabilities making it suitable for conducting sensitive observations, such as detection of incipient sooting.
2. Premixed combustion gives user the control on fuel – air ratio due to the capability of varying both as per requirement. In our study as obtaining the fuel – air ratio corresponding to incipient sooting is of prime importance, premixed combustion is a suitable choice.
3. Laminar flows are comparatively easier to model numerically which is helpful in predicting combustion characteristics if required.

The key properties of flame such as structure, chemiluminescence, temperature and speed are studied for different fuels and different flame types to understand the chemical behavior of the fuels. These key flame properties are explained in brief with

reference to premixed laminar flame as the Meker burner study involves only such kind of a flame. Prior to discussing the properties of the flame the different zones of combustion around the flame as mentioned before are re – iterated. These are a) the zone of unburnt premixed gases before the luminous region or *Preheat zone*, b) the luminous region or the flame sheet where the primary combustion reaction occurs or *Reaction zone* and c) a region of diffused luminosity and comparatively lower temperature where the radicals generated in the flame recombine or *Recombination zone*. (see **Figure 1.2**)

The structure of the flame in case of a laminar flow field is perceived in conjunction with concept of laminar flame speed (S_L). Laminar flame speed is termed as the speed at which the unburnt gas flows through the combustion wave in a direction normal to the surface of the wave.[5] This implies that normal to the flame surface, the velocity of product gases remains at a constant value S_L which can be related mathematically to the unburnt gas flow speed U_1as

$$S_L = U_1 \cos\theta \qquad 1.3$$

where U_1 generally is a mean value of poiseuille velocity profile[6] which is a function of radial length (r) from the axis of the burner tube and is given by the relation

$$V(r) = \frac{1}{4\eta}.\frac{dp}{dz}.(r_o^2 - r^2) \qquad 1.4$$

where r_o is the inner radius of the tube carrying the unburnt mixture, r is the radial location of interest inside the tube, η is the gas viscosity and $\frac{dp}{dz}$ is the axial pressure gradient along the tube. Thus, knowing the value of S_L at any location on the flame corresponding to a value of unburnt gas velocity, the value of θ can be deduced using **Equation 1.3**. This process can be repeated for other values of V(r) obtained from **Equation 1.4** and a flame shape corresponding to the velocity profile can be determined. This flame shape is similar to a cone with the cone being able to stretch vertically depending on the change in flame temperature (T_f) which is in turn dependent on the change in ϕ for the fuel – air mixture being studied. This relation is expressed as

$$S_L \sim \left[\exp\left(-\frac{E}{RT_f}\right)\right]^{\frac{1}{2}} \quad 1.5$$

where E is the activation energy and R is the universal gas constant. In certain cases the flame cone appears to open up at the tip thus having a truncated cone like shape which can be accounted for due to $U_1 >> S_L$ whereas for the flame to exist at the tip $S_L \equiv U_1$.

The energy released during combustion is partly luminous and is perceivable by the eye. This luminosity is due to the chemiluminescence in the visible spectrum from the radical species constituting the flame. Glassman[7] mentions that the luminosity of the primary flame changes from deep blue to aqua – greenish as fuel – air ratio is varied from lean to rich. The deep blue color of the flame is due to a majority of $\dot{C}H$ radicals in the flame and a blue – green or aqua green color at fuel – rich conditions is due to a majority of $\dot{C}_2$ radicals. The products of combustion like CO_2 and H_2O give a reddish hue to the post flame zone. Soot particles in the post flame zone give off a bright yellow luminosity on excitation, due to black body radiation.

In addition to this, the determination of the flame temperature is of great importance too. The flame temperature is usually theoretically computed assuming complete combustion and no heat loss to the surroundings within a certain temperature limit. It is termed as adiabatic flame temperature ($T_{adiabatic}$), which is also the maximum temperature a flame can attain. $T_{adiabatic}$ is useful parameter for comparing fuels in terms of the obtainable energy and in selection for energy specific operations. $T_{adiabatic}$ is computed by applying the first law of thermodynamics around the flame which results in the relation

$$\sum H_P - \sum H_R = 0 \quad 1.6$$

as the system is adiabatic and no work is done. The value of $T_{adiabatic}$ varies with ϕ with the peak temperature around stoichiometric combustion conditions and the curve falling off both in the lean and rich combustion regimes. The lower temperature in the lean combustion regime can be accounted for due to excess air which acts as a sink to the heat while in the rich combustion regime the unburnt fuel acts as a sink.

In context with the Meker burner study, flame structure and chemiluminescence of the flame are of importance and thus the focus of the study so as to determine the combustion behavior of fuel.

1.2.3. Soot

Hydrocarbon fuels upon combustion yield certain products and by – products, either gaseous or fine particulate matter, which pose a danger to the environment and by extension its inhabitants. Black carbon or soot, a flaky particulate matter, formed due to conglomeration of several un-oxidized carbon atoms in case of fuel – rich combustion (see **Figure 1.6**) is one such emission and in the recent past has been a focus for several emissions research. This research study is also based on studying soot emissions from liquid hydrocarbon fuels which requires a basic understanding about its composition and formation as well as methods for detection.

Soot comprises mostly of black carbon particles and some trace amount of unburnt

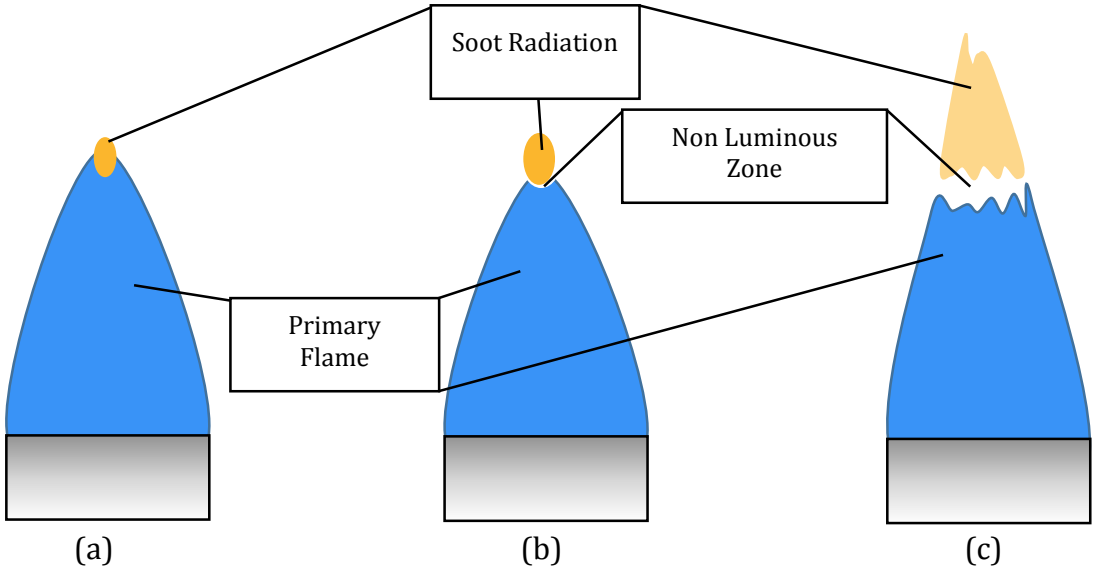

Figure 1.5: Three different types of incipient soot flames observed in the Meker burner study.

hydrocarbons. Microscopically, it can be viewed as numerous spherical carbon particles joined to each other randomly. The mechanism involving the formation of soot from hydrocarbon fuels is common for liquid or gaseous fuels. Several studies

[7] have suggested and concluded that the tendency to soot among different hydrocarbon families follow this trend

Aromatics > Alkynes > Alkenes > Alkanes

implying that if aromatic hydrocarbons are the dominating constituents in a fuel sample then the fuel will most likely show sooting behavior at a lower value of ϕ in comparison to a fuel having alkane as the dominating constituent.

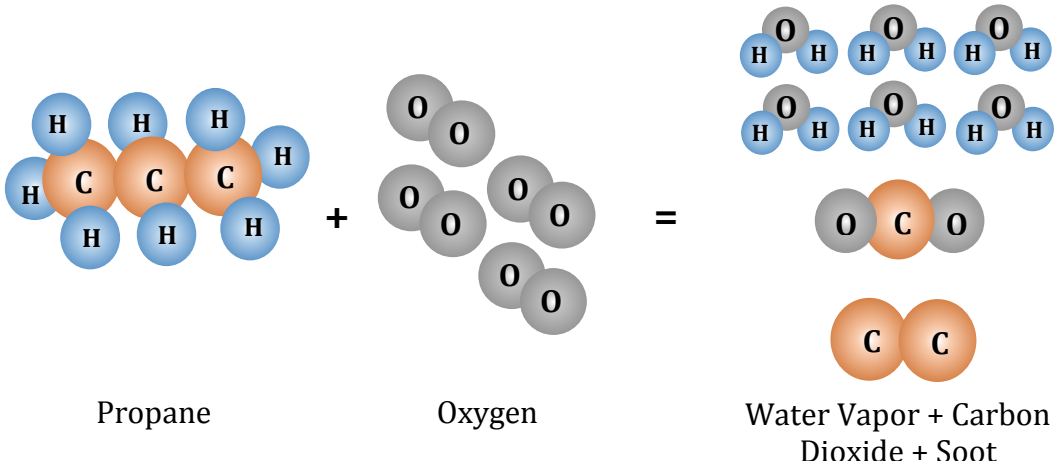

Figure 1.6: Graphical representation of Methane combustion for $\phi > 1$ resulting in soot particle formation.

The formation of soot or black carbon is a very straightforward process at the macroscopic level. Any material comprising of carbon, in majority, has the capability to produce soot particles when subjected to a combustion process, where the un – oxidized carbon atoms bond together and grow to form structures which are perceived as black flaky particulate matter emanating from the flame. In the interest of this research study and to thoroughly understand the process of soot formation understanding the chemistry occurring at the microscopic level has a greater advantage. The soot formation process at microscopic level can be broken down into four major successive steps, i.e. a) nucleation, b) coagulation, c) growth and oxidation and d) agglomeration.

The soot build up is initiated with the formation of soot precursors. These are chemically activated species or compounds which are formed upon decomposition of

the hydrocarbons in the fuel at high temperature. The precursors are susceptible to oxidation due to the interaction with oxygen atoms in the flame and for lean flames end up being oxidized. For richer flames, the possibility of these precursors to proceed with soot growth is much more likely. Some of the soot precursors mentioned over time include polyacetylenes[8], ionic species[9] and polycyclic aromatic hydrocarbons (PAH)[10].

Recent work in determining the pathways to soot formation by Frenklach et al.[11] mention the PAH soot precursor as a dominant pathway. Frenklach et al. [12] propose a mechanism termed HACA (H – abstraction – C_2H_2 – addition), to predict growth of soot particles, comprising of two major steps as suggested by the name itself. The mechanism involves removal of an H atom from the aromatic compound resulting in the formation of an aromatic radical which is followed by its interaction with a gaseous acetylene molecule leading to the formation of products. The steps involved in the HACA mechanism are highly susceptible to running in reverse despite of recovering some of the lost entropy.[11] Frenklach et al. [13] mention a coupling between the entropy recovery and thermodynamic resistance to reversibility as a key to ascertain irreversibility in the HACA mechanism which eventually results in the growth of soot particles. Glassman [14] mentions that hydrocarbon species that exist with conjugate structures i.e. the species in which electron – bond – electron transfer exists, are prime candidates for assisting in the soot growth. On the basis of this statement, recent work has shown that hydrocarbon radicals like methyl, propargyl and cyclopentadienyl [15]–[17] can also result in the formation of soot or PAH depending on the availability of these radicals and the composition of the fuel being studied.

The formation of soot is a thermodynamic process and is found to be entropy driven where the hydrogen removed from the hydrocarbon goes freely. Consider carbon formation from propane pyrolysis. How enthalpy and entropy impact the Gibbs free energy in each step of a possible reaction sequence is found by Wang.[18] He mentions that acetylene formation is an endothermic process but there is a sudden increment in the entropy of the system due to dehydrogenation process. These two

processes results in the overall reduction of Gibbs free energy thus making acetylene a dominant hydrocarbon specie in cases of fuel – rich combustion.[9], [19] Acetylene being an intermediate in soot formation process, further leads to the formation of benzene, which is an exothermic process but causes a reduction in entropy. The process of particle growth from benzene to PAH shows a mild but gradual reduction in the Gibbs free energy. On the whole the process of soot formation is neither highly exothermic nor it involves huge release of entropy thus making the process of particle growth a relatively reversible process. [18]

Finally, the soot particles produced in the flame radiate both thermal and luminous energy due to their high temperature in the flame. In theory, the soot particles exhibit characteristics of black body radiation. The luminosity from these particles is found to be in the longer wavelength regime of the visible spectrum i.e. yellow – red in color. The intensity of the yellow radiation from the soot is found to vary which is a function of temperature and soot particle number. Thus, a qualitative reasoning regarding the sooting behavior of a fuel can be made by observing the luminous radiation from soot in the flames.

1.3. Literature Study

Progressing on the fundamental concepts discussed in the previous section several research works pertaining to studying soot emissions from different kinds of hydrocarbon fuels have been conducted. This section discussed these works which directly and indirectly relate the Meker burner study of liquid hydrocarbon fuels. The section is divided into sub – sections with a focus on a) Effect of Fuel on soot formation b) Effect of fuel on flame structure and chemiluminescence.

1.3.1. Effect of Fuel on Soot formation

The most extensive work in determining the correlation between the fuel chemistry and threshold sooting was conducted by Street et al. [20] in 1955. A premixed Bunsen flame was used for the study of a number of hydrocarbon fuels by observing the chemiluminescence of the flame tip for bright yellow radiation due to soot particles. Based on their results, the propensity to form soot among pure hydrocarbon fuels such as n – paraffins, iso – paraffins, olefins, cyclo paraffins and aromatics can be summarized in the following points:

1. Heavy aromatic compounds like tetralin, α-methylnaphthalene and dicycloparaffin like decalin show the lowest sooting threshold. These have either a benzene ring or a heavy cyclic structure and thus they skip the soot precursor formation step as per Frenklach et al. [11], [13], [21]sooting mechanism. This leads to rapid soot formation.
2. The paraffin and iso – paraffin compounds show a very limited variation in the sooting threschold with the increase in carbon atoms per molecule whereas aromatic and olefins show a drastic fall in threshold sooting with the increase in carbon atoms.
3. Aromatic compounds with carbon atom counts greater than 8 show lower threshold sooting in comparison to paraffin and iso – paraffin compounds having the same number of carbon atoms. Also aromatic compounds with number of carbon atoms less than 7 have a nearly similar propensity to soot as olefins with carbon atoms around 5.

Street et al. in their study also mention an increase of 3 – 5 % in the critical equivalence ratio (ϕ_C) of soot formation per 100K increase of the unburnt gas temperature. Building upon this study Millikan[22] in 1962, Calcote et al. [23] in 1982, determined the impact of flame temperature on soot threshold and formation. Glassman et al. [7] in 1984 performed an extensive research similar to Street et al. [20] by studying a variety of pure hydrocarbon fuels for their sooting propensity with a focus on effect of adiabatic flame temperature. The behavior of the fuel types on the basis of their results can be summarized as follows:

1. The variation in the propensity to soot shows a similar trend as observed from the study by Street et al. [20] with the heavy aromatic compounds having the highest propensity and the low carbon atom olefins the least.
2. For any given fuel the propensity to soot appears to decrease with the increase in the adiabatic flame temperature. Hence, along with the type of fuel the flame temperature is also a key factor in determining the soot behavior of fuels.

Ono et al. [24] in early 2015 published their work on determining the effect of increasing molecular weight of polycyclic aromatic hydrocarbons and temperature rise on the formation of soot. The study involved sampling the particles from pyrolysis of the test fuels with a Differential Mobility Analyzer (DMA) and Condensation Particle Counter (CPC) and determining the particle count variation with respect to the particle diameter. The results from the study suggest that with the increase in pyrolysis temperature the number concentration of the particles increases. It also confirmed the HACA mechanism of soot formation suggested by Frenklach et al. [11][21] by showing that adding acetylene to benzene a significant rise in soot particle numbers occurs.

In recent years with the advancement in alternative fuels from synthetic and renewable resources and their feasibility as a replacement of the conventional fossil fuels in the aerospace and automotive industry, emission characteristics of these fuels is considered to be of utmost importance. As these fuels are composed of different hydrocarbon families having different number of carbon atoms in varying

proportions certain predictions of their soot propensity can be made on the basis of the results obtained for individual components from Street et al. [20] and Glassman et al. [7] studies though specific tests of these fuels are a necessity.

Yang et al. [25] studied the sooting tendency of jet fuels and formulated two levels of correlation between the fuel composition and soot formation to predict soot emissions in actual gas combustors. The study involves relating lumped fuel composition parameters like hydrogen content and smoke point with sooting tendency followed by relating detailed hydrocarbon composition with the lumped fuel parameters. The work is based upon the Threshold Sooting Index model used by Olson et al. [26] in 1985. The TSI reference values from Olson et al.'s work mentions naphthalene with a TSI = 100, *n* – butylbenzene with a TSI = 62, decalin with a TSI = 15 and *n* – dodecane with a TSI = 5.1. The updated TSI model by Yang et al. is found to perform well for a variety of fuels, combustor operations and soot formation parameters. The results also show Jet fuels like JP – 8 and Jet A-1 having a TSI value of around 14 and 20.1 which suggest that JP – 8 has a lower propensity to soot in comparison to Jet A – 1.

The TSI concept was also used by Mensch et al. [27] in modelling complex jet fuels like JP – 8 and Jet – A using surrogate fuels composed of pure hydrocarbon fuels for which the TSI data exists or is easy to obtain. The surrogate fuels were attained by matching H/C ratio to that of the jet fuel. In the surrogate fuels, 1,3,5 – trimethylbenzene or mesitylene and 1 – methylnaphthalene are used as the aromatic hydrocarbon. The two JP – 8 surrogate studied are composed of 52% iso – cetane, 23% *n* – dodecane, 25% 1,3,5 – trimethylbenzene and 64% iso – cetane, 23% *n* – dodecane, 13% 1- Methylnaphthalene, respectively with an H/C ratio of 2.0 and a similar TSI value of $\sim$ 29.0. The results of the study further confirm that heavy aromatic fuels have a higher sooting propensity as for the same TSI value lower amount of 1 – methylnaphthalene is required than 1,3,5 – trimethylbenzene. Another key observation from this study is that with the variation in aromatic content of the jet fuels their sooting propensity can be varied and reduced for good measure.

Synthetic jet fuels like those obtained from the Fischer Tropsch process were also studied for their sooting behavior by Saffaripour et al. [28]. The study is conducted for laminar, co-flow diffusion flames at atmospheric pressure. The test fuels used in the study are Jet A-1 (18.9% vol. aromatics), fully synthetic jet fuel – CtL (10.7% vol. aromatics), Fischer Tropsch – synthetic paraffinic kerosene – GtL (<0.1% vol. aromatics), SPK + 50% Naphthene (4.6% vol. aromatics) and SPK + 20% Hexanol (<0.1% vol. aromatics). It is evident from the results that fuels with higher aromatic content have higher volume fractions while those with very low or no aromatics show significantly low fractions.

Other than the SPK fuels there are bio – derived fuels usually termed as HRJ (Hydro processed Renewable Jet) fuels which are being currently used to with additives in aircrafts. Liu et al. [29] compared the sooting behavior of HRJ fuels derived from Camelina and Tallow with Jet – A using the spherically symmetric droplet flame configuration. The results of the study show that the HRJ fuels have a lower sooting propensity in comparison to the Jet – A fuel which can be related to the difference in aromatic content of the test fuels. To further understand the effect of aromatics on sooting Liu et al. also test a blend 50/50% vol. blend of Jet – A and HRJ Camelina. The sooting propensity of the blend is found to be between pure HRJ Camelina and pure Jet – A as expected.

1.3.2. Effect of Fuel on Flame structure and Chemiluminescence

As mentioned earlier the flame is a composition of radical species in their excited states denoted with a superscript (*) which is the cause of the flame luminosity. The key radical species responsible for the hue of the flame luminosity are OH^*, CH^*, C_2^* and CO_2^* [30] as specified by Gaydon and further supported by his subsequent work in studying the absorption spectra of free radicals in oxy – acetylene flames on flat flame burners. Gaydon et al. [31] mention that the C_2 absorption of 5165Å wavelength peaked in richer flames with mixture ratios about three times the stoichiometric, CH absorption peaked in three bands of 4315Å , 3900Å and 3143Å for leaner flames with no detection in the luminous mantle above the inner cone. Another absorption, though weak at 4050Å is mentioned just above the tip of the reaction zone in flames

having mixture strengths around 3 – 4 times stoichiometric and accounted for by the presence of C_3 radicals which are also considered to be responsible for the formation of soot precursors. Haber et al. [32] in his study of premixed methane air flame on a flat flame burner setup for modelling OH* chemiluminescence presented the spectrum of the flame at an equivalence ratio of 1.0. These trends have been observed in other hydrocarbon flames too thus making the presence of these radicals the cause for the color of the flame as it appears.

The structure of the flame as observed in Bunsen flame experiments especially and similar to the cases presented by Street et al. [20] in their study (see **Figure 1.4**) can be viewed as a simple flow problem and a characteristic of the laminar flame speed (S_L). Certain flames appear to open up near the tip as the equivalence ratio ϕ is increased.

1.4. Summary

On the basis of the information provided regarding this research study in this chapter concerning its objective, motivation and justification as well as the fundamental theory necessary to understand and conduct this study the following summary points are drawn:

1. Developing an understanding of the correlation between the sooting tendency of a hydrocarbon fuel and its principal components is a necessity to set a basis for further complex investigations.
2. Adverse impacts on the environment and its inhabitants and components of engine in various machinery due to particulate matter like soot dispersed upon combustion draws enough motivation and justification for the research study.
3. Using a Premixed Laminar flame for studying combustion properties and emissions is a promising approach due to stability and adequate user control over the process.

4. Certain hydrocarbon families show higher tendency to form soot in comparison to others. Noticing such trends in the research study can help validate the results obtained.

With a fair knowledge about the key terms and processes involved in the study, a detailed discussion on literature mentioning similar studies and results is talked about in the next chapter. This literature serves as both justification for the experimental approach considered for the study as well as a source for validating the outcome of the Meker Burner study.

***

2. LIQUID FUELS

This chapter discusses in detail the liquid hydrocarbon fuels which serve as the core of this research study. A fuel in the most generic terminology is a chemical mixture, composed of various compounds belonging to different hydrocarbon families. Thus, the source of these fuels, proportion of different hydrocarbon compounds in the fuel as well as their physical properties are necessary to relate and predict the soot formation characteristics upon combustion.

2.1. Liquid Fuel Production

The majority of liquid fuels used for transportation are primarily composed of hydrocarbon compounds in varying proportions along with certain impurities such as nitrogen and sulfur, which upon combustion results in NO_x and SO_x emissions, respectively. N_2 from air also adds to the NO_x emission. The liquid hydrocarbon fuels are obtained from various sources and employ different techniques for production. A broad classification of the liquid fuel sources are *Non – Renewable Sources* such as crude oil, coal, natural gas and *Renewable Sources* such as Oil Seeds, Animal Fat (Tallow) and Lignocellulose biomass. The fuels used in the research study are obtained from various sources using different extraction and processing methods. **Table 2.1** provides details of these fuels which are further explained in the chapter. On the basis of the information provided in **Table 2.1** the key major processes for obtaining these liquid fuels are enumerated as follows:

1. Fractional Distillation Method.
2. Fischer – Tropsch Method.
3. Hydro – Processing Method.
4. Fermentation Method.

Fuel Name/ IUPAC Name	Global Formula	C:H Ratio	Molecular Weight (g/mol)	Density (kg/m^3)	Stoichiometric fuel – air ratio
Iso – Octane	C_8H_{18}	0.444	114	690	0.066
Mesitylene	C_9H_{12}	0.750	120	863.7	0.073
Toluene	C_7H_8	0.875	92	867	0.0745
Cyclohexane	C_6H_{12}	0.500	84	770	0.0675
Petroleum Aromatic Blend	$C_{9.9}H_{12.9}$	0.767	132	925	0.0726
JP – 5	$C_{11.9}H_{22.6}$	0.527	166	810	0.0684
Jet – A	$C_{11.4}H_{22.1}$	0.516	159	820	0.0681
JP – 8	$C_{10.8}H_{21.8}$	0.495	114	790	0.0676
FT – Coal	$C_{10.8}H_{23.6}$	0.458	154	760	0.0664
FT – Natural Gas	$C_{11.8}H_{25.6}$	0.461	168	760	0.0669
HRJ – Camelina	$C_{12.0}H_{25.9}$	0.463	170	750	0.0666
HRJ – Tallow	$C_{12.1}H_{26.3}$	0.460	172	793	0.0664
Gevo Jet Blend Stock	$C_{12.5}H_{27.0}$	0.463	178	800	0.0669

Table 2.1: List of key properties for Liquid Fuels used in the Meker burner study.

2.1.1. Fractional Distillation Method

The majority of the transportation fuel i.e. Gasoline, Kerosene, Diesel Oil and Fuel Oil is obtained from Crude Oil drilled from the earth's crust. Crude oil is a highly viscous and dense hydrocarbon liquid mixture formed from decomposed organisms subjected to intense pressure and temperature. The process of fractional distillation is employed to the crude oil in order to obtain hydrocarbon mixtures having different molecular structure, physical properties and especially the boiling points as shown in **Figure 2.1**. These components are further subjected to catalytic cracking and reforming to obtain the fuel for final usage.

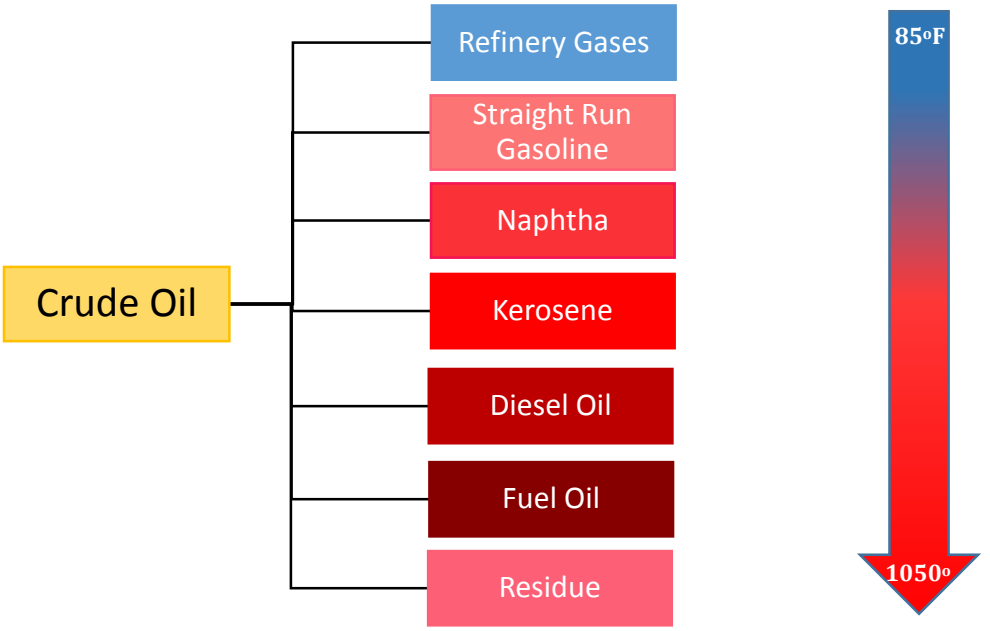

Figure 2.1: Fractional Distillation of Crude Oil with products separated at different temperatures. [38]

The transportation fuels obtained from this process, as mentioned previously, have been put to use for over a century during which they have been further refined and modified to suit the needs. Gasoline, has a boiling point in the range of (85 – 185^{0}F) and comprises mostly of C_5 – C_{10} straight chained or branched hydrocarbons along with aromatic hydrocarbons. Its primary usage is in cars to convert thermal energy to kinetic energy using an engine. Kerosene forms the parent compound for several classes of jet propellants currently in use. Its boiling point is in the range of (350 – 450^{0}F) while comprising majorly of C_{10} – C_{17} hydrocarbons along with fair amount of

aromatic hydrocarbons. Due to the availability of higher number of carbon atoms in a single chain, this fuel is able to provide much higher energy than gasoline and hence is a prime fuel for aircrafts. Another distillate, Diesel oil with a fairly higher boiling point in the range of (450 – 650^{O}F) comprises of hydrocarbon chains with even higher carbon numbers i.e. C_{14} – C_{20}. Other distillates, with higher carbon numbers are dense and have a wax like composition making the suitable for other applications beyond transportation fuel. **Figure 2.2** shows the chemical composition, both at component level and elemental level for the Kuwait crude oil. The presence of naphthenic and aromatic is found to promote formation of soot upon combustion as suggested by several studies mentioned in the previous chapter.

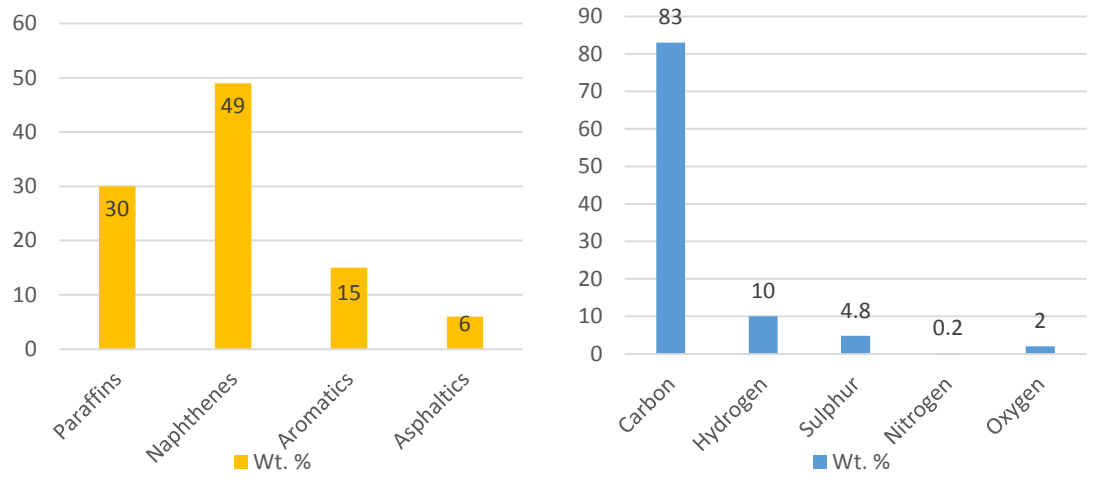

a) b)

Figure 2.2: Percentage chemical composition of Kuwait crude oil. [33]

2.1.2. Fischer – Tropsch Method

In the 1920s, Franz Fischer and Hanz Tropsch developed a process to formulate liquid hydrocarbon fuels from other solid or gaseous fossil fuels; it is termed the Fischer – Tropsch Method. The process employs conversion of syngas (a combination of CO and H_2) in presence of a catalyst (usually transition metals like cobalt, iron and ruthenium) into liquid hydrocarbons of varying chain lengths. This chemical process, in a general sense, is depicted by chemical reaction given as **Equation 2.1** below. A prelude to this gas-to-liquid conversion reaction step, is obtaining syngas from

carbon rich sources such as coal and natural Gas. As an example when natural gas is subjected to steam in a steam reformer process, which is essentially a de-hydrogenation reaction, the products contain carbon monoxide and molecular hydrogen (see **Equation 2.2**).

$$(2n + 1)H_2 + nCO \rightarrow C_nH_{2n+2} + nH_2O \quad 2.1$$

where, $n \in [1, N]$ describing the number of carbon atoms.

$$CH_4 + H_2O \rightarrow CO + 3H_2 \quad 2.2$$

For syngas production, coal is subjected to partial combustion under controlled air and/or steam supply, called gasification. Volatiles released from coal undergo pyrolysis to produce char particles (mostly carbon) which upon interaction with air result in carbon dioxide (CO_2) and carbon monoxide (CO) formation (see **Equation 2.3** and **Equation 2.4**). In case of steam, the char particles undergo partial oxidation to form carbon monoxide and di-hydrogen as shown in **Equation 2.5**. Finally, syngas obtained from these different sources is converted to liquid fuel as per **Equation 2.1**. [34]

$$C + O_2 \rightarrow CO_2 \quad 2.3$$

$$CO_2 + C \rightarrow 2CO \quad 2.4$$

$$C + H_2O \rightarrow H_2 + CO \quad 2.5$$

Varying the temperature in a Fischer – Tropsch process results in formation of liquid fuels with different molecular structure. On the basis of this temperature difference, two classifications exist, namely *High Temperature Fischer – Tropsch* (HTFT) and *Low Temperature Fischer – Tropsch* (LTFT). **Table 2.2** discusses a comparison among these two classifications. The HTFT process was commercialized by Sasol specifically for coal-to-liquid conversion with light paraffins and olefins as products whereas the LTFT process has been mainly used on natural gas for gas-to-liquid conversion with heavy paraffins and waxy hydrocarbons as its products.

		HTFT Process	LTFT Process
Temperature Range (^{0}C)		310 – 340	210 – 260
Pressure (bar)		~25	10 – 45
Catalyst Used		Iron	Cobalt
Product Distribution (Carbon basis) %	**CH_4**	4.0	7.0
	n – Alkenes (C_2 to C_4)	4.0	24.0
	n – Alkanes (C_2 to C_4)	4.0	6.0
	C_5 – C_{10}	18.0	36.0
	C_{11} – C_{16}	19.0	12.0
	> C_{17}	48.0	9.0
	Oxygenated Hydrocarbons	3.0	6.0
Reactor Type		Circulating fluidized bed reactor	Multi tubular fixed bed reactor

Table 2.2: HTFT and LTFT Process comparison table. [35]

2.1.3. Hydro – Processing Method

The renewable feedstock for transportation fuel i.e. plant oil seeds, animal fat and algae are first used for extracting oil and fat (rich in C,H and O) to be used for further chemical conversion processes. The plant oil seeds and algae are fed into an oil press which separates the oil and the biomass. The biomass formed is generally used as an additive to organic fertilizers and in animal fodder. Similarly, the animal fat obtained from slaughter houses after the rendering process serves as good as the oil obtained from plant sources. The oil and fat collected from these primary extraction processes is composed principally of triglycerides. A simple triglyceride as shown in **Figure 2.3** can be described as three ester compounds joined together. In structure, a triglyceride is similar to a glycerol ($C_3H_8O_3$) but instead of the hydroxyl group (-OH) there exists a carboxylate group (RCOO-) at each of the three carbon atoms.

The triglyceride rich oil and fat can be chemically converted into glycerol and fatty acids with the hydrolysis process. This process is conducted at high temperature and high pressure with water. The reaction conditions result in breaking of the triglyceride into three different carboxylate radicals ($R_aCO\dot{O}$, $R_bCO\dot{O}$ and $R_cCO\dot{O}$) and a $H_3\dot{C} - \dot{C}H - \dot{C}H_3$ radical which then reacts with the hydroxyl radical ($\dot{O}H$) and hydrogen radical ($\dot{H}$) produced from H_2O dissociation. Another method to dissociate the triglyceride is to react it with an alcohol (generally methanol) in presence of a catalyst. This is termed as the transesterification method, as one ester gets converted into another ester along with the formation of glycerol. As methanol is the reacting alcohol the resulting ester is termed as Fatty Acid Methyl Ester (FAME). FAMEs can be directly used as biodiesel in land based vehicles but for using them as jet fuels the esters need to be converted into long chained pure hydrocarbons for them to mimic

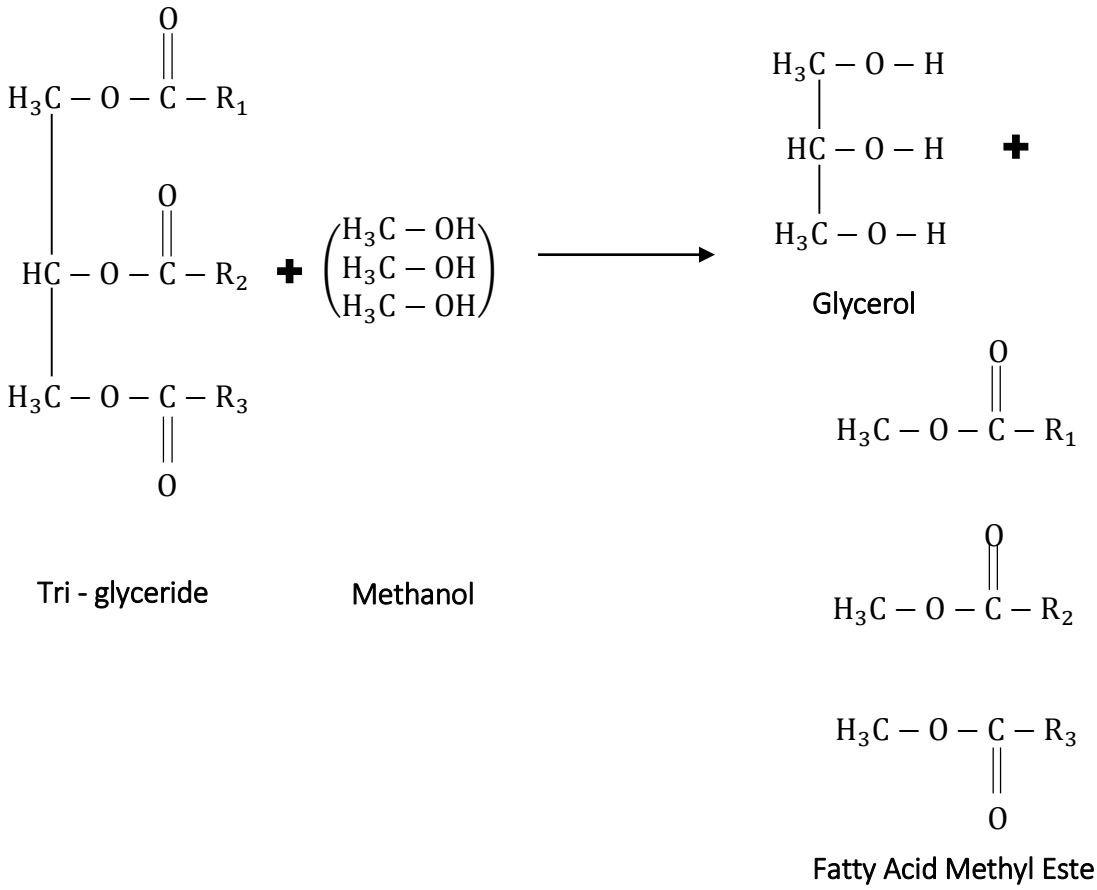

Figure 2.3: Trans – esterification process of tri – glyceride using methanol to obtain fatty acid methyl esters (FAME).

physical and chemical properties of prevalent jet fuels obtained from non – renewable sources. Hydrotreated Renewable Jet (HRJ) or Hydrogenated Esters and Fatty Acids (HEFA) fuels are formed from hydro – processing the fatty acid methyl ester or other fatty acid esters obtained from hydrolysis process. The hydro – processing method comprises of deoxygenation/hydrogenation, isomerization and hydrocracking steps. These steps are discussed in brief points as follows:

1. *Deoxygenation/Hydrogenation:* This process is a catalytic reaction conducted at a low temperature in presence of hydrogen. The oxygen atom attached to alkyl groups is replaced with a hydrogen atom and the carbon – carbon double bonds are replaced with single bonded carbon atoms. The outcome of the process are long chained n – alkanes along with water and carbon dioxide.

These n – alkanes have high density and show poor fuel flow capabilities which can be improved from the next two steps.

2. *Isomerization:* This is also a catalytic process involving interaction of n – alkanes and hydrogen in moderate temperature and pressure conditions. The long chained n – alkanes obtained from step 1 are converted to branched hydrocarbons.
3. *Hydrocracking:* This final step aims at reducing the hydrocarbon chain size by reacting the branched isomers of n – alkanes with hydrogen in presence of a catalyst at higher temperature and pressure values.

It has been noticed that based on the temperature and pressure values employed for the isomerization and hydrocracking processes hydrocarbons with different chain sizes and branches can be obtained. [36]

2.1.4. Fermentation Method

As a renewable feedstock, in addition to the oil seeds from the plants there is an abundance of plant sugars (sucrose) which comprises of monosaccharides like glucose and fructose, both represented by a chemical structure: $C_6H_{12}O_6$. The process of fermentation is well known for converting such monosaccharides with the help of enzymes (such as zymase) present in yeast and fermenting bacteria into alcohol and carbon dioxide as depicted in **Equation 2.6**. The enzymatic fermentation process is not very helpful in fermenting the complex sugars (polysaccharides) and starch. By reacting them with acids such as sulfuric acid or hydrochloric acid the complex sugars are hydrolyzed to simple sugars (monosaccharides) which can then be reacted with fermenting enzyme.

$$C_6H_{12}O_6 \xrightarrow{\text{zymase}} 2C_2H_5OH + 2CO_2 \qquad 2.6$$

The most common product of such a fermentation process is ethanol with other products like methanol, propanol and butanol. [34] The ethanol obtained is subjected to dehydration process for obtaining ethylene followed by oligomerization process which combines the short chained alcohols into n – alkanes of desired length. This final product is then usable for propulsion in aircrafts.

2.2. Chemical Properties of Test Fuels

The hydrocarbon liquid fuels mentioned previously in **Table 2.1** possess a varying chemical composition owing to the difference in the extraction and secondary refinement processes employed. Gas chromatography analysis of these fuels conducted by AFRL show n - Paraffins, Iso - Paraffins, Monocycloparaffins, Dicycloparaffins, Tricycloparaffins, Alkylbenzenes, Diaromatics and Cycloaromatics as the major hydrocarbon families present. These hydrocarbon families possess different structural arrangement of carbon and hydrogen atoms which results in varying chemical and physical properties. **Figure 2.4** shows a comparison among the test fuels (used for the study) on the basis of % wt. composition of four major hydrocarbon families i.e. n – paraffins, iso – paraffins, cyclo – paraffins and aromatics.

The paraffinic hydrocarbons include straight chained hydrocarbons (n – paraffins or n - alkanes) varying from C_1 – C_{23} as well as branched hydrocarbons or isomers of straight chained hydrocarbons (iso – paraffins or iso - alkanes) varying from C_4 – C_{23}. Paraffinic hydrocarbons are a major component of gasoline, diesel fuel and jet fuels obtained from both non – renewable and renewable sources. The straight chained hydrocarbons or n – paraffins show easy thermal decomposition due to their low flash point which is a result of low C – C and C – H bond dissociation energy of 348 kJ/mol and 413 kJ/mol, respectively.

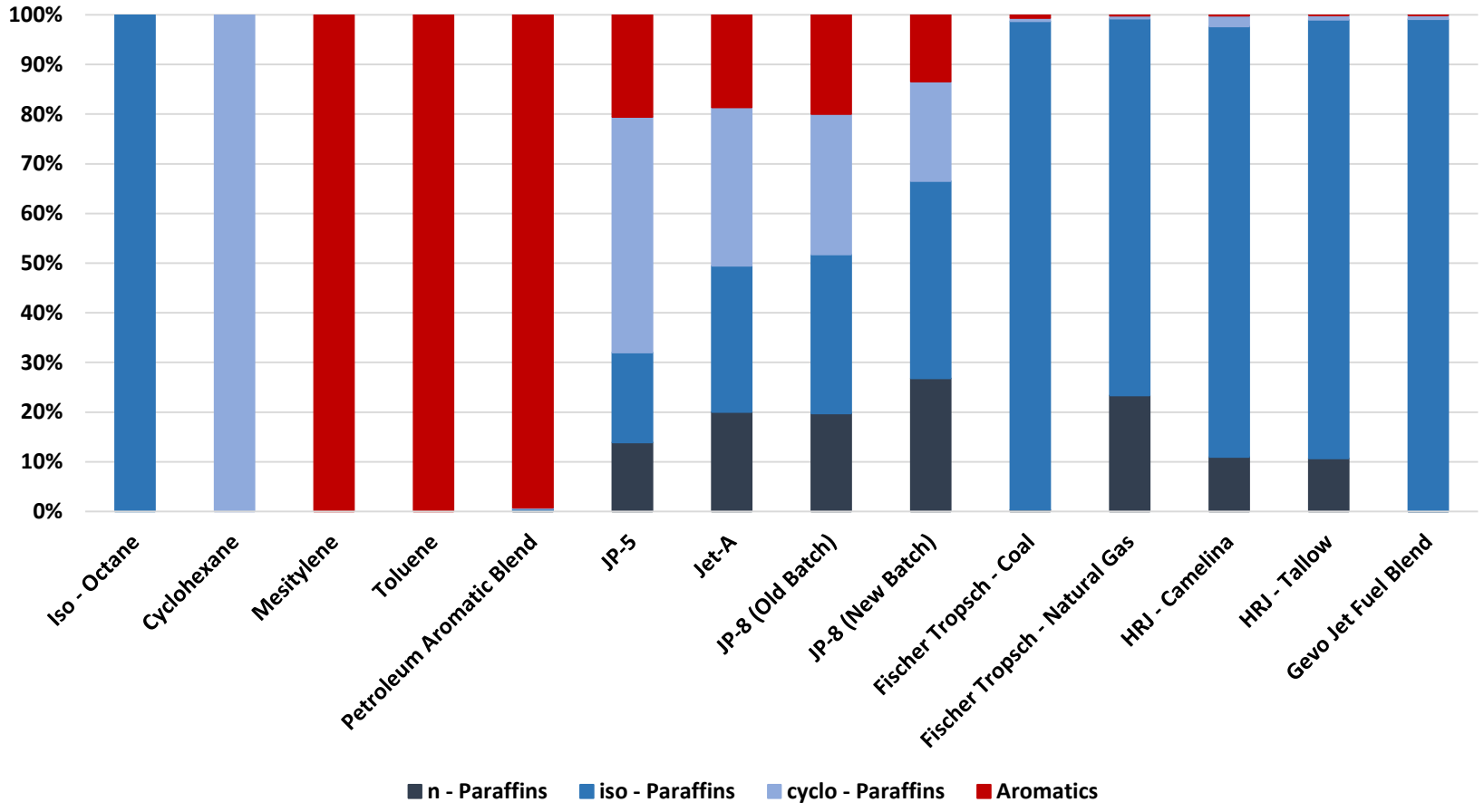

Figure 2.4: Percentage by weight n – paraffin, iso – paraffin, cyclo – paraffin and Aromatic composition of the test fuels.

In case of Iso – Paraffinic hydrocarbons in addition to the C – C and C – H bond energies, the well – defined and close packed structure of the C and H atoms induces resistance to thermal decomposition, thus making it comparatively slightly difficult to undergo combustion. Gasoline is a great example to understand the impact of n – paraffins and iso – paraffins on combustion. 'Knock' in internal combustion engines is generally due to n – paraffins while iso – paraffins prevent engine knock. The term Octane rating for gasoline is in reference to iso – octane which has a value of 100.

Another point of comparison among straight chained hydrocarbons is the number of bonds between the carbon atoms. Hydrocarbons containing double bonded carbon atoms (C = C) are termed olefins or n –alkenes and those containing triple bonded carbon atoms (C ≡ C) are termed n – Alkynes. In terms of the bond energy, both n – alkenes and n – alkynes exceed n – alkanes by a large margin, making them comparatively difficult to undergo thermal decomposition. As the C – H bond dissociation energy is nearly 348 kJ/mol in comparison to 614 kJ/mol for C = C bond and 839 kJ/mol for C ≡ C bond, the de-hydrogenation of n – alkenes and n – alkynes precedes carbon atom dissociation which propels aromatization and eventually soot formation as described by Frenklach et al.[21] The cyclo – paraffinic compounds have a cyclic structure with carbon atoms located at the vertices. This type of hydrocarbon generally has a well – defined, closely packed structure making it difficult to undergo thermal decomposition. Also based on the concept of bond energies the cyclo – paraffinic compounds can be expected to behave similar to n – alkanes in terms of soot formation.

The aromatic compounds are also cyclic in structure but have alternate C = C bonds instead of only C – C bonds as in cyclo – paraffins. These compounds are generally added in the range of 10 – 20% to the fuel to assist in seal swell of crucial plumbing components of the engine and fuel delivery system and provide lubricity. Benzene (C_6H_6) is a common aromatic hydrocarbon which is resonance stabilized by its two Kekulé forms. (see **Figure 2.5**) These two forms suggest that the electron pair forming the double bond among the adjacent carbon atoms is not stable and tends to switch the double bond location. This process is very rapid, thus making the bond

dissociation energy between two adjacent carbon atoms approximately as the average of bond dissociation energy of C – C and C = C bonds.

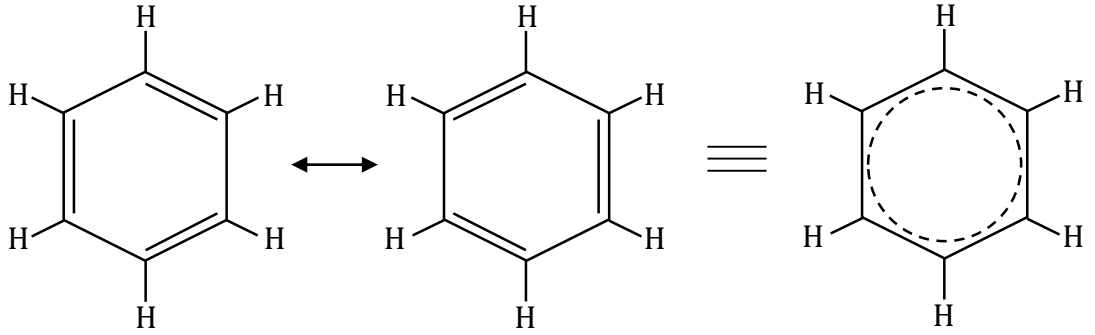

Figure 2.5: Resonance stabilized Kekulé forms of Benzene.

In terms of bond dissociation energies as, C – H bond has a higher chance of dissociating before the adjacent carbon atoms in the rings and form radicals. As this step is a part of the soot mechanism proposed by Frenklach et al.[11] and skips the soot precursor steps of acetylene formation, it becomes a prime candidate for rapid soot formation in the fuels. In general, these fuels contain just carbon and hydrogen but can also include impurities in the form of other elements such as sulfur and nitrogen. These impurities have the potential to impact the soot formation in these fuels and even contribute in the formation of SO_x and NO_x emissions. Some of the presently used bio – derived fuels contain a hydroxyl group (-OH) and belong to the alcohol family of organic compounds such as the B100 (Bio – Diesel).

Most of the test fuels for the study, though complex in composition, undergo a similar combustion process as a simple hydrocarbon like methane. The general stoichiometric combustion reaction (see **Equation 1.2**) mentioned in Chapter I is applicable to these fuels by using the Global formula mentioned in **Table 2.1**. The stoichiometric combustion reactions for them are listed as **Equations 2.7 – 2.19**.

Iso – Octane:	$C_8H_{18} + 12.5[O_2 + 3.76N_2] \rightarrow 8CO_2 + 9H_2O + 47N_2$	2.7
Cyclohexane:	$C_6H_{12} + 9[O_2 + 3.76N_2] \rightarrow 6CO_2 + 6H_2O + 33.84N_2$	2.8
Mesitylene:	$C_9H_{12} + 12[O_2 + 3.76N_2] \rightarrow 9CO_2 + 6H_2O + 45.12N_2$	2.9
Toluene:	$C_7H_8 + 9[O_2 + 3.76N_2] \rightarrow 7CO_2 + 4H_2O + 33.84N_2$	2.10
PET Aromatic	$C_{9.9}H_{12.9} + 13.13[O_2 + 3.76N_2] \rightarrow 9.9CO_2 + 6.45H_2O + 49.35N_2$	2.11
JP – 5	$C_{9.9}H_{12.9} + 13.13[O_2 + 3.76N_2] \rightarrow 9.9CO_2 + 6.45H_2O + 49.35N_2$	2.12
Jet – A	$C_{11.4}H_{22.1} + 16.93[O_2 + 3.76N_2] \rightarrow 11.4CO_2 + 11.05H_2O + 63.64N_2$	2.13
JP – 8	$C_{10.8}H_{21.8} + 16.25[O_2 + 3.76N_2] \rightarrow 10.8CO_2 + 10.9H_2O + 61.1N_2$	2.14
FT – Coal	$C_{10.8}H_{23.6} + 16.7[O_2 + 3.76N_2] \rightarrow 10.8CO_2 + 11.8H_2O + 62.79N_2$	2.15
FT – Natural Gas	$C_{11.8}H_{25.6} + 18.2[O_2 + 3.76N_2] \rightarrow 11.8CO_2 + 12.8H_2O + 68.43N_2$	2.16
HRJ – Camelina	$C_{12}H_{25.9} + 18.48[O_2 + 3.76N_2] \rightarrow 12CO_2 + 12.95H_2O + 69.47N_2$	2.17
HRJ – Tallow	$C_{12.1}H_{26.3} + 18.68[O_2 + 3.76N_2] \rightarrow 12.1CO_2 + 13.15H_2O + 70.24N_2$	2.18
Gevo Jet Blend	$C_{12.5}H_{27} + 19.25[O_2 + 3.76N_2] \rightarrow 12.5CO_2 + 13.5H_2O + 72.38N_2$	2.19

In addition to these test fuel samples obtained directly from stores and AFRL (Air Force Research Laboratory, Ohio) a few samples prepared by blending two fuels from the primary fuel inventory were also studied.

2.3. Blended Test Fuels

On the basis of the literature on soot formation studies conducted for different hydrocarbon liquid fuels a consensus can be made for aromatic hydrocarbons to form soot more readily than paraffinic hydrocarbons. This theory is mostly confirmed from the experiments conducted on the Meker burner and is further discussed in Chapter 3. To understand the impact of aromatic hydrocarbons on incipient soot phi ($\phi_{incipient}$) a few test samples obtained by blending Mesitylene with HRJ – Camelina and HRJ – Tallow in varying % vol./vol. proportion are studied. The impact of cyclo – paraffins on the incipient soot phi ($\phi_{incipient}$) is also studied by blending Cyclohexane with HRJ – Camelina in a similar way as the previous cases. The blend ratios of these samples are provided in **Figure 2.6**. HRJ – Camelina and HRJ – Tallow are chosen for

they have almost no aromatic hydrocarbons as per the composition showed in **Table 2.1** and are mostly composed of iso – paraffinic hydrocarbons. The results pertaining to incipient soot phi ($\phi_{incipient}$) for these blended fuel samples are discussed at length in Chapter V.

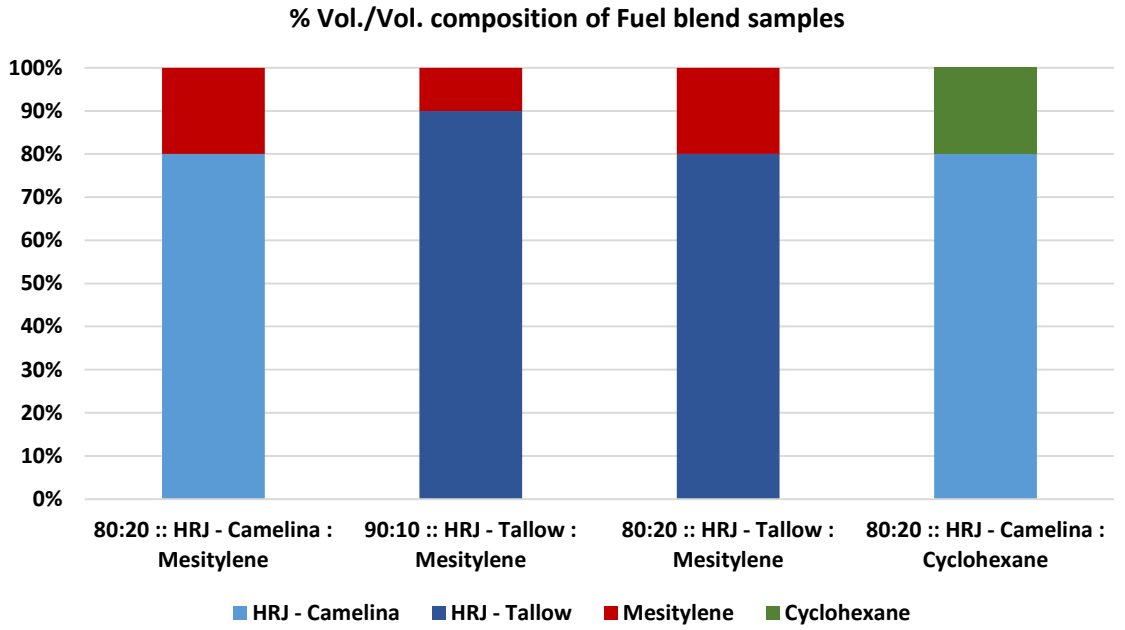

Figure 2.6: Percentage Vol./ Vol. composition of blended fuel samples.

2.4. Summary

The information presented regarding the synthesis, properties and emissions in relation to liquid jet fuels in this chapter, establishes a firm basis, useful in analyzing the results obtained from the research study. The key information can be summarized in a few points as follows:

1. Jet fuels obtained from renewable sources are processed such that they can be considered as a possible candidate to replace the currently used jet fuels obtained from non – renewable resources like kerosene.
2. In reference to gas turbine engines used in aircrafts, pure hydrocarbon fuels are of interest in comparison to fuels containing additional elements such as oxygen as in case of bio – diesel.

3. Different hydrocarbon families present in a jet fuel mixture provide an amalgamation of properties to a fuel which could be beneficial in terms of performance but detrimental in emissions. Presence of alkene, alkyne and aromatic hydrocarbons in the fuel appears to accentuate sooting as per literature.

Beginning from the next chapter, a transition into the experimental proceedings of the Meker burner study. The chapter provides detailed information on the experimental design, setup, steps undertaken for conducting experiments and instrument calibrations and observation techniques implemented.

***

3. MEKER BURNER CONCEPT & EXPERIMENTAL SETUP

A laminar flame configuration is used to determine the incipient soot phi ($\phi_{incipient}$). The development of the experimental setup along with a detailed discussion on the design and performance relevant to the study are discussed in this chapter. The plane jet atomizer assembly and design are used from thesis of Lee.[37] A brief description of the calibration of measurement systems and observation recording methodology is also provided.

3.1. Meker Burner Design Concept

The earliest studies conducted on liquid fuel combustion by Glassman et al. [7] and Street et al. used the Bunsen type flame, which is a premixed laminar flame. The selection of such a type of flame is justified due to its relatively stable structure which allows easy observation of changes in the flame. In these studies the flame is shrouded by a non – reactive gas to prevent air entrainment effects on the flames which can potentially impact the incipient soot phi ($\phi_{incipient}$).

The Meker Burner experimental setup, in principle, is similar to the Bunsen burner but instead of having a single flame cone at burner head a Meker burner uses a multi-pore burner head design allowing multiple flame cones. The setup uses a nickel coated off-market Meker head which is connected to a steel mixing tube with Swagelok connector. A fully developed laminar flow of the fuel – air mixture is obtained at the exit of the burner owing to the gradually increasing cross – section of the mixing tube and Meker burner assembly. This is further connected to a chamber allowing heated air to interact with atomized fuel from the plane jet atomizer and force through the drilled hole in the nozzle plate. The plane jet atomizer injects liquid fuel from the pressurized fuel tank into the system. The setup uses a non-reactive noble gas as a medium to generate the required pressure in the tank which in this case was nitrogen or helium. The air fed into the system is preheated to assist in fuel vaporization using an inline air heater connected upstream of the mixing chamber which is regulated using a thermostat and set – point controller. **Figure 3.1** shows a

schematic of the Meker burner experimental setup used in the study. The components of the system are further discussed in detail for a better understanding.

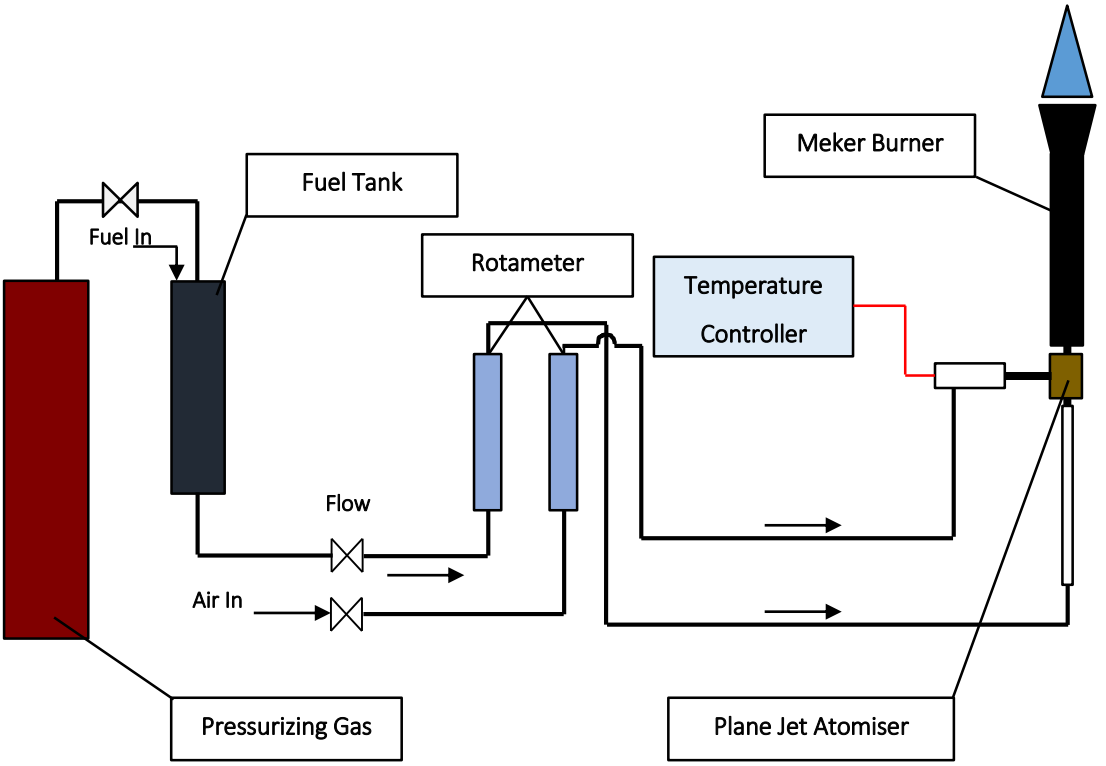

Figure 3.1: Schematic representation of the Meker burner experimental setup.

3.1.1. Fuel Pressurization, Delivery and Air heater System

The experimental setup uses liquid fuel for combustion which requires to be vaporized prior to being mixed with a stream of air to obtain a premixed combustion flame. The fuel is loaded into a stainless steel cylindrical container which is fitted with a $\frac{7''}{8}$ diameter fuel inlet port and a $\frac{9''}{16}$ diameter inlet port for the pressurizing gas at the top end. An outlet port of $\frac{9''}{16}$ diameter is provided at the bottom along with a separate drain port for removing the fuel from the system and/or air bubbles trapped in the lines. Both of the ports are fitted with a manual valve to allow the contents to flow when desired. The fuel container is designed to sustain high enough pressure

allowing a wide range of settings before a final setting of 65 psig or ~448.2 KPa gauge for fuel pressure was selected. Helium is used to pressurize the fuel in the container. The selection was made due to the non-corrosive and non-reacting nature of helium (being a noble gas) with the fuel under analysis. A pressure gauge is put in line with the gas inlet port to the container to adjust the pressure as and when required. The

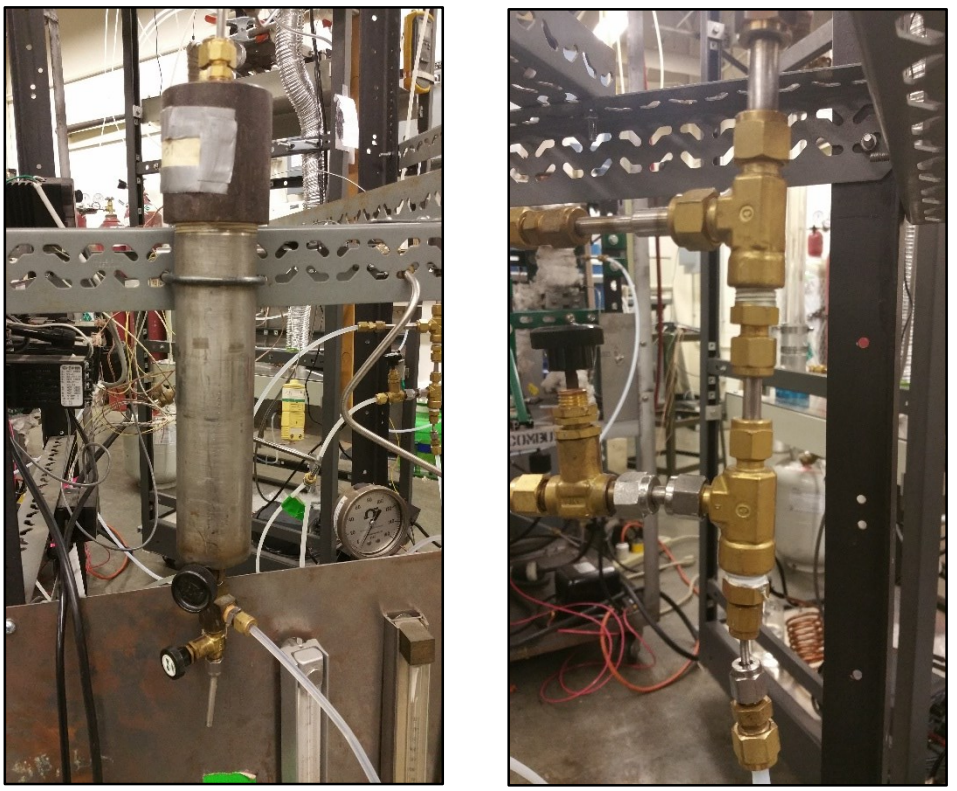

(a) (b)

Figure3.2: Fuel Tank and Plane Jet Atomizer used in the experimental setup represented by (a) and (b), respectively.

$\frac{9}{16}''$ outlet port at the bottom of the tank is connected to the lower inlet port of a liquid flow rotameter with a $\frac{1}{4}''$ flexible tubing. The rotameter is a mechanical flow device which is used to adjust flow rate as per requirement. The rotameter is discussed under the Flow Control sub-topic. After the rotameter, the fuel is transferred further to the plane jet atomizer using the $\frac{1}{4}''$ flexible tubing.

A Plane Jet Atomizer is described as a flow device that intakes high – pressure liquid at one end and releases atomized liquid droplets from the other end. The plane jet

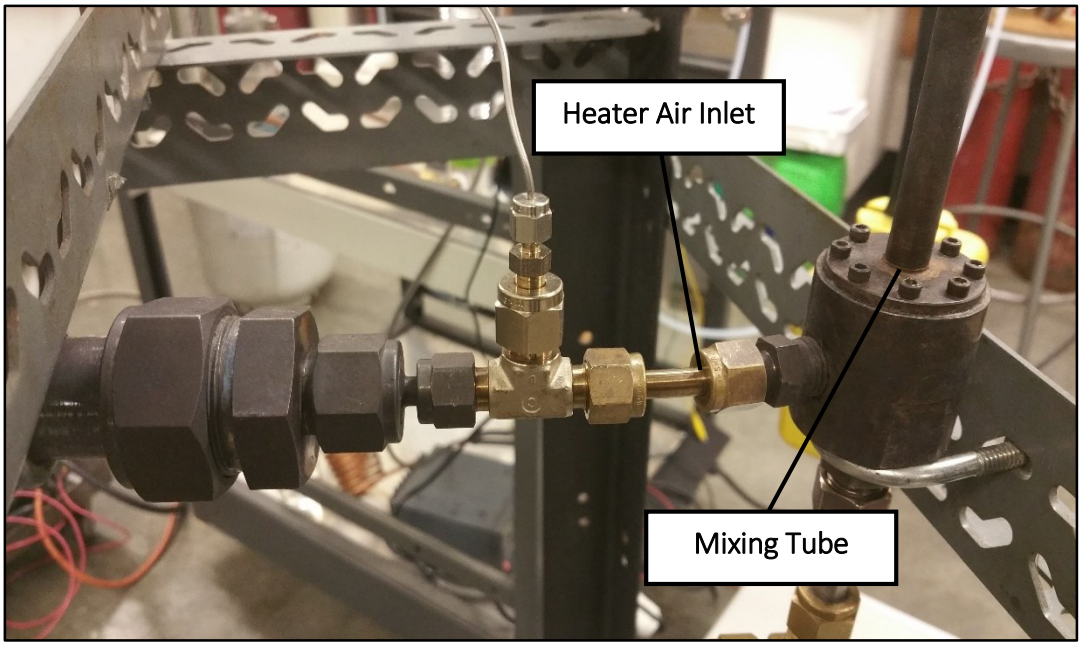

(a)

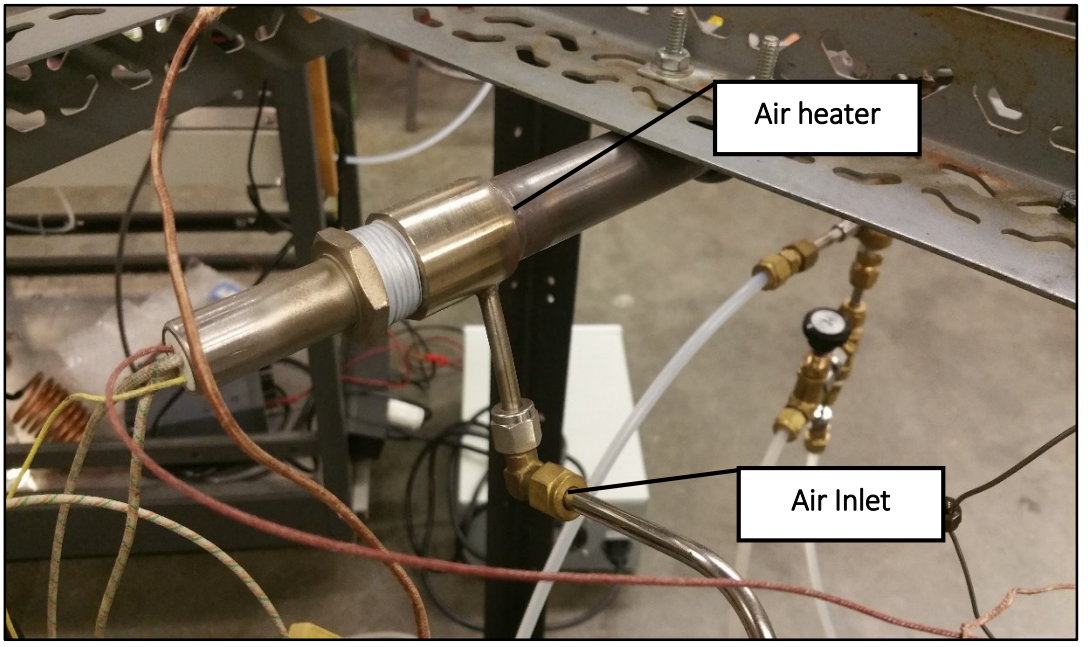

(b)

Figure3.3: Air heater assembly to preheat the air for fuel vaporization in the mixing tube.

atomizer used in the experiment is a liquid cooled to prevent vaporization inside the atomizer which will cause vapor lock inside the atomizer and disrupt fuel flow. The PJA *(Plane Jet Atomizer)* consists of 3 concentric tubes arranged such that the inner

tube carries the pressurized fuel for atomization while the two outer tubes circulate the water for cooling purposes. The inner tube is 0.125″ OD SS tubing, the middle tube is $\frac{1}{4}''$ OD and the outermost tube is $\frac{3}{8}''$ OD in dimension. The exit of the PJA is a truncated jeweler's torch tip, made of tapered 0.125″ OD copper tubing with a ruby inset which is silver – soldered onto the stainless steel tube assembly. The exit diameter of the orifice is 0.006″.

The air heater assembly is located upstream of the fuel – air mixing assembly. Air at room temperature and at a pressure of 62 psig or ~427.5 kPa gauge is directed through a rotameter device at a fixed mass flow rate of $4.32\,x10^{-4}$ Kg/s which corresponds to a reading of 55 on the rotameter tube. Air at this controlled flow rate is directed through the air heater which is a 1″OD stainless steel tube fitted with a 500 W, 4″(0.102m) long and $\frac{3}{4}''$ (19mm) of a diameter Inconel sheathed heater cartridge concentrically. The assembly allows the heater to interact with the incoming air and eventually raise its temperature to $360^{o}C$. The air temperature required is provided as an input through a Watlow series 989 temperature controller. The user inputs at the controller interface and a PID control signal is sent to the SCR. The air

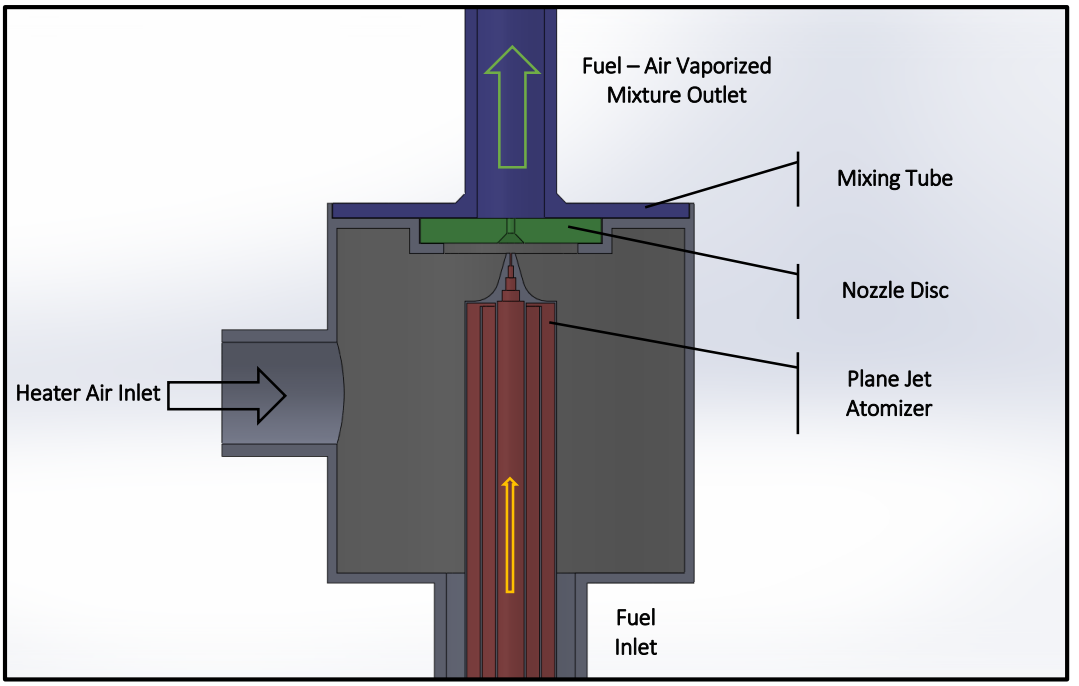

Figure3.4: Cross – sectional view of the mixing tube assembly.

heater operates on 110VAC single phase. A K-type thermocouple is installed in the interior of the Inconel sheath which gives the heater element temperature this forming a feedback loop and prevent over – heating. The heated air then enters the mixing tube assembly where the interaction of heated air and atomized fuel results in instant fuel vaporization. The mixing tube assembly and the Meker burner design are discussed in the sub – section.

3.1.2. Mixing Tube Assembly and Meker Burner

The pressurized hot air through the super heater system and fuel from the PJA, interact with each other in a stainless steel hollow cylinder of 1.5" OD (38.1mm) as shown in the **Figure3.4**. The pressure difference drives the air to exit into the mixing tube through the 90º countersunk, #68 (ϕ 0.031′′ or 0.787 mm) drilled hole in the middle of the solid stainless steel disk, depicted in green color in **Figure3.4**. The countersunk proves useful in preventing loss of fuel due to recirculation upon interaction with the disc surface. The exit tip of the PJA is located at a distance of 0.040′′ (1.016mm) below the lower surface of the steel disk. This allows enough gap between the nozzle plate and PJA tip for the air to force the atomized fuel through the plate nozzle and simultaneously initiate fuel vaporization. The mixture exits as a jet from the plate nozzle into a 0.25′′ ID (6.35mm) stainless steel tubing, 5′′ (127mm) in length. A one piece nickel – plated Humboldt Meker burner, as shown in **Figure3.5** is fastened to the 5′′ mixing tube with a Swagelok. The off – market Meker burner is custom – fitted with a pipe fitting to complete the required assembly. The Meker burner has an axial length of 10′′ (254mm) with a varying ID so as to obtain a fully developed laminar flow. The inlet ID of the Meker burner is 0.25′′ (6.35mm) and it expands to a maximum of 1.75′′ (44.45mm) ID. The burner head is fitted with a mesh of equally spaced, nearly 70 circular holes with 0.118′′ (2.99mm) diameter each. The mesh on the burner head results in several smaller Bunsen flames which together represent almost a flatter flame.

The assembly is wrapped in an insulation tape to minimize heat loss across the surface of the assembly. The temperature of the hot air exiting the burner head is

observed to be in the range of $110 - 120^{o}$ C in comparison to 360^{o} C near the super – heater. This suggests that even with insulation around the assembly there is a considerable heat loss which must be accounted for while conducting the experiment. The entire experimental setup is fastened on to a portable rack with the burner in the upright position. The experiments are conducted beneath a fume hood to prevent inhalation of product toxic gases and other emissions.

(a) (b)

Figure3.5: Side view of the Meker burner top as used in the experimental setup. (a) Actual Meker burner, (b) CAD model of the Meker burner.

3.2. Instrumentation

The experimental setup till this point is analogous to a black box or a function which uses inputs, processes them and provides an input. Instrumentation devices are an integral part of the experimental setup which provide various functions to the user and behave as an interface to the setup. In this experiment, the instrumentation devices used can be classified into two broad categories: (a) Flow Control and (b) Flow Calibration. These categories are discussed in the subsequent sub – sections.

3.2.1. Flow Control

In the Meker burner experimental setup (see **Figure 3.1**), two devices, the rotameter and ball valve are used. The ball valve is a type of control/safety valve with two modes, i.e. allows fluid flow or blocks the fluid flow. This valve is located both on the fuel and the air line, just before the Rotameter inlet. The purpose of the valve is to stop the fuel or air flow in case of emergency or to stop the experiment.

(a) (b)

Figure3.6: Rotameter flow meters installed in the experimental setup. (a) Fuel Rotameter and (b) Air Rotameter.

A rotameter is a flow control and measuring device installed inline of the fluid flow (see **Figure3.6**). It is a mechanical device and functions entirely on the basis of force balancing. The device has two ports, inlet and outlet for the fluid to flow. Near the inlet, a flow control valve is provided for adjusting the flow as per requirement. The device also has a graduated hollow glass tube with a metallic bead in it. When there is no flow the bead sits at the bottom of the tube, due to gravity which corresponds to a reading of "zero" on the scale. As the valve is opened and pressurized fluid is allowed to flow, the force imparted by the fluid on the bead offsets this force due to gravity thus making the bead rise vertically in the tube and eventually stabilize at a point. The graduations on the tube provide a numerical value corresponding to the flow. Rotameters being a flow measuring device require calibration for different fluids to

obtain a flow value. The process of calibration and devices used are discussed in **Section 3.2.2**.

In the experiment, two separate rotameter devices are installed on the fuel and air line. To reduce variables affecting the fuel and air composition, the rotameter controlling the air flow is set to a fixed value while the flow on the fuel rotameter is varied to obtain different values of phi (ϕ). Digital flow control devices are currently being used which provide a higher precision and increased repeatability in comparison to the rotameters. Such control devices can be installed on the setup for future work.

3.2.2. Flow Calibration

Calibration of the fuel rotameter is conducted for the different fuels under analysis to determine the mass flow rate associated with each fuel for a given rotameter reading. Physical properties of a liquid such as viscosity and density play a vital role in determining the flow rates. The calibration of the same was conducted using a simple methodology involving collecting a fixed volume of fuel for a given rotameter setting and fixed experimental conditions in a graduated cylinder and simultaneously recording the time required to collect the fixed volume.

In this procedure, the fuel is loaded in the fuel tank and pressurized with helium to 65 psig as in the experimental process. The flexible tubing connecting the outlet of the rotameter and inlet of the PJA is re-directed to collect the fuel in the graduated cylinder. The fuel is allowed to flow through the system by opening the control valve. Before the calibration is done, air trapped in the system is vented out to avoid error in the calibration process. The calibration process is started by setting the rotameter bead to read 10 on the scale and timing the collection of 1 ml of fuel in the graduated cylinder. A set of four observations are made at this setting to lower the chances of error in recording the observations. These steps are repeated for every 10^{th} reading until the maximum reading on the scale. This entire procedure is repeated for the other fuels and the calibration curves for the fuels and fuel blends are provided in the Appendix B for reference. A comparison of the calibration curves for the fuels is

provided in **Figure 3.7**. As evident from the figure the calibration curves for almost all the fuels is nearly linear in nature and appears to have a similar slope.

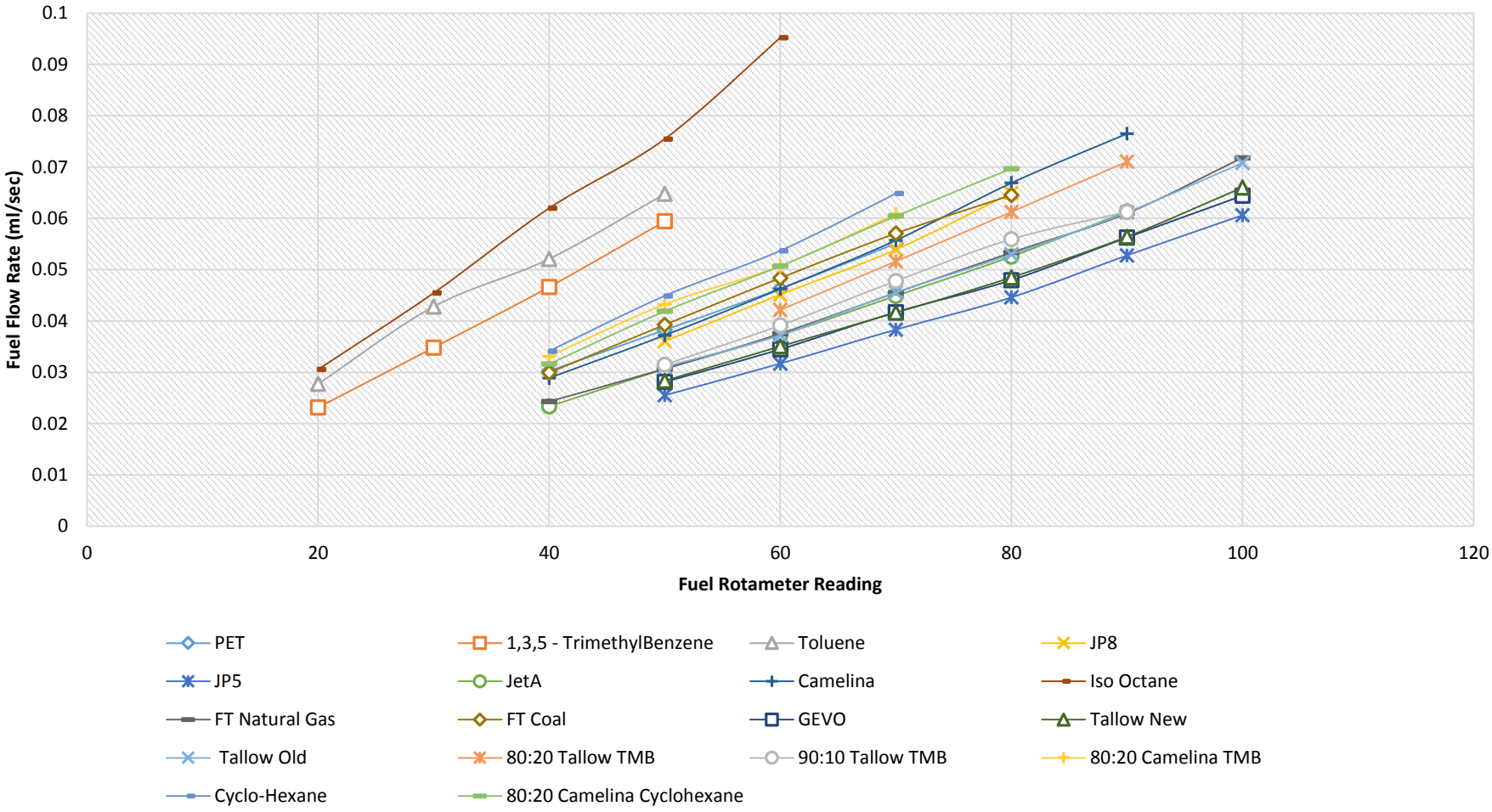

Figure 3.7: Calibration curves for the test fuel samples at 65 psig pressure.

A difference in the location of the curves on the XY plot is due to the variation in fuel viscosity.

The rotameter controlling the air flow is also calibrated for the experimental setting of 62 psig feed pressure into the system. A wet test meter is used to determine the air flow rate for a given rotameter setting. The meter is connected using the flexible tubing to the outlet of the rotameter while the rotameter inlet is connected to pressurized air. The rotameter bead is set to read 10 on the scale and air is allowed to flow through the calibration setup. This causes the needle on the wet test meter dial to rotate clockwise. One revolution of the needle corresponds to a volume of 0.1 cu. ft..The time for a revolution is recorded with a stopwatch and a total of four observations for a fixed rotameter setting are recorded. These steps are repeated for every 10^{th} reading on the scale until the maximum reading on the scale. A suitable flow rate for the experiment was found corresponding to a reading of 55 on the rotameter scale which corresponds to a value of 21.6 LPM. A detailed excel sheet on the calibration calculation is provided in the Appendix B.

3.2.3. Recording Observations

The experiment after calibration for a given test fuel is initiated by allowing air to flow through the system and simultaneously rising its temperature from the super heater. Once the thermocouple downstream of the super heater signals a steady value for the air temperature, fuel is allowed to flow through the PJA into the Meker burner assembly. After a delay of few seconds, the fuel – air vaporized mixture is released at the burner head. If for the given setting the fuel – air ratio (ϕ) is high enough to sustain combustion, then on igniting the mixture with a lighter gives combustion flame for the test fuel. The structure and chemiluminescence of the flame can be varied by changing ϕ using the fuel rotameter because mass flow rate of air ($\dot{m}_{air}$) is kept constant for all the experiments. For a given test fuel, observations are made for *Incipient Sooting* combustion condition mainly. To provide a perspective and reference for this state, observations are also made for *Complete Sooting, No Sooting* and *Very Lean* combustion

conditions. Observations are primarily made on the mass flow rate of the fuel ($\dot{m}_{fuel}$) and the flame shape and color for the before mentioned combustion conditions.

The $\dot{m}_{fuel}$ observations are made based on the fuel rotameter readings. The rotameter readings are conducted with a naked eye and are prone to parallax errors. Hence, the experiment is conducted at least twice for all the test fuels to improve the precision of the recorded data and observe the repeatability of the experiment.

Flame photography is done by Canon Rebel T5i DSLR with an EF 100mm f/2.8 Macro USM lens is used to capture digital photographs for the different combustion conditions for all the test fuels. The camera is setup on a tripod and placed next to the experiment such that the primary and post flame zone are in field of view. The camera settings were fixed at ISO 800, $f = 5.0$ and a shutter speed of $\frac{1}{40}s$. The digital photographs provide observable information about the flame structure and the chemiluminescence from the flames.

3.3. Summary

The contents of the chapter provided information related to the design and setting up of the Meker burner experiment. The components of the experiment were discussed for their operation and design as well as significance in the setup. Apart from the mechanical components, instrumentation devices used were also discussed. The approach to use these devices and calibrate them was also provided in brief. Finally, the method followed for recording experiment observations is also discussed. The selection of this method and the approach hold a significance in maintaining uniformity among the fuels and ease of understanding.

The next chapter provides the observations, results and discussion for the different fuels tested on the Meker burner setup.

***

4. OBSERVATIONS AND RESULTS

The experimental setup as described in Chapter 3 was used for a total of 17 different test fuel samples. The emphasis of the experiments is on determining the Fuel– Air ratio at incipient soot stage ($\phi_{incipient}$) for these test fuels. In addition to this, the structure of the flame and its chemiluminescence are also observed. As mentioned in the previous chapter, the methodology implemented for recording observations is using digital photography which is somewhat similar to the observation method used by Street et al.[20] and Glassman et al.[7] in their studies.

The contents of the chapter are categorized mainly under three sections, namely:

1. Effect on Incipient Soot.
2. Effect on Flame Structure and Luminescence.
3. Effect on Heat Loss at the Burner Surface.

The first section discusses the 17 fuel samples under separate sub – sections, classified on the basis of their hydrocarbon composition. The sub-sections are described as follows:

1. **Paraffinic and Cyclo – Paraffinic Fuels**

   Fuels composed of straight – chained or branched hydrocarbons having alkane, alkene or alkyne groups. It also includes fuels having an *n* – cyclic structure, where *n* is the number of cyclic rings. Aromatic hydrocarbons are not accounted for under this classification.

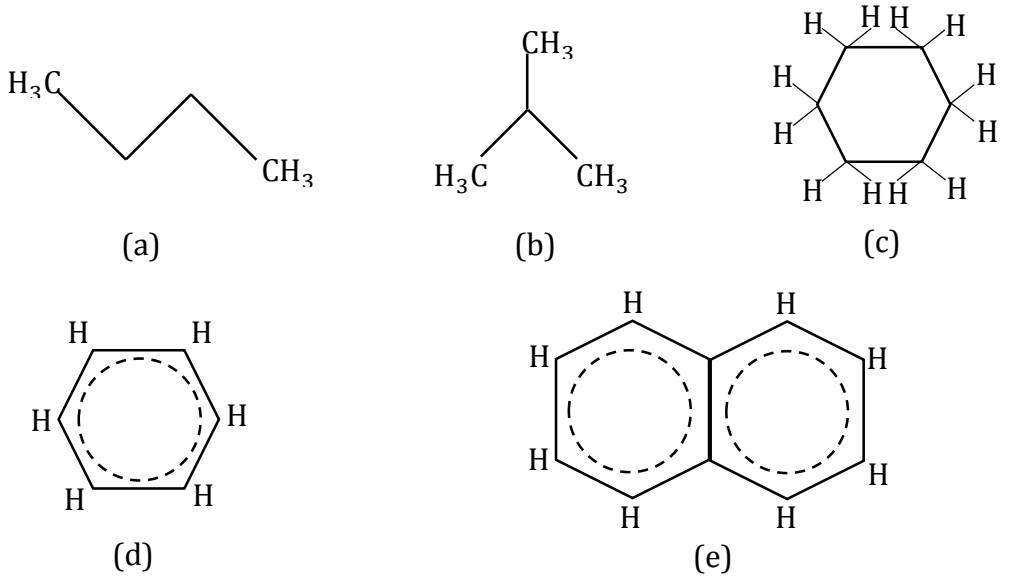

Figure 4.1: Structural representation of different hydrocarbon compounds. (a) n – Butane, (b) iso – Butane, (c) Cyclohexane, (d) Benzene and (e) Naphthalene.

2. **Aromatic Fuels**

   Fuels composed of compounds having single or more benzene like rings with or without alkyl groups attached to the ring periphery.

3. **Jet Fuels**

   Comprises of different Jet fuel grades which are a blend of several paraffin, cyclo – paraffin, aromatic hydrocarbons. These fuels are used in the aviation industry at present.

4. **Renewable Jet Fuels**

   Comprises of hydrocarbon fuels obtained from renewable sources or feed – stock. These fuels too are a blend of several paraffin, cyclo – paraffin and iso – paraffin hydrocarbons with no or very low aromatic hydrocarbons.

5. **In – house Blended Fuels**

Comprises of fuels obtained as a result of blending two fuels in different percentage by volume. The parent fuels are taken from one of the previously described sub – sections.

4.1. Effect on Incipient Soot

The primary motive of this experimental study was to determine the fuel – air ratio or phi (ϕ) corresponding to the onset of soot formation in a laminar premixed flame. This is obtained by first determining the fuel flow rate ($\dot{Q}_{fuel}$) in ml/s from the fuel rotameter reading and obtaining a corresponding mass flow rate ($\dot{M}_{fuel}$) in kg/s value using the density of the fuel followed by obtaining a ratio of fuel – air at the current observation ($\frac{F}{A}_{observed}$) and eventually calculating the incipient phi ($\phi_{incipient}$) using the fuel – air ratio at stoichiometric combustion ($\frac{F}{A}_{stoichiometric}$). The calculation process is shown in **Equation 4.1** for reference.

$$\phi_{incipient} = \left[\frac{(\dot{Q}_{fuel} * \rho_{fuel} * 1E-6)/\dot{M}_{air}}{\frac{F}{A}_{stoichiometric}}\right] \quad 4.1$$

Here, $\dot{m}_{air}$ is the mass flow rate of air which is fixed to a value of $4.32E-04\,\frac{kg}{s}$ for all the experiments. The onset of soot is considered to be the condition of the flame tip when a yellow chemiluminescence due to radiation from soot is observed through the digital camera. Based on this approach the observations and results deduced for the 17 fuel samples are provided. The results in this section include tabular readings obtained from the fuel rotameter and digital photographs corresponding to four different soot conditions.

4.1.1. Paraffinic and Cyclo – Paraffinic Fuels

This sub – section involves incipient soot results for iso – octane or 2,2,4 – trimethylpentane (C_8H_{18}), which is an isomer of n – paraffinic compound n – octane. It is a pure hydrocarbon with only C – C and C – H bonds. As an isomer, it has a more refined structure in comparison to n – octane. Another fuel, cyclohexane (C_6H_{12}) which is a

hydrocarbon with a cyclic structure, is also included in the study and presented in this sub – section. Cyclohexane is generally represented by a hexagon with carbon atoms at the vertices. Each of the carbon atoms is bonded to the adjacent carbon atoms and two hydrogen atoms to complete its octet.

	Iso - Octane		Cyclo - Hexane	
Observation	RM Reading Run #1	RM Reading Run #2	RM Reading Run #1	RM Reading Run #2
No Sooting – Lean Mixture	21	22	34	34.5
No Sooting – Rich Mixture	39	39	62	61.5
Incipient Sooting	40	40.5	64	63.5
Complete Sooting ǂ	44	46	70	71

ǂ: Equivalence ratio higher than incipient sooting with bright soot streaks.

Table 4.1: Rotameter readings recorded for Iso – Octane and Cyclohexane at four different soot stages.

The rotameter readings recorded for the two fuels are provided in **Table 4.1** and the corresponding images of the combustion flame are provided in **Figure 4.2** and **Figure4.3**. Based on these observations the following statements can be made for these two fuels:

1. The rotameter readings suggest that $\phi_{incipient}$ for Iso – Octane and Cyclohexane are 1.51 and 1.54, respectively.
2. The results suggest that these two fuels tend to soot comparatively later which can be associated with the fact that the alkanes do not tend to soot fast.
3. The occurrence of incipient soot in case of these fuels is slightly harder to determine with precision by crude observation. This is apparently due to the soot luminescence in these cases being mostly diffused and dull.

4. These fuels are not a blend and comprise upto 99% of similar hydrocarbon compound, respectively. Thus, the results obtained can be accounted for the hydrocarbon compound itself.
5. Though the value for $\phi_{\text{incipient}}$ is nearly close for both the fuels, Cyclohexane has a higher value which implies it is harder to make it soot in comparison to Iso – Octane.

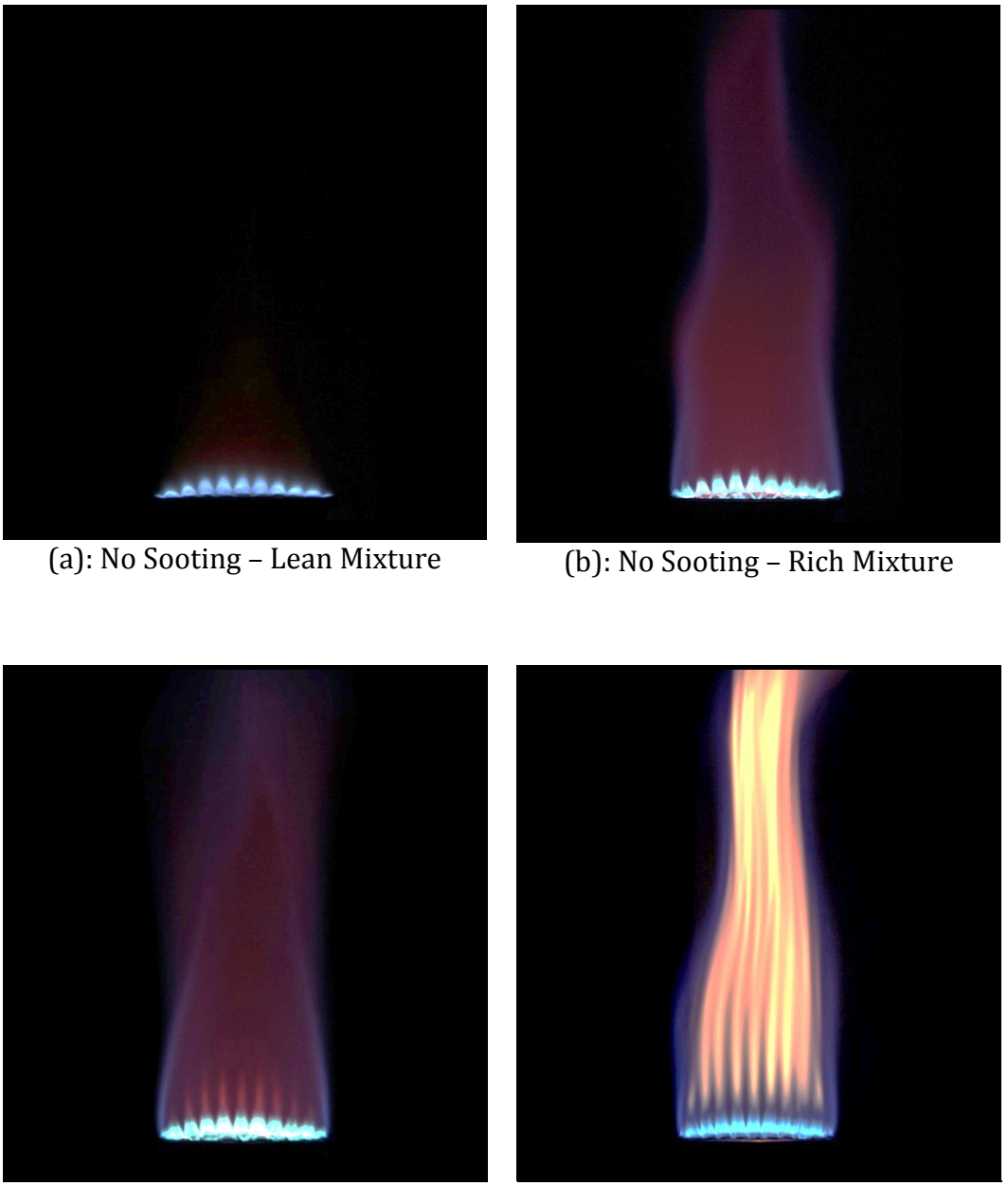

(a): No Sooting – Lean Mixture

(b): No Sooting – Rich Mixture

(c): Incipient Sooting

(d): Complete Sooting

Figure 4.2: The four different stages of Sooting for Iso-Octane. Φ for the different stages are: a) 0.78 ± 0.02 ; b) 1.46 ± 0.00 ; c) 1.51 ± 0.01 and d) 1.69 ± 0.04.

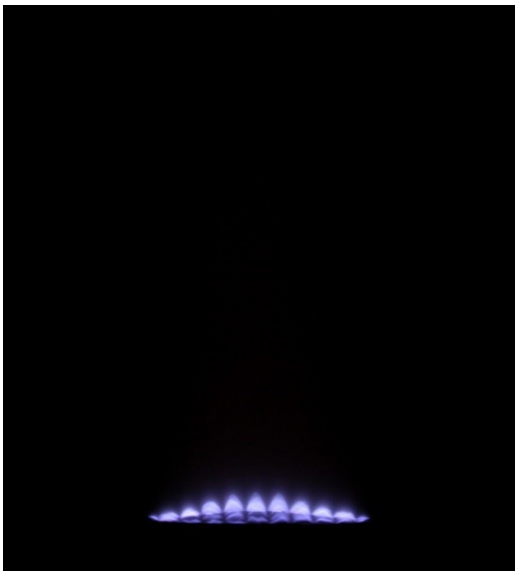

(a): No Sooting – Lean Mixture

(b): No Sooting – Rich Mixture

(c): Incipient Sooting

(d): Complete Sooting

Figure4.3: The four different stages of Sooting for Cyclo – Hexane. Φ for the different stages are: a) 0.75 ± 0.01 b) 1.48 ± 0.00 c) 1.54 ± 0.01 and d) 1.71 ± 0.01.

4.1.2. Aromatic Fuels

The fuels covered under this subsection are cyclic in structure but with alternating C = C carbon bonds making them different from the cyclo – alkanes. The compounds can have a mono – aromatic ring or poly – cyclic aromatics. Certain aromatic compounds are also found to have alkyl groups on the periphery. Mesitylene or 1,3,5 – trimethylbenzene (C_9H_{12}) is a mono – aromatic compound with methyl groups bonded to every odd peripheral carbon atom. Toluene or 1 – methylbenzene (C_7H_8) is another mono – aromatic compound with a single methyl group bonded to the peripheral carbon atom. Along with these two mono – aromatic fuels, a blend of Petroleum Aromatic ($C_{9.9}H_{12.9}$) is also tested on the Meker burner setup. The Petroleum Aromatic Blend comprises of various light and heavy aromatic compounds which contain mostly naphthalene like di – aromatic structures. On the basis of the literature study, these fuels are expected to have an incipient soot phi ($\phi_{incipient}$) value much lower than the paraffinic and cyclo – paraffinic compounds discussed in the previous sub – section.

	PET blend		Mesitylene		Toluene	
Observation	RM Reading Run #1	RM Reading Run #2	RM Reading Run #1	RM Reading Run #2	RM Reading Run #1	RM Reading Run #2
No Sooting – Lean Mixture	42	41	29	28	--	--
No Sooting – Rich Mixture	58	58	38	39	36	35
Incipient Sooting	61	60	41	41	38	37
Complete Sooting	64	63	43	43	40	39

Table4.2: Rotameter readings recorded for Petroleum Aromatic Blend, Mesitylene and Toluene at four different soot stages.

The rotameter readings recorded for the three fuels are provided in **Table4.2** and the corresponding images of the combustion flame are provided in **Figure4.4**, **Figure4.5**

and **Figure4.6**. Based on these observations the following statements can be made for these three fuels:

1. The values of $\phi_{incipient}$ for Petroleum Aromatic blend, mesitylene and toluene are obtained from the rotameter reading as 1.14, 1.33 and 1.34, respectively.
2. The results for these fuels are in accordance with the expectations as per the referred literature i.e. aromatic hydrocarbons tend to soot the earliest.
3. The flame tips at incipient soot stage show a prominent bright yellow button like shape, which is helpful in obtaining the corresponding $\phi_{incipient}$ value with a much higher precision in comparison to the fuels mentioned in sub – section **4.1.1**.
4. If closely observed the Petroleum Aromatic Blend produces soot much earlier than Mesitylene or Toluene. It can be argued that di – aromatic compounds, such as naphthalene in Petroleum Aromatic Blend, produce soot comparatively earlier than mono – aromatics. Thus, the following trend can be generalized in the order of their sooting tendency from high to low:

   Poly – Aromatic > Di – Aromatic > Mono – Aromatic
5. Further, on comparing the sooting behavior of Mesitylene and Toluene, Mesitylene appears to soot earlier than Toluene but not by a huge difference. This small difference can be accounted for by the availability of methyl radicals ($C\dot{H}_3$) which is higher in Mesitylene in comparison to Toluene.
6. As the values of $\phi_{incipient}$ are closer to the value of 1, it can be said that the mechanism to form soot has a much higher rate in comparison to the paraffinic and cyclo – paraffinic hydrocarbons.

(a) No Sooting – Lean Mixture (b) No Sooting – Rich Mixture

(c) Incipient Sooting (d) Complete Sooting

Figure4.4: The four different stages of Sooting for PET blend. Φ for the different stages are: a) 0.68 ± 0.01 b) 1.08 ± 0.00 c) 1.14 ± 0.01 and d) 1.21 ± 0.01.

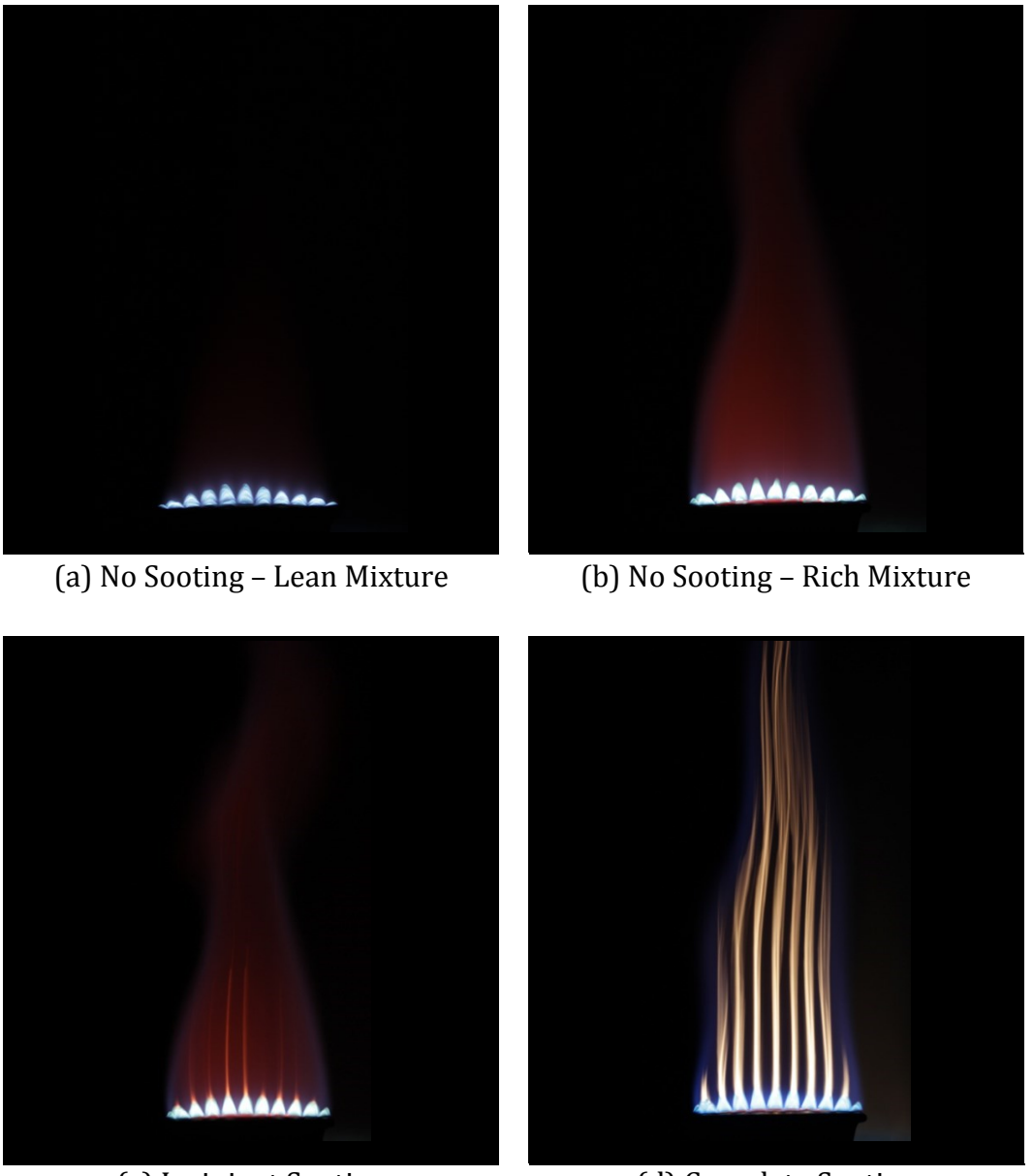

(a) No Sooting – Lean Mixture (b) No Sooting – Rich Mixture

(c) Incipient Sooting (d) Complete Sooting

Figure4.5: The four different stages of Sooting for Mesitylene. Φ for the different stages are: a) 0.91 ± 0.01 b) 1.24 ± 0.01 c) 1.33 ± 0.003 and d) 1.39 ± 0.00.

(a) No Sooting – Rich Mixture

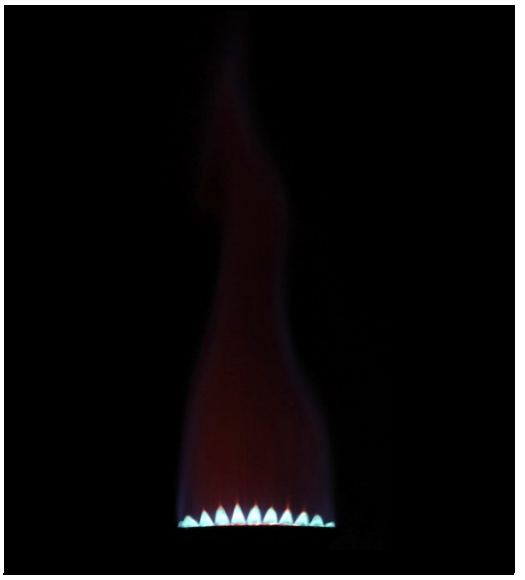

(b) Incipient Sooting

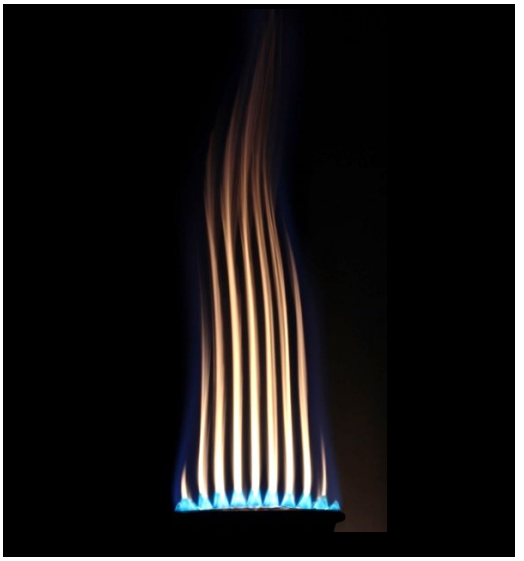

(c) Complete Sooting

Figure4.6: The four different stages of Sooting for Toluene. Φ for the different stages are: a) 1.28 ± 0.02 b) 1.34 ± 0.02 c) 1.41 ± 0.01

4.1.3. Jet Fuels

The Jet Fuels obtained primarily from fractional distillation of crude oil and subsequent refinement contain an amalgamation of different hydrocarbon families such as n – paraffins, cyclo – paraffins, iso – paraffins and aromatics. The results obtained for pure paraffinic, cyclo – paraffinic and aromatic compounds in previous sub – sections are useful in understanding the results for the jet fuels.

The jet fuel samples tested in this study include JP – 5 ($C_{11.9}H_{22.6}$), a low grade jet fuel with ~21% aromatics, Jet – A ($C_{11.4}H_{22.1}$), a slightly higher grade jet fuel with ~19% aromatics and JP – 8 ($C_{10.8}H_{21.8}$), a much refined and higher grade fuel with ~13% aromatics.

On the basis of the results obtained for aromatic fuels in sub – section **4.1.2**, the expected result for the jet fuels is for JP – 5 to have a higher sooting propensity in comparison to JP – 8 with the least amount of aromatic content. With reference to the observations recorded in **Table4.3** and corresponding images of the flame in **Figure4.7**, **Figure4.8** and **Figure4.9** the following statements can be made for these jet fuels:

1. The values of $\phi_{incipient}$ for JP – 5, Jet – A and JP – 8 are obtained from the rotameter reading as 1.45, 1.46 and 1.51, respectively.
2. The results for these fuels are in accordance with the fact that the jet fuel with least amount of aromatic, soots at a higher phi in comparison to the jet fuel with the maximum aromatics.
3. Similar to the observation made for pure aromatic compounds in sub – section **5.1.2 t**he flame tips at incipient soot stage show a prominent bright yellow button like shape, which is helpful in obtaining the corresponding $\phi_{incipient}$ value with a much higher precision.

	JP – 5		Jet – A		JP – 8	
Observation	RM Reading Run #1	RM Reading Run #2	RM Reading Run #1	RM Reading Run #2	RM Reading Run #1	RM Reading Run #2
No Sooting – Lean Mixture	56	55	45	44	42	43
No Sooting – Rich Mixture	89	88	76	75.5	67.5	68
Incipient Sooting	90.5	90	78.5	79.5	72	70.5
Complete Sooting	98	97	88	86	79	78

Table4.3: Rotameter readings recorded for JP – 5, Jet – A and JP – 8 for four different sooting stages.

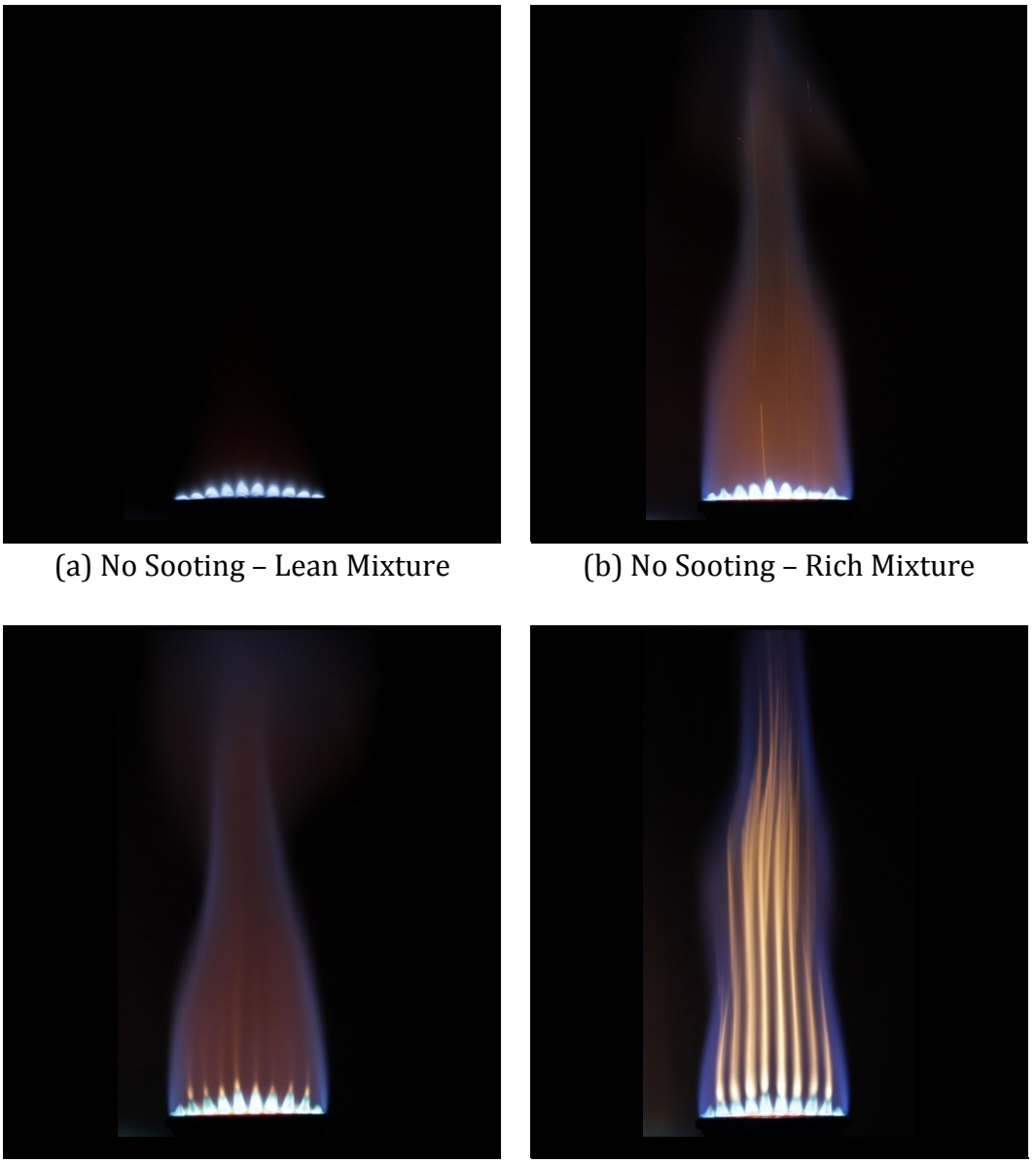

(a) No Sooting – Lean Mixture (b) No Sooting – Rich Mixture

(c) Incipient Sooting (d) Complete Sooting

Figure4.7: The four different stages of Sooting for JP – 5. Φ for the different stages are: a) 0.78 ± 0.00 b) 1.42 ± 0.01 c) 1.45 ± 0.00 and d) 1.59 ± 0.01.

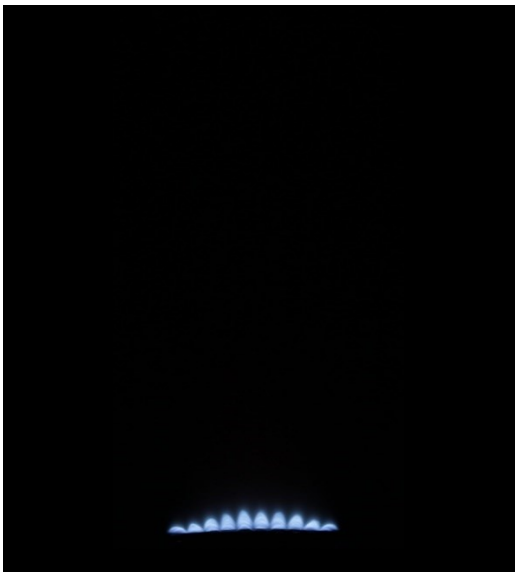

(a) No Sooting – Lean Mixture

(b) No Sooting – Rich Mixture

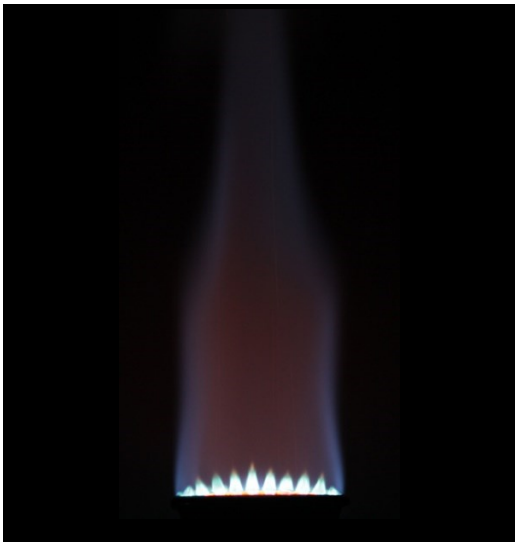

(c) Incipient Sooting

(d) Complete Sooting

Figure4.8: The four different stages of Sooting for Jet – A. Φ for the different stages are: a) 0.73 ± 0.01 b) 1.39 ± 0.00 c) 1.46 ± 0.01 and d) 1.63 ± 0.02.

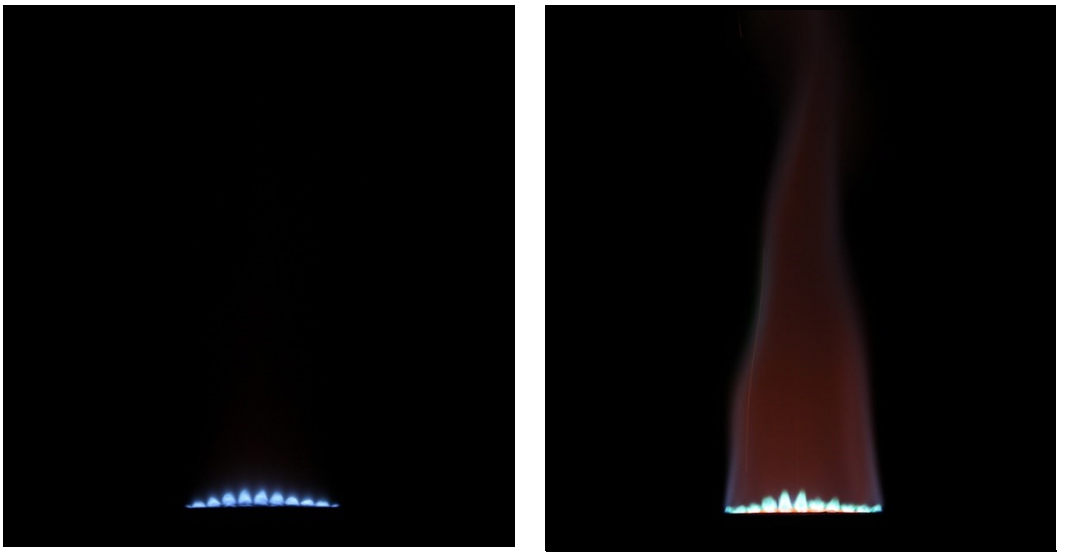

(a) No Sooting – Lean Mixture (b) No Sooting – Rich Mixture

(c) Incipient Sooting (d) Complete Sooting

Figure4.9: The four different stages of Sooting for JP – 8. Φ for the different stages are: a) 0.77 ± 0.01 b) 1.42 ± 0.00 c) 1.51 ± 0.02 and d) 1.70 ± 0.01.

4.1.4. Synthetic and Renewable Jet Fuels

Synthetic jet fuels are obtained by processing carbon rich sources like coal and combustion waste gases to form liquid hydrocarbon fuels such as the Fischer Tropsch fuels. Renewable jet fuels are obtained from renewable sources like plant oil seeds and animal fat. The chemical properties of these jet fuels are as similar as possible to the conventional jet fuels. This feature of the synthetic and renewable jet fuels makes them a viable option for blending with the petroleum jet fuels and eventually being used as a "drop – in" fuel in the aircrafts. Referring to the gas chromatography data for hydrocarbon composition presented in **Table A. 2** , the fuels discussed in this subsection have an aromatic content $< 0.64\%$ which implies the threshold soot in these fuels is controlled my some other hydrocarbon family than aromatics.

The synthetic jet fuel samples tested on the Meker burner setup include Fischer Tropsch – Coal ($C_{10.8}H_{23.6}$) and Fischer Tropsch – Natural Gas ($C_{11.8}H_{25.6}$). Both of these fuels are processed using the Fischer Tropsch method using coal or natural gas as the source. The renewable jet fuels are HRJ – Camelina ($C_{12.0}H_{25.9}$) and HRJ – Tallow ($C_{12.1}H_{26.3}$) which are obtained from Camelina oil seeds and Animal Fat (Tallow) by processing them through hydro – treatment method. Two different batches of the HRJ Tallow were tested and are hence forth mentioned as old batch and new batch for reference. Finally, a new fuel obtained through the fermentation process, GEVO Jet blend ($C_{12.5}H_{27.0}$) is also considered under this sub – section.

On the basis of observations recorded in

Table4.4 and **Table4.5** as well as corresponding images of the flame in **Figure4.10**, **Figure4.11**, **Figure4.12**, **Figure4.13** and **Figure4.14**, the following statements can be made for these renewable jet fuels:

1. The values of $\phi_{\text{incipient}}$ for HRJ Tallow old batch, HRJ Tallow new batch, HRJ Camelina, FT Coal, FT Natural Gas and GEVO Jet Blend are obtained from the rotameter reading as 1.68, 1.56, 1.47, 1.51, 1.51 and 1.53, respectively.

2. The $\phi_{incipient}$ values as noted for the fuels under this section are somewhat in the same range suggesting almost similar chemical composition which is evident from **Table A. 2**.
3. The data presented in **Table A. 2** shows that the renewable jet fuels have a very high composition of iso – paraffinic compounds. Presence of high amount if iso – paraffinic compounds validates the lower sooting propensity of these fuels for iso – paraffins are found to be highly impervious to soot.
4. Among the renewable jet fuels, HRJ Tallow appears to produce soot at the highest ϕ possible. The fact that the chemical composition in terms of major hydrocarbon families is almost similar it is not easy to ascertain the reason.
5. The HRJ tallow old batch and HRJ tallow new batch, show two different values for $\phi_{incipient}$ despite of being obtained from the same source. A possible cause for this difference can be a variation in the physical property of the fuel i.e. density or viscosity. Upon referring to the calibration chart for HRJ tallow old batch and HRJ tallow new batch it is evident that the fuel flow rate ($\dot{Q}_{fuel}$) vs Rotameter reading curve for the HRJ tallow old batch is much steeper than that for HRJ tallow new batch. Thus, the possibility of difference in viscosity of the two fuels is a huge possibility.

	HRJ Tallow (Old Batch)		HRJ Tallow (New Batch)		HRJ Camelina	
Observation	RM Reading Run #1	RM Reading Run #2	RM Reading Run #1	RM Reading Run #2	RM Reading Run #1	RM Reading Run #2
No Sooting – Lean Mixture	55	54	53	55	41	41
No Sooting – Rich Mixture	83	80	88	90	66	65
Incipient Sooting	90	91	91	92	71	70.5
Complete Sooting	94	94	95	96	77	75

Table4.4: Rotameter readings recorded for HRJ Tallow old batch, HRJ Tallow new batch and HRJ Camelina at four different sooting stages.

	GEVO Fuel		FT – Natural Gas		FT - Coal	
Observation	RM Reading Run #1	RM Reading Run #2	RM Reading Run #1	RM Reading Run #2	RM Reading Run #1	RM Reading Run #2
No Sooting – Lean Mixture	56	56	44	50	40	40
No Sooting – Rich Mixture	87	85	78	78	67	66
Incipient Sooting	89	88	83	85	70	70.5
Complete Sooting	96	95	88	89	78	77

Table4.5: Rotameter readings recorded for GEVO fuel, Fischer Tropsch – Natural Gas and Fischer Tropsch – Coal at four different sooting stages.

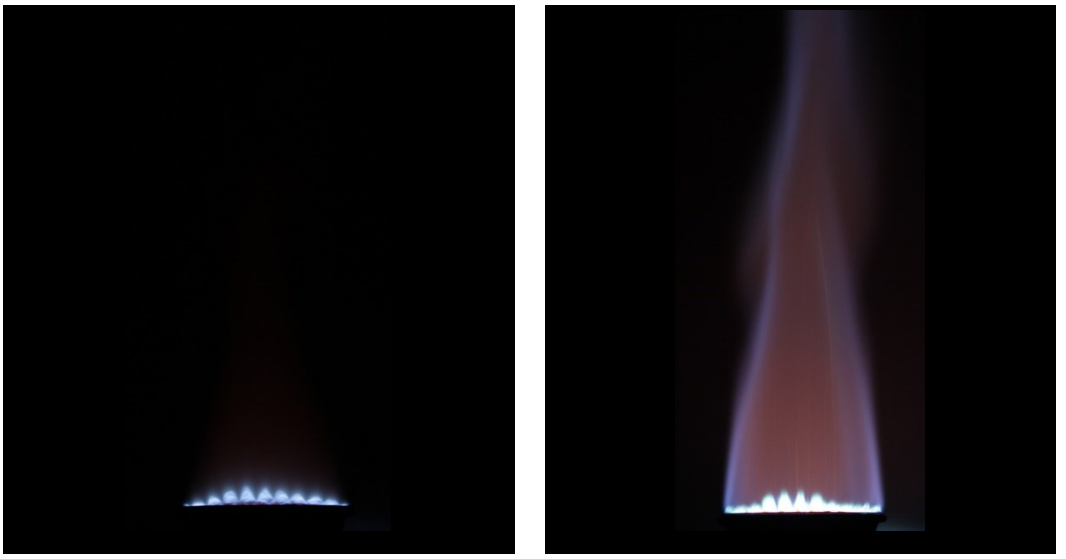

(a) No Sooting – Lean Mixture (b) No Sooting – Rich Mixture

(c) Incipient Sooting (d) Complete Sooting

Figure4.10: The four different stages of Sooting for HRJ Tallow new batch. Φ for the different stages are : a) 0.79 ± 0.02 b) 1.51 ± 0.02 c) 1.56 ± 0.01 and d) 1.65 ± 0.01.

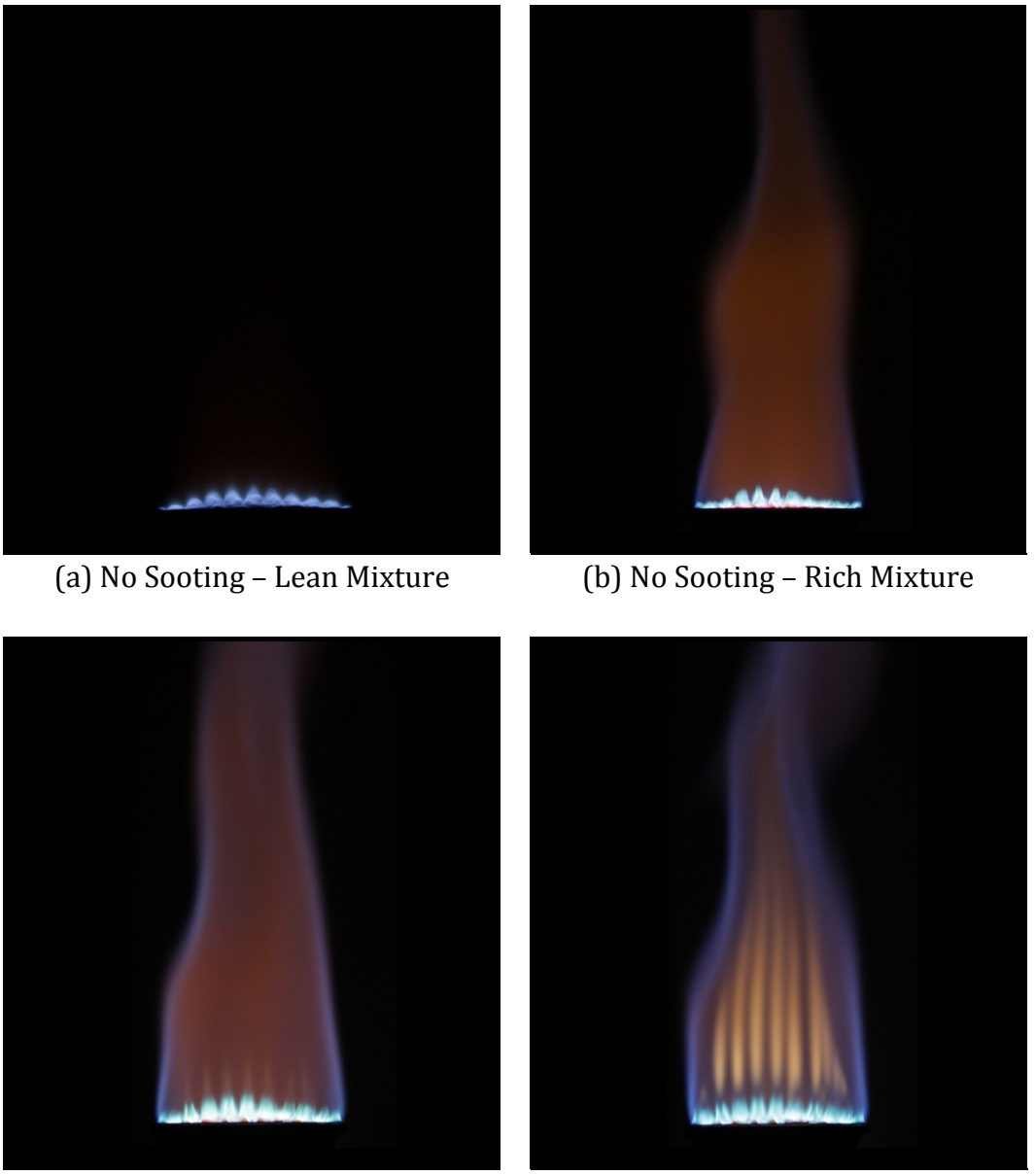

(a) No Sooting – Lean Mixture (b) No Sooting – Rich Mixture

(c) Incipient Sooting (d) Complete Sooting

Figure4.11: The four different stages of Sooting for HRJ Camelina. Φ for the different stages are : a) 0.75 ± 0.00 b) 1.37 ± 0.01 c) 1.47 ± 0.02 and d) 1.63 ± 0.02.

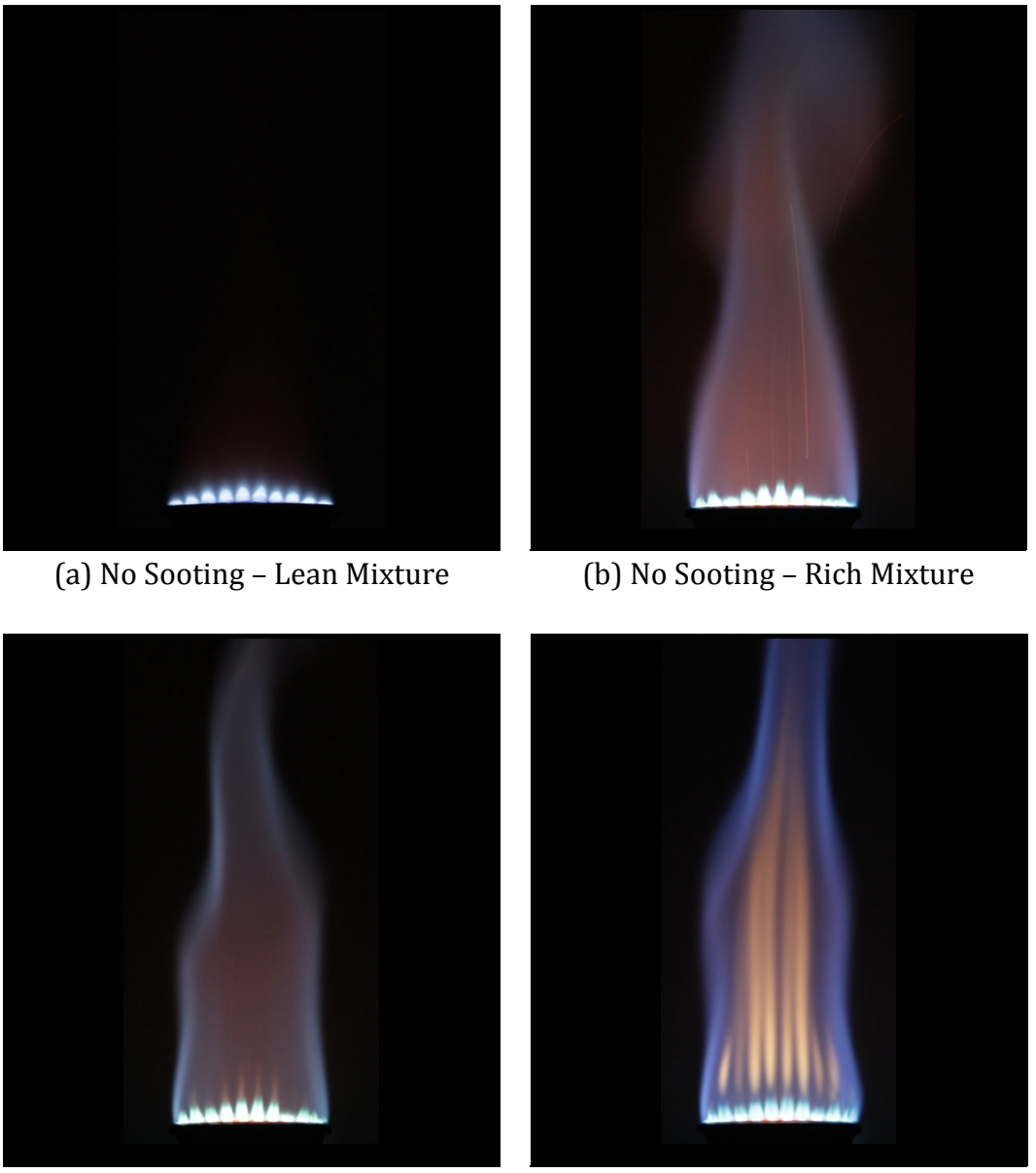

(a) No Sooting – Lean Mixture (b) No Sooting – Rich Mixture

(c) Incipient Sooting (d) Complete Sooting

Figure4.12: The four different stages of Sooting for Fischer Tropsch – Natural Gas fuel. Φ for the different stages are : a) 0.75 ± 0.07 b) 1.38 ± 0.00 c) 1.51 ± 0.02 and d) 1.60 ± 0.01.

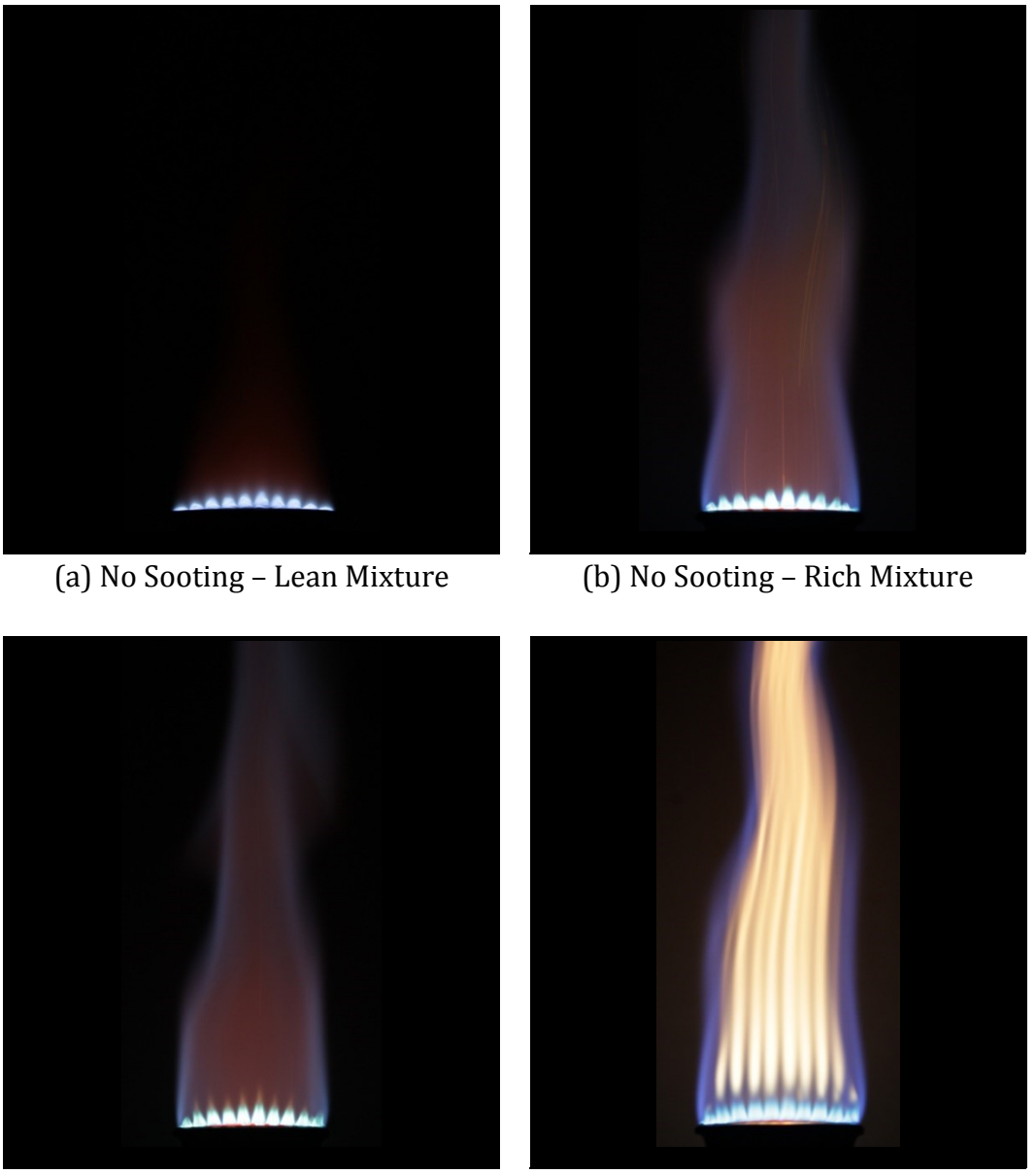

(a) No Sooting – Lean Mixture (b) No Sooting – Rich Mixture

(c) Incipient Sooting (d) Complete Sooting

Figure4.13: The four different stages of Sooting for Fischer Tropsch – Coal fuel. Φ for the different stages are : a) 0.81 ± 0.00 b) 1.42 ± 0.01 c) 1.51 ± 0.00 and d) 1.67 ± 0.02.

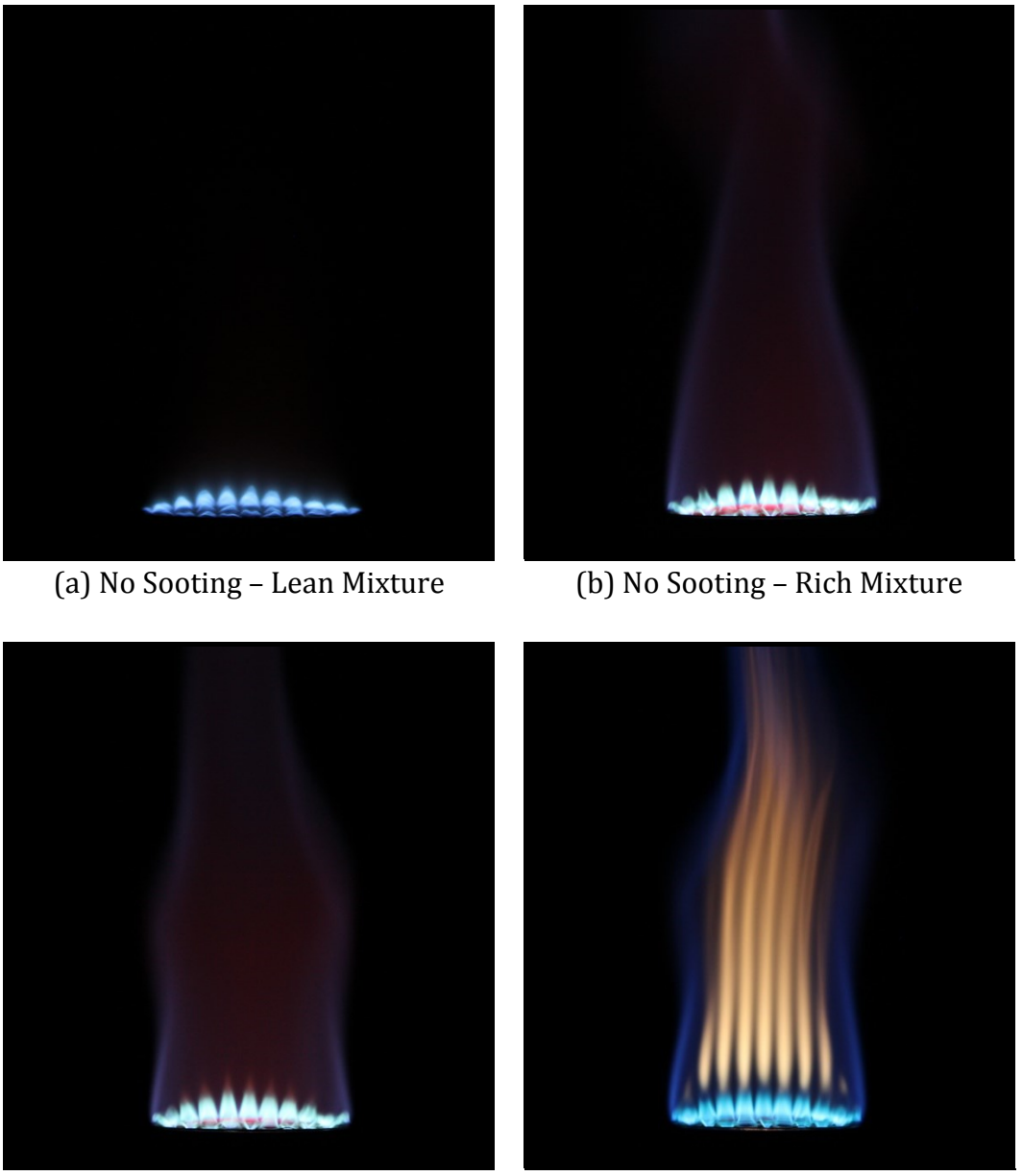

(a) No Sooting – Lean Mixture (b) No Sooting – Rich Mixture

(c) Incipient Sooting (d) Complete Sooting

Figure4.14: The four different stages of Sooting for GEVO Renewable Jet fuel. Φ for the different stages are : a) 0.88 ± 0.00 b) 1.48 ± 0.02 c) 1.53 ± 0.01 and d) 1.67 ± 0.01.

4.1.5. In – house Blended Fuels

The study of different fuel samples till now has provided crucial information about the sooting behavior and also a relation between the sooting propensity and different hydrocarbon families which are present in these fuels. To further understand this relation between sooting propensity and hydrocarbon families, in – house blends of a few primary fuels is also studied. The fuel blends are percentage vol./vol. in composition. The mole fractions and corresponding density values for these blends are computed with the relations provided in **Equations 4.2 – 4.6**.

$$\rho_{blend} = V_A^{\%} * \rho_A + V_B^{\%} * \rho_B \quad 4.2$$

$$n_A = V_A * \frac{\rho_A}{MW_A} \quad 4.3$$

$$n_B = V_B * \frac{\rho_B}{MW_B} \quad 4.4$$

$$x_A = \frac{n_A}{n_A + n_B} \quad 4.5$$

$$x_B = \frac{n_B}{n_A + n_B} \quad 4.6$$

Using the values of mole fraction x_A and x_B calculated for the two fuels used in a blend the corresponding fuel air ratio at stoichiometric ($\phi_{\text{stoichiometric}}$) can be obtained by writing a stoichiometric combustion equation.

The fuels used for making these blends include HRJ tallow new batch, HRJ camelina, mesitylene and cyclohexane. Out of these fuels, HRJ tallow new batch and HRJ camelina have a higher sooting threshold whereas mesitylene being a pure aromatic compound has a lower sooting threshold. The four in – house fuel blends obtained from these primary fuels are 90:10 :: HRJ tallow : mesitylene (90% by volume of HRJ tallow + 10% by volume of mesitylene), 80:20 :: HRJ tallow : mesitylene (80% by volume of HRJ tallow + 20% by volume of mesitylene), 80:20 :: HRJ camelina : mesitylene (80% by volume of HRJ camelina + 20% by volume of mesitylene) and 80:20 :: HRJ camelina : cyclohexane (90% by volume of HRJ camelina + 20% by volume of cyclohexane). **Figure 2.6** provides a bar chart representation of the composition of these blended fuels.

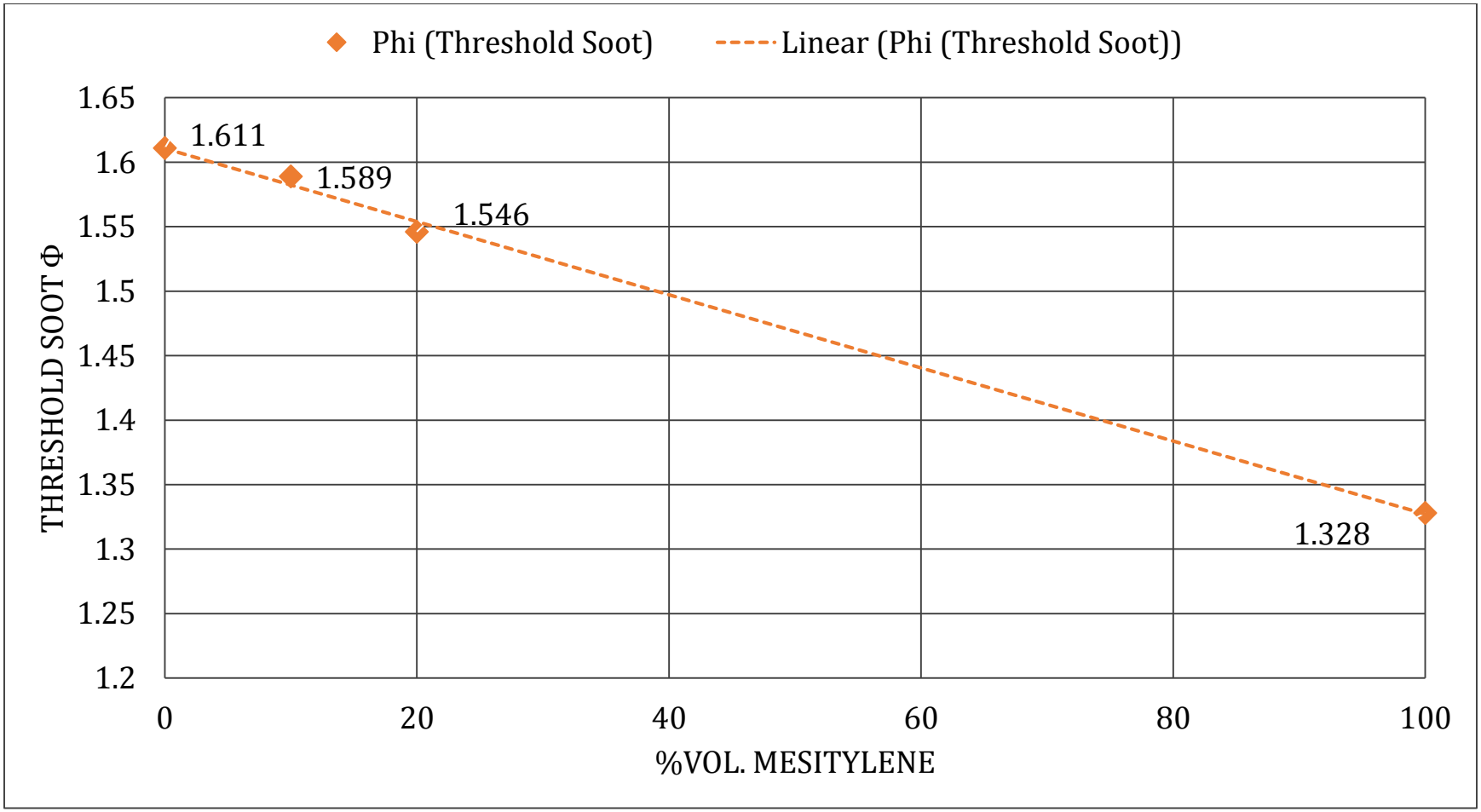

Figure4.15: Variation of $\phi_{incipient}$ with variation in percentage by volume of Mesitylene in HRJ Tallow and Mesitylene blend.

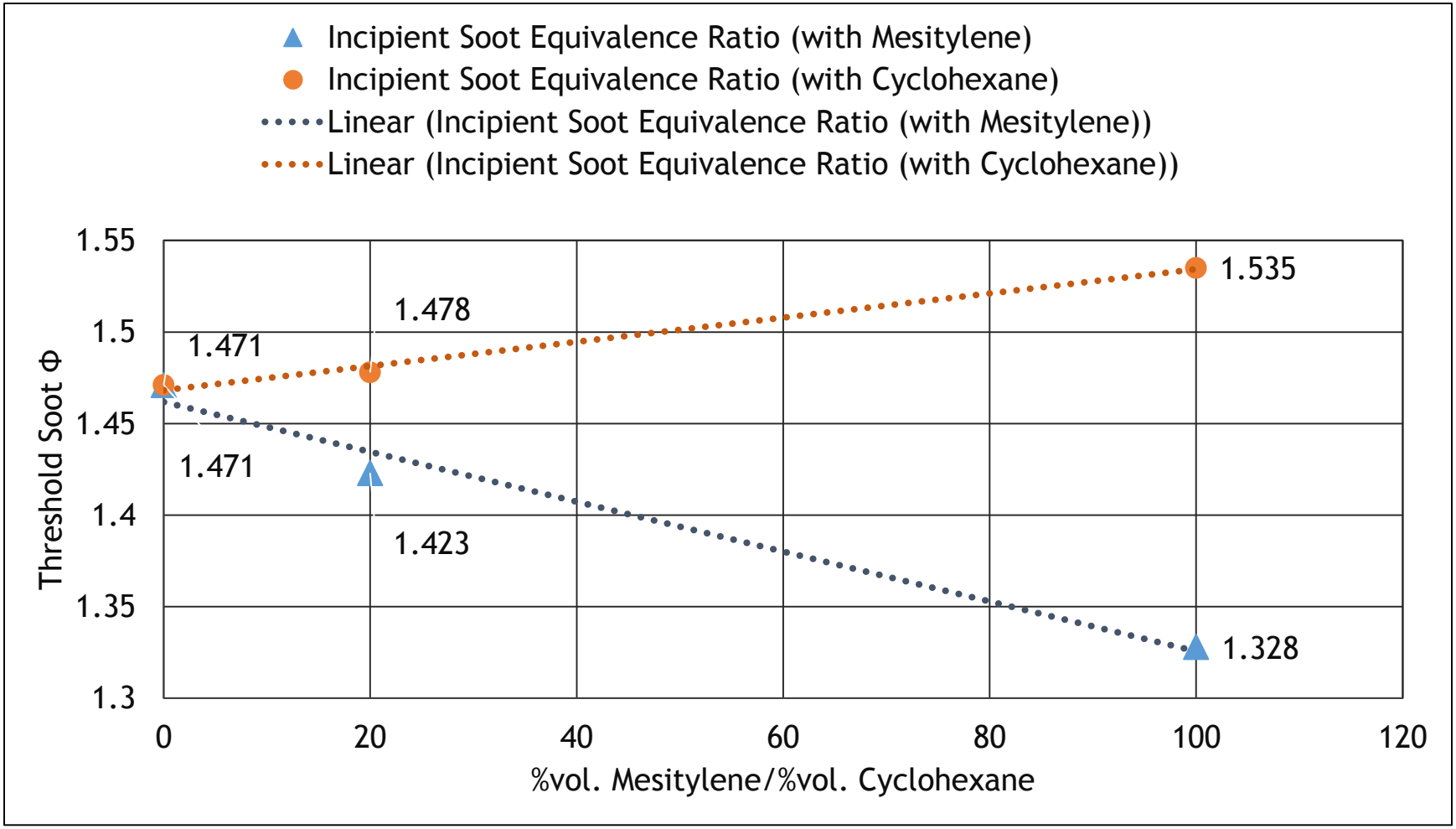

Figure4.16: Variation of $\phi_{incipient}$ with variation in percentage by volume of Mesitylene and Cyclohexane in blend with HRJ Camelina.

On the basis of observations recorded in **Table4.6** as well as corresponding images of the flame in **Figure4.17**, **Figure4.18**, **Figure4.19** and **Figure4.20**, the following statements can be made for these in – house fuel blends:

1. The values of $\phi_{incipient}$ for 90:10 :: HRJ Tallow : Mesitylene, 80:20 :: HRJ Tallow : Mesitylene, HRJ Camelina, 80:20 :: HRJ Camelina : Mesitylene and 80:20 :: HRJ Camelina : Cyclohexane are obtained from the rotameter reading as 1.51, 1.48, 1.42 and 1.47, respectively.
2. For the 90:10 HRJ Tallow + Mesitylene blend and 80:20 HRJ Tallow + Mesitylene blend the propensity to soot is found to increase with the increase in aromatic content. Taking into account the sooting propensity of pure HRJ Tallow and Mesitylene, separately, it appears that as the Mesitylene proportion increases the $\phi_{incipient}$ reduces linearly.
3. 80:20 HRJ Camelina + Mesitylene blend shows a similar change in the propensity to soot when put into perspective with the $\phi_{incipient}$ values corresponding to pure HRJ Camelina and Mesitylene as mentioned in the previous point.
4. 80:20 HRJ Camelina + Cyclohexane blend on the other hand appears to have decreased the sooting propensity of HRJ Camelina. This result is expected as Cyclohexane has a lower sooting propensity than HRJ Camelina.

The comparison of these blends with the primary fuels in terms of $\phi_{incipient}$ is provided as an XY plot in **Figure4.15** and **Figure4.16** for reference.

	90% HRJ Tallow + 10% Mesitylene		80% HRJ Tallow + 20% Mesitylene		80% HRJ Camelina + 20% Mesitylene		80% HRJ Camelina + 20% Cyclo – Hexane	
Observation	RM Reading Run #1	RM Reading Run #2	RM Reading Run #1	RM Reading Run #2	RM Reading Run #1	RM Reading Run #2	RM Reading Run #1	RM Reading Run #2
No Sooting – Lean Mixture	48	47	46	44	39	40	34.5	35
No Sooting – Rich Mixture	79	79	73	69	58.5	60	62	64
Incipient Sooting	83.5	83	75	73	63	62	65.5	66
Complete Sooting	91	89	80	77	68	68	71.5	71

Table4.6: Rotameter readings recorded for 90% (vol.) HRJ Tallow + 10% (vol.) Mesitylene, 80% (vol.) HRJ Tallow + 20% (vol.) Mesitylene, 80% (vol.) HRJ Camelina + 20% (vol.) Mesitylene and 80% (vol.) HRJ Camelina + 20% (vol.) Cyclo – Hexane at four different sooting stages.

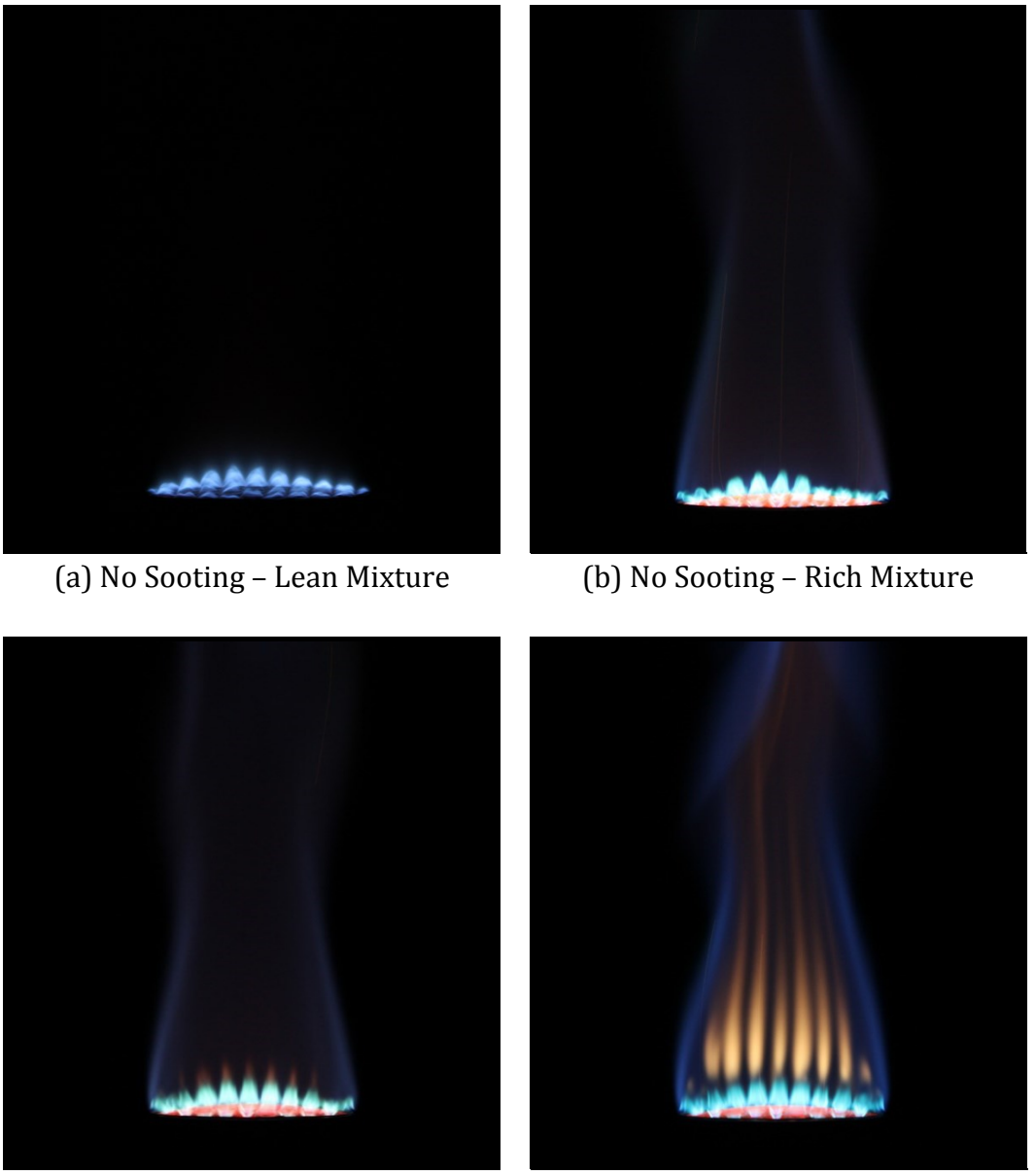

(a) No Sooting – Lean Mixture (b) No Sooting – Rich Mixture

(c) Incipient Sooting (d) Complete Sooting

Figure4.17: The four different stages of Sooting for 90% (vol.) HRJ Tallow + 10% (vol.) Mesitylene fuel blend. Φ for the different stages are : a) 0.79 ± 0.01 b) 1.43 ± 0.00 c) 1.51 ± 0.01 and d) 1.65 ± 0.02.

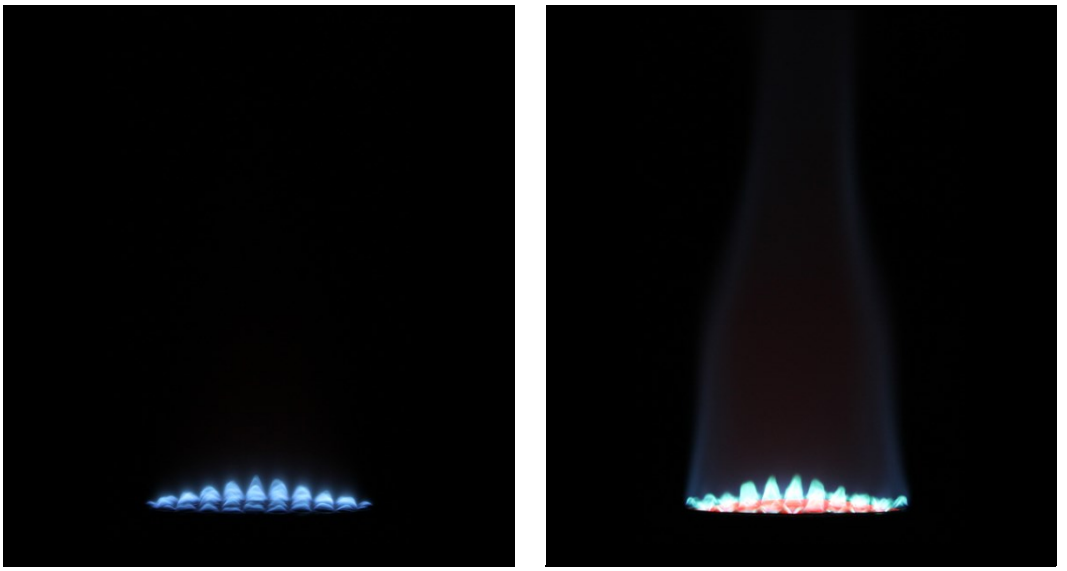

(a) No Sooting – Lean Mixture (b) No Sooting – Rich Mixture

(c) Incipient Sooting (d) Complete Sooting

Figure4.18: The four different stages of Sooting for 80% (vol.) HRJ Tallow + 20% (vol.) Mesitylene fuel blend. Φ for the different stages are : a) 0.74 ± 0.03 b) 1.41 ± 0.05 c) 1.48 ± 0.03 and d) 1.60 ± 0.04.

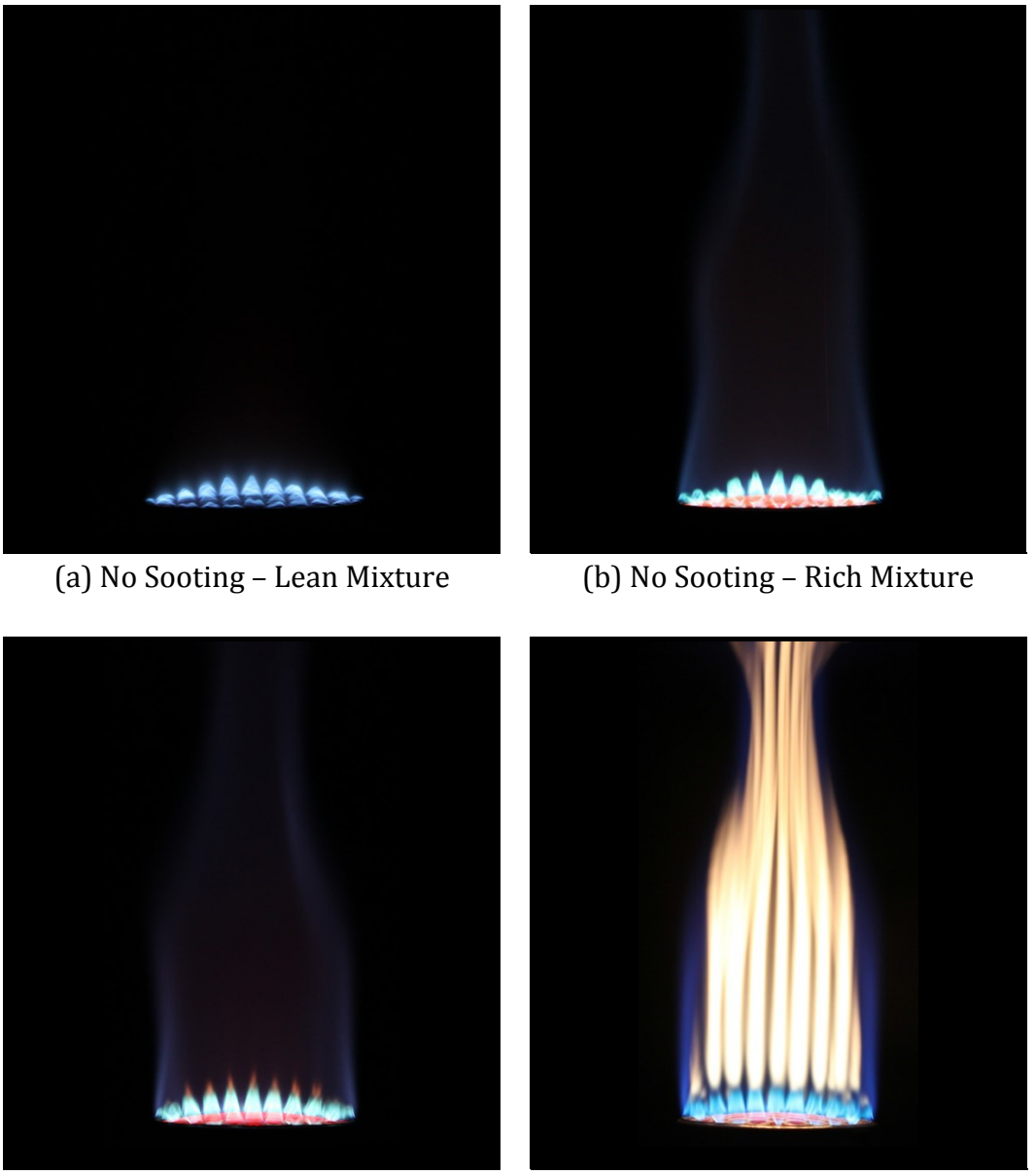

(a) No Sooting – Lean Mixture (b) No Sooting – Rich Mixture

(c) Incipient Sooting (d) Complete Sooting

Figure4.19: The four different stages of Sooting for 80% (vol.) HRJ Camelina + 20% (vol.) Mesitylene fuel blend. Φ for the different stages are : a) 0.87 ± 0.01 b) 1.35 ± 0.01 c) 1.42 ± 0.02 and d) 1.56 ± 0.00.

(a) No Sooting – Lean Mixture (b) No Sooting – Rich Mixture

(c) Incipient Sooting (d) Complete Sooting

Figure4.20: The four different stages of Sooting for 80% (vol.) HRJ Camelina + 20% (vol.) Cyclo – Hexane fuel. Φ for the different stages are : a) 0.71 ± 0.01 b) 1.41 ± 0.02 c) 1.47 ± 0.01 and d) 1.61 ± 0.01.

4.2. Effect on Flame Structure and Luminescence

The effects of fuel composition (carbon and hydrogen only) on the propensity to soot, calculated as $\phi_{incipient}$ were recorded and are presented along with the observations in previous section. The observations of the flame for these different test fuels shows certain similar behavior in terms of the flame structure and chemiluminescence and can be linked to the hydrocarbon composition of the test fuels.

Upon observing the digital photographs displaying the stage of incipient soot formation for the test fuels, three different types of flame structures were observed. The first type of flame structure is observed to have a well – defined elongated parabolic structure with a tiny button like shape at the tip of the parabola. This shape is found to be radiating a bright yellow luminescence which is due to soot. Pure aromatic fuels such as Petroleum Aromatic Blend, mesitylene and toluene are found to have a flame structure similar to the first type. The second type of flame structure observed also represents an elongated parabola with a button like shape radiating yellow at the flame tip. On closer observation of the flame tips it is found that unlike the first type of flame the yellow soot button and the primary flame front have a very small gap or no luminescence zone. Jet fuels like JP – 5, Jet – A and JP – 8 are found to have their flame structure of the second type. The third type of flame structure is the one with a distorted parabolic tip which appears as if the flame tip has opened up along with a streak of yellow radiation near the flame tip due to soot. A considerable gap between the primary flame and the streak of soot can be observed. Fuels like iso – octane, cyclohexane, Fischer Tropsch – coal, Fischer Tropsch – natural gas, HRJ – camelina, HRJ – tallow (both old and new batch) and GEVO Jet fuel blend. **Figure4.21** depicts these three types of flame structures for reference.

Upon close observation of the third type of flame, the region of no luminosity between the primary flame and streak of soot is found to vary in vertical length for different fuels classified under this type. **Figure4.22** shows a comparison between the fuels enlisted under the third type of flame. On the basis of this figure it can be stated that HRJ camelina, HRJ tallow and FT – natural gas have a higher gap length in comparison to iso – octane and cyclohexane.

(a) (b) (c)

Figure4.21: Three different types of flame structures at incipient soot stage for (a) PET Aromatic blend, (b) JP – 8 and (c) HRJ Tallow new batch.

Figure4.22: Complete sooting stage of flames of the third type for (a) HRJ Camelina, (b) HRJ Tallow new batch, (c) FT – Coal , (d) FT – Natural Gas, (e) GEVO Jet fuel blend, (f) Iso – Octane and (g) Cyclohexane.

Apart from the flame structure, the luminescence of these flames are also worth studying to deduce a co – relation with the chemical composition of the fuels as the chemiluminescence in combustion flames is due to $C\dot{H}$ and $\dot{C}_2$ radicals produced from dissociation of hydrocarbon fuels. On observing the different stages of soot formation for all the fuels the following statements can be made:

1. The primary flame gives a dark blue chemiluminescence at $\phi < 1$ which becomes a more blue – green or aqua colored chemiluminescence for $\phi > 1$. This variation is consistent with all the fuels.
2. The brightness of the primary flame is found to be much higher for fuels with aromatics in it than those without aromatics.
3. The soot chemiluminescence is also found to be brighter for fuels with aromatic content in comparison to those without it if considered at a similar value of ϕ. **Figure4.23** shows this comparison between three different fuels with varying aromatic percentages by weight. The flames are at $\phi = 1.7$.

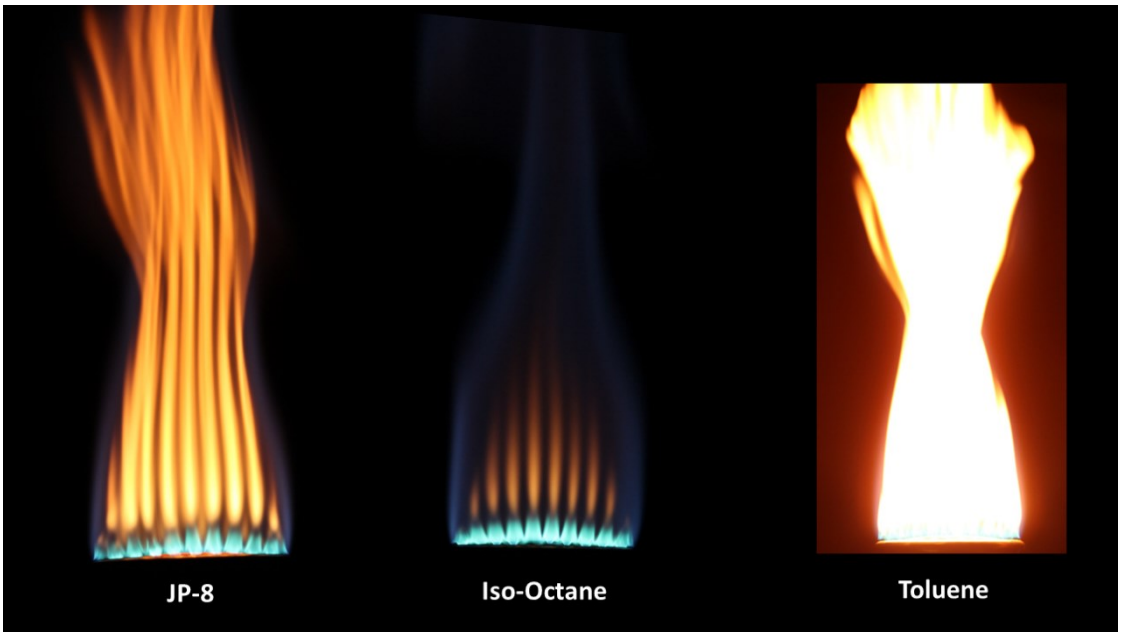

Figure4.23: Comparison of JP – 8, Iso – Octane and Toluene flames at $\phi = 1.7$.

4.3. Effect on Heat Loss at the Burner Surface

In the observations made during the study it is noticeable that the surface of the burner appears to give off radiation of a bright orange – red, especially in the range of $1 < \phi < 1.3$. The observed radiation is apparently due to the rise in temperature at the surface of the burner due to heat transfer from the flame. The loss of heat from the flame to the burner could impact the results obtained for $\phi_{incipient}$ making it crucial to obtain the corresponding heat loss value. An optical pyrometer is used to obtain the radiation temperature ($T_{radiation}$) by focusing the pyrometer lens on the burner surface. Two fuels: iso – octane and toluene are tested for the heat loss. The optical pyrometer readings are considered to be blackbody temperature (T_b) by assuming the surface emissivity (ϵ) as 1. This assumption allows the usage of Stefan – Boltzmann relation to obtain radiated energy (P_{loss}) as represented by **Equation 4.7** below.

$$P_{loss} = \sigma . \epsilon . A . T_b^4 \tag{4.7}$$

Here, σ is the Boltzmann constant and A is the metallic surface area of the burner top where the flame is anchored. Using the mass flow rate ($\dot{m}_{fuel}$) information for these fuels at different values of ϕ, the amount of energy that enters the system can also be computed using the Lower Heating Value (LHV) of these fuels as represented by **Equation 4.8**.

$$P_{in} = \dot{m}_{fuel} * LHV \tag{4.8}$$

Finally, percentage of heat lost is computed as a ratio of P_{loss}: P_{in}. The results of this study are presented as a plot (see **Figure4.24**) with percentage of heat loss along the Y – axis and ϕ along the X – axis. The results convey that the percentage of heat loss is maximum near $\phi = 1.1$ and drops down on either side. It is also ascertained that the percentage of heat loss is not very high which could potentially impact the behavior of the flame. The images of the burner surface at $\phi = 1.2$ and $\phi = 1.3$ for Iso – Octane and Toluene can be referred to in **Figure4.25**.

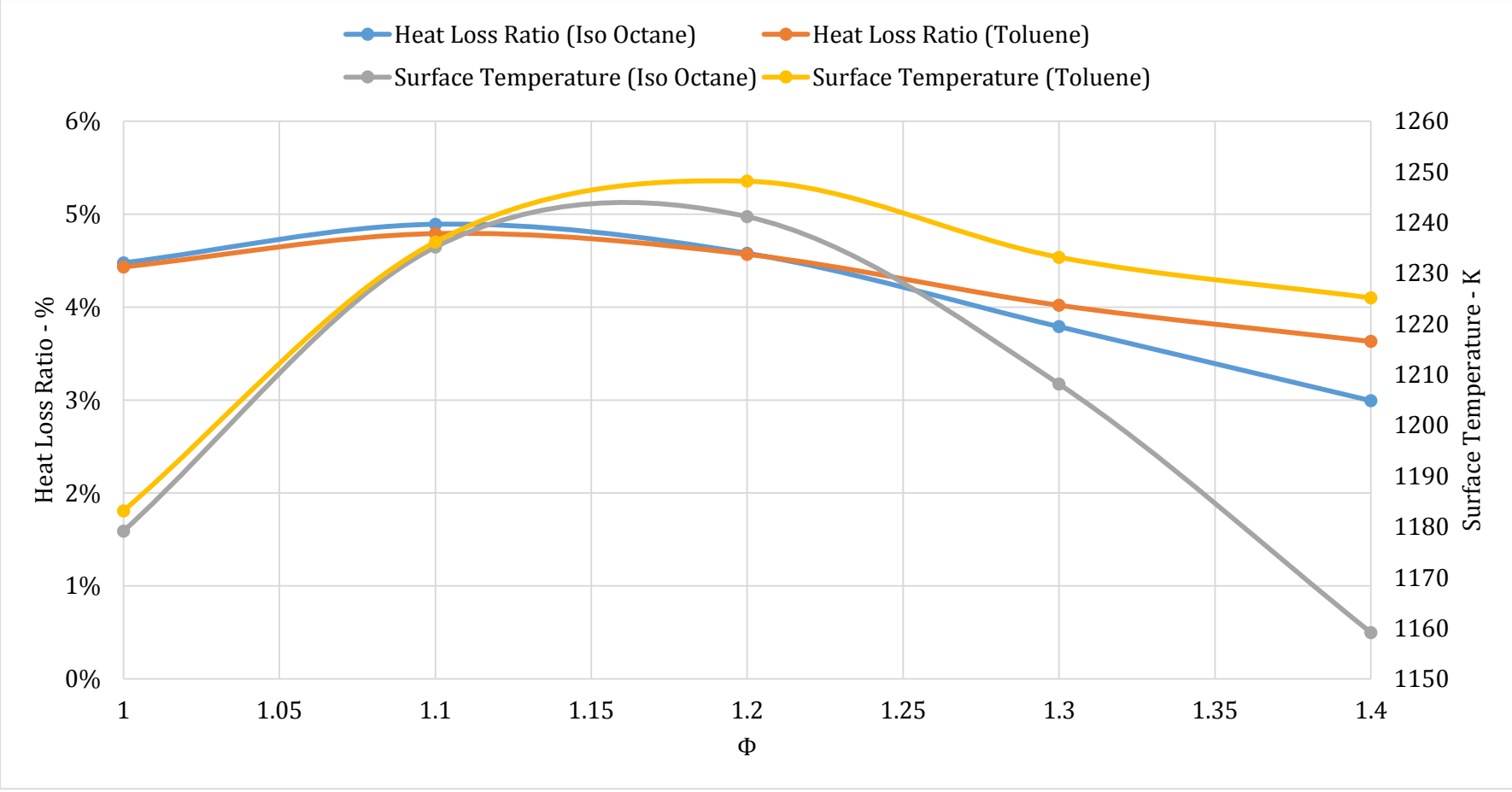

Figure4.24: Percentage of heat loss and burner surface temperature as the value of ϕ varies.

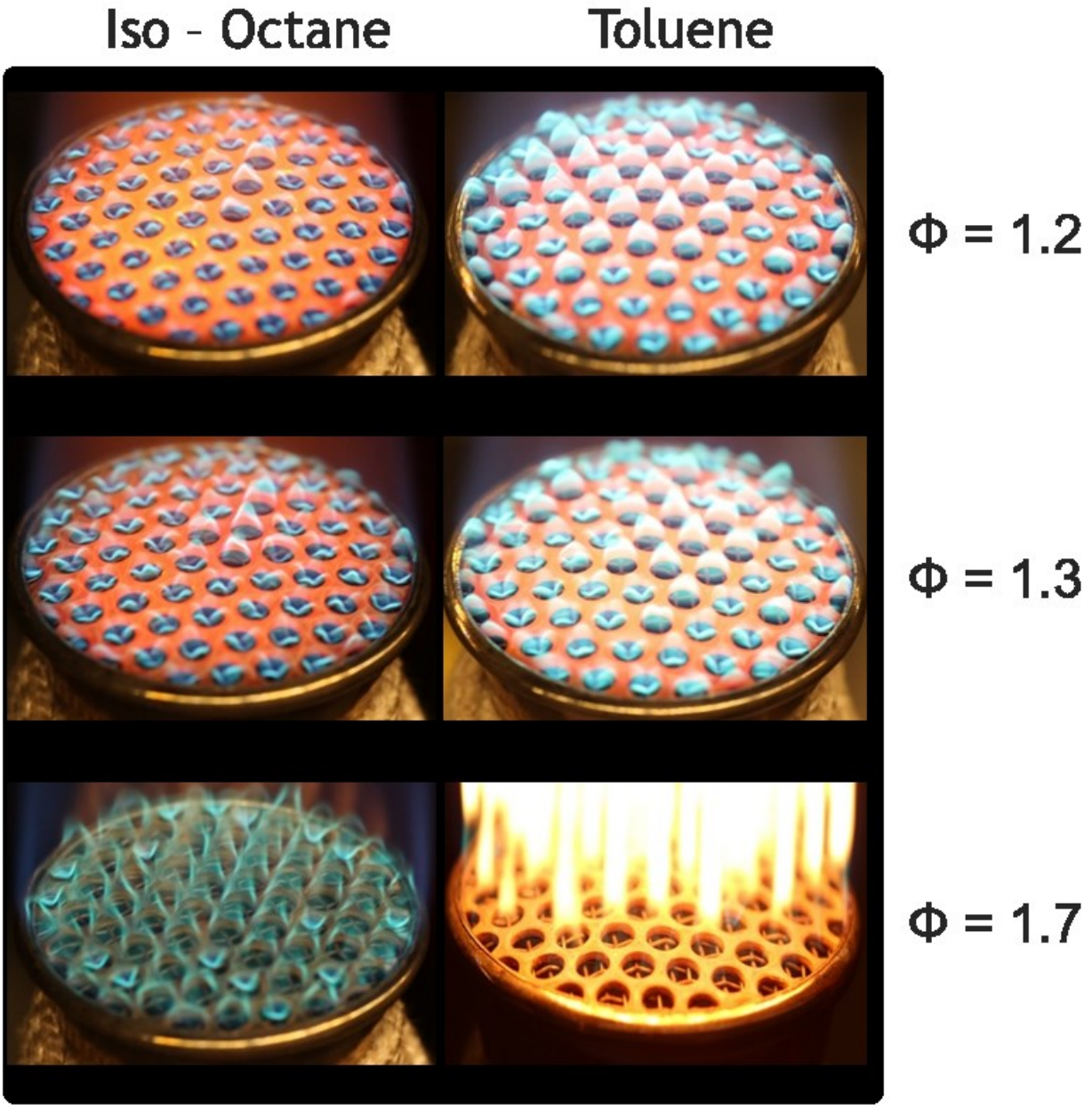

Figure4.25: Radiation from the Meker burner surface for (a) Iso – Octane and (b) Toluene at $\phi = 1.2$ and $\phi = 1.3$, respectively.

4.4. Summary

On the basis of the observations and results computed for the Meker burner experiments, following points summarize the findings:

1. The chemical composition of the fuel shows a direct impact on the sooting threshold of the fuel. Presence of aromatic compounds i.e. mono – aromatics and di – aromatics reduces sooting threshold. Paraffinic compounds such as iso – alkanes and cyclo – alkanes increase sooting threshold. Variation of percentage aromatic in a fuel directly correlates with the variation in threshold sooting.
2. Radiation from the soot at incipient sooting and complete sooting stages shows variation among fuels. Fuels with higher aromatic content definitely show a much brighter radiation from soot in comparison to pure paraffinic fuels like iso – octane and cyclo – hexane. Flame brightness is also observed to vary with the fuel similar to the variation in soot brightness.
3. The soot streaks are found to vary in their location above the flame tip as a function of the fuel composition. Fuels with higher aromatic content show the soot streak and the flame tip in an overlap whereas fuels with no aromatic content like iso – octane and cyclo – hexane show an observable region of no luminosity or a gap between the flame tip and soot streak.
4. The radiation from the surface of the burner is due to the high temperature at the surface caused due to heat loss from the flame. The computation of this heat loss in reference with the total heat capacity of the fuel is found to be ~ 5%. Hence, the impact of this heat loss on the flame properties is assumed to be negligible.

***

5. DISCUSSION

5.1. Effect of fuel chemistry on sooting threshold

The observations and results presented in Chapter 4 pertaining to incipient soot, flame structure and luminescence as well as heat loss at the surface of the Meker burner require a thorough analysis to deduce a reasonable conclusion to this research study and suggest possible improvements for future work.

The results for $\phi_{incipient}$ obtained for the different test fuel samples suggests the following trend for constituent hydrocarbon families in the decreasing order of sooting propensity:

$$\text{Aromatics} > \text{n} - \text{alkanes} \cong \text{iso} - \text{alkanes} > \text{cyclo} - \text{alkanes}$$

Street & Thomas, in their work on premixed flames using a Bunsen burner setup, test a variety of pure hydrocarbon fuels for their sooting propensity which forms a benchmark for validation of the results obtained from this study.[20] **Table 5.1** provides a comparison of $\phi_{incipient}$ values for the common fuels. Based on this comparison of values, the results from the study seem to be close enough to the reference values though a noticeable difference in the Iso – Octane value is undeniable.

Fuel	$\phi_{incipient}$ [20]	$\phi_{incipient}$ (Meker)
Iso - Octane	1.44	1.51
Cyclohexane	1.51	1.54
Toluene	1.33	1.34

Table 5.1: Comparison of recorded $\phi_{incipient}$ values with literature values from Street et al. [20]

Similar to the work of Street et al. another pair of researchers conducted study on the premixed flames and deduced a correlation between the sooting propensity and the fuel composition. [7] also study the premixed fuels using a Bunsen burner setup. The experiments conducted by them involve cases with and without air and are presented

as a function of the adiabatic flame temperature. **Table5.2** shows a comparison of the $\phi_{incipient}$ values recorded in the Meker burner study with those reported by Takahashi et al.[7] for the common fuels.

Fuel	$\phi_{incipient}$ [7]	$\phi_{incipient}$ (Meker)
Cyclohexane	1.43	1.54
Toluene	1.33	1.34

Table5.2: Comparison of recorded $\phi_{incipient}$ values with literature values from Takahashi et al.

Based on this comparison, the validity of the results obtained is somewhat ascertained although a definitive dissimilarity among the values for cyclohexane can be observed. The experimental setup mentioned by [7], [20] is very similar. Both the setups use a Pyrex shroud around the primary flame to prevent entrainment effect and also use N_2 as a diluent in the fuel – air mixture. This along with other factors pertaining to the conditions of experiment can be accounted for the marginal dissimilarities in the $\phi_{incipient}$ values.

The effect of the fuel chemistry on threshold sooting for the fuel samples tested is shown by **Figure 5.1**. Here, the fuel samples are distributed into four sections with varying aromatic content along the abscissa and the corresponding fuel – air equivalence ratios at incipient sooting along the ordinate. The addition on aromatics in the fuel shows reduction in the threshold sooting with the variation being almost linear. Internal variation in $\phi_{incipient}$ for the <0.1 %wt. aromatic and >20 %wt. aromatic is considerable. For the >20 %wt. aromatic section this variation confirms the impact of heavy aromatics (i.e. naphthalene, cumene) on reducing threshold sooting by a larger margin than that by lighter aromatics (i.e. benzene, toluene). In the <0.1 %wt. aromatic section the HRJ tallow and Gevo jet blend fuels show a considerable difference in the $\phi_{incipient}$ despite having nearly the

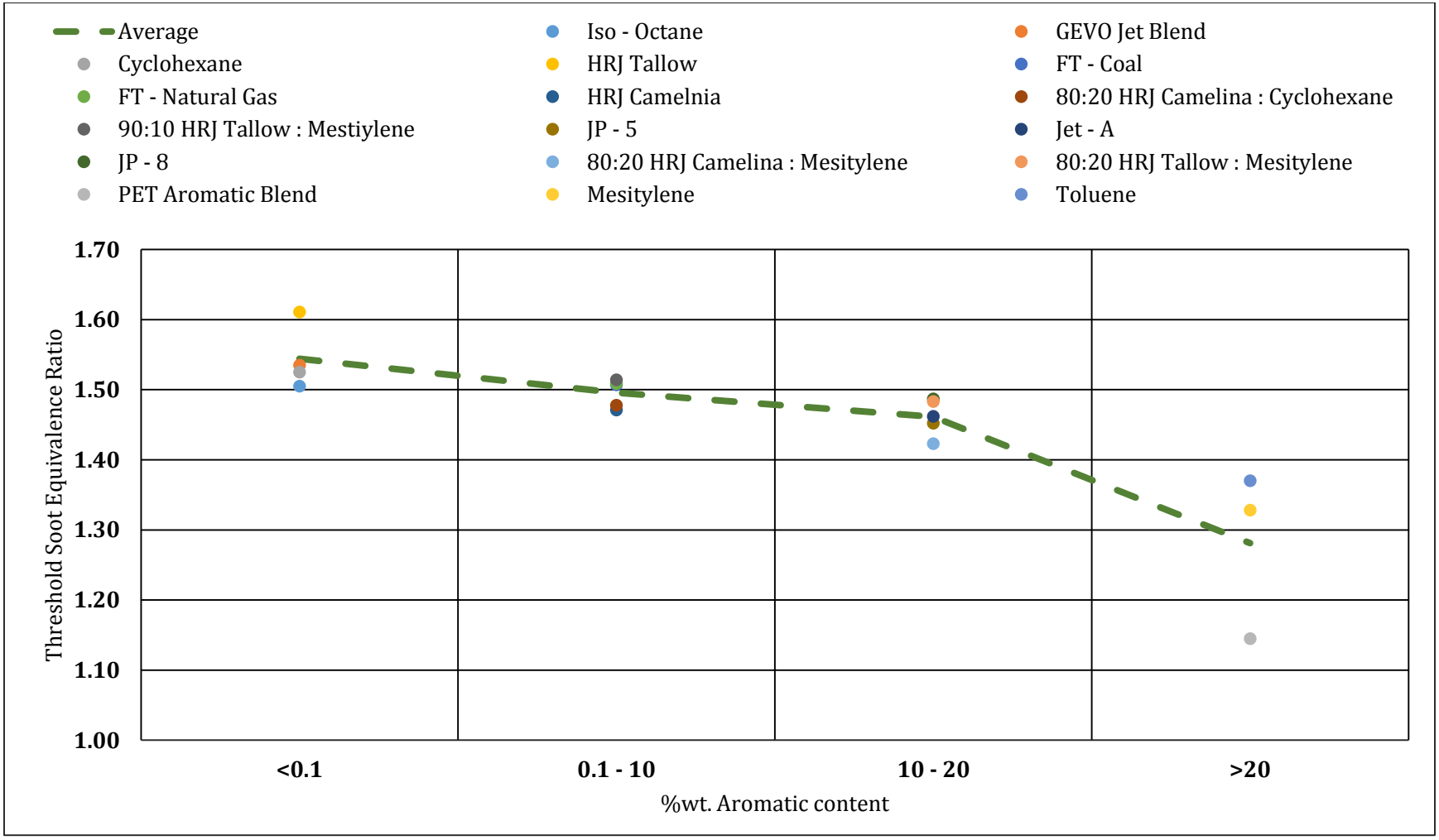

Figure 5.1: Variation in the threshold sooting with %wt. aromatic content of fuel.

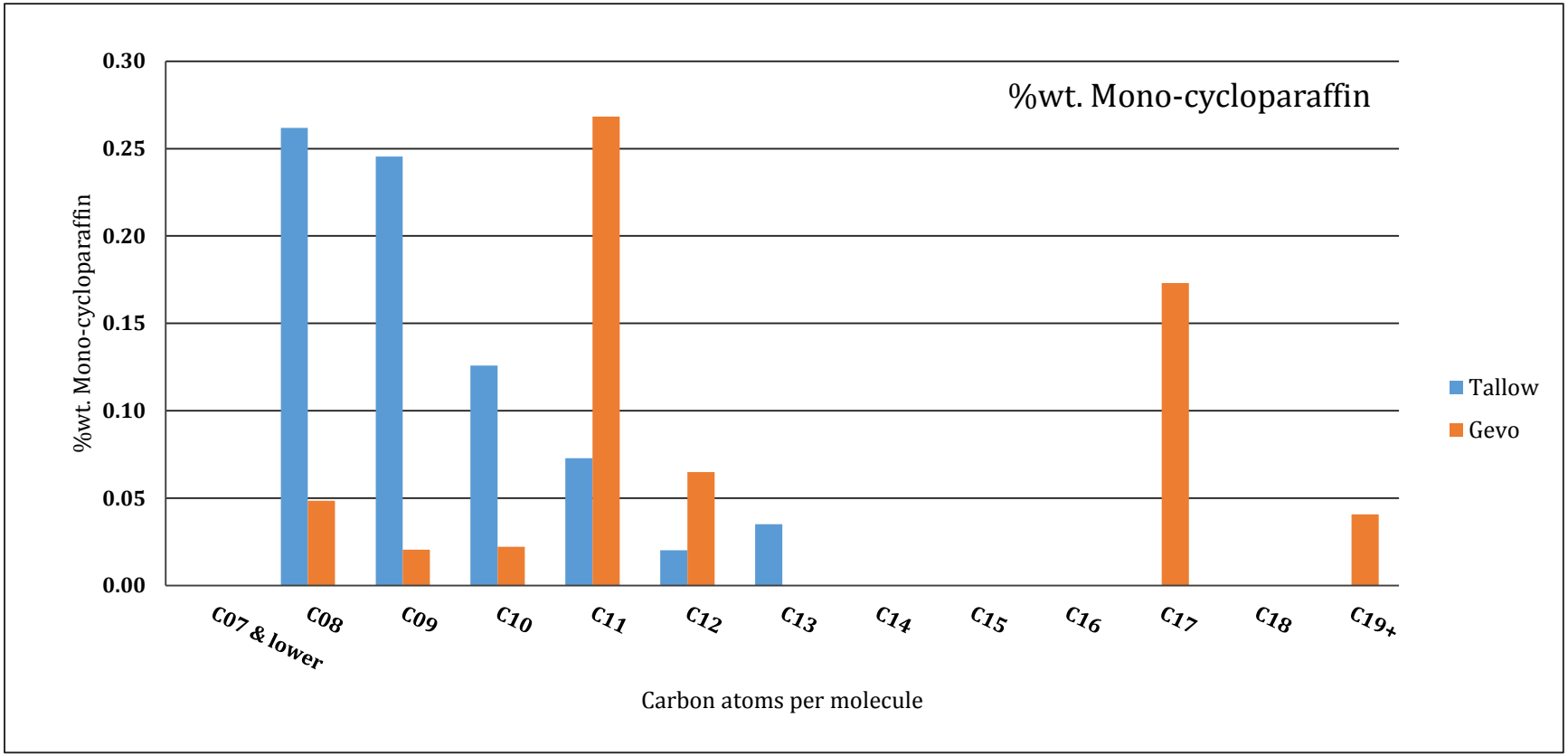

Figure 5.2: Percent by weight monocyclic paraffins in HRJ tallow and Gevo jet blend from AFRL gas chromatography data.

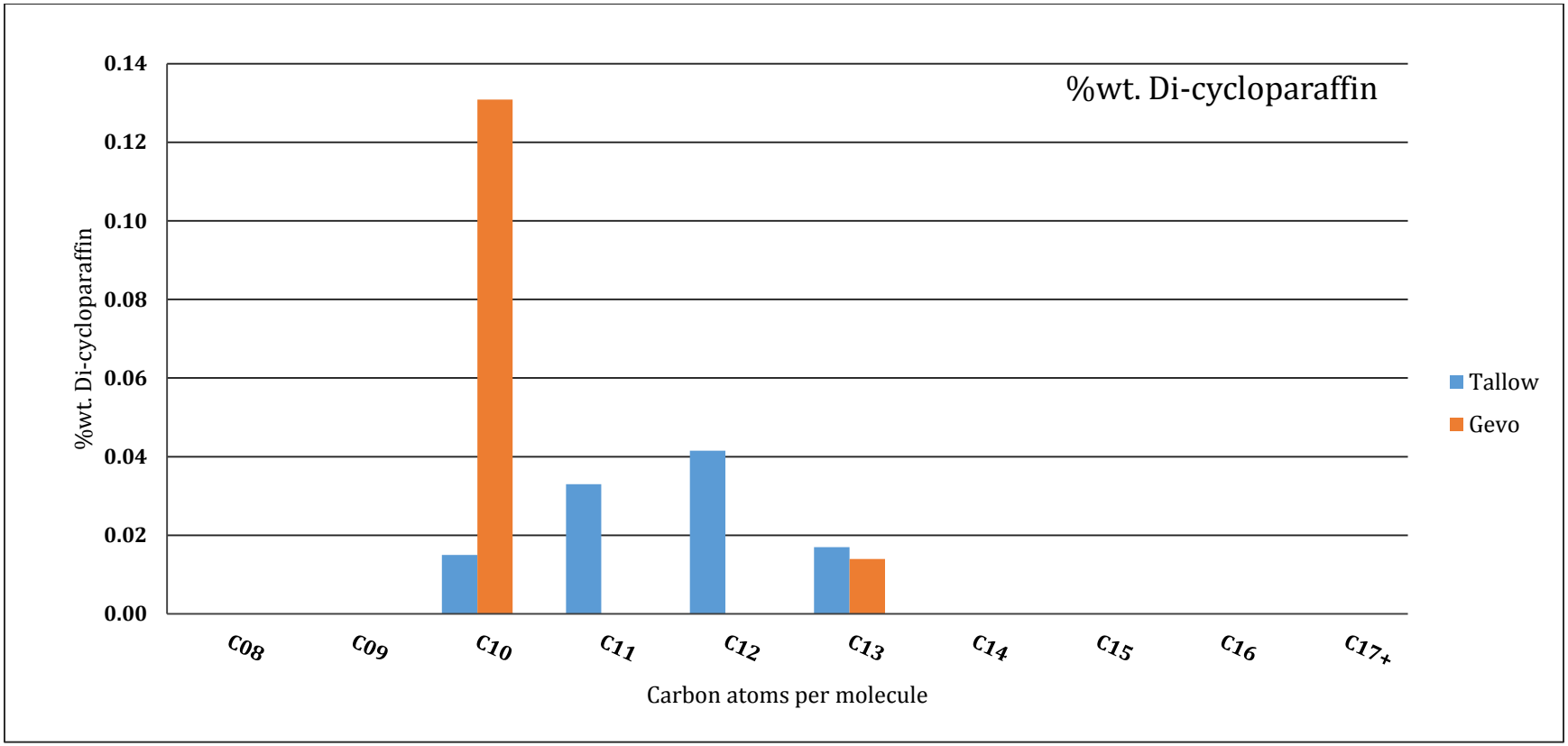

Figure 5.3: Percent by weight dicyclic paraffins in HRJ tallow and Gevo jet blend from AFRL gas chromatography data.

same amount of aromatic content. This implies some other hydrocarbon specie is responsible for such a variation.

Upon further comparing the gas chromatography data for these two fuels and referring to the results published by Street et al. [20] a considerable variation in the monocyclic paraffins and dicyclic paraffins was observed. In **Figure 5.2**, the lower molecular weight monocyclic paraffins are greater in concentration for HRJ tallow i.e. C10 and lower while higher molecular weight monocyclic paraffins i.e. C11 and higher are greater in concentration for Gevo jet blend. In addition to this, as per **Figure 5.3**, the dicyclic paraffin C10 (decalin), which as per Street et al. [20] has a low sooting threshold, has a high concentration in Gevo jet blend than in HRJ tallow. Both of these trends, can be considered to be the reason for such a difference in the fuel – air equivalence ratios of HRJ tallow and Gevo jet blend.

5.2. Flame structure at threshold sooting

The non – luminous zone or gap observed in paraffin rich fuels between the primary blue from and the streak of soot can be argued to be due to an intermediate reaction step where the radicals responsible for luminosity in the flame are undergoing recombination with similar or dissimilar molecules in the flow resulting in the loss of luminosity. To further strengthen this argument the flames pertaining to Toluene, JP – 8 and Iso – Octane at $\phi_{incipient}$ can be compared. From comparison of the flames it is observed that the pure aromatic fuel Toluene shows no gap between the primary flame and soot. JP – 8 with nearly 13% aromatics shows a very small gap and Iso – octane shows a large enough gap which is easy to observe. With reference to the mechanism of soot formation [11]–[13], [18], [21] aromatic compounds require less number of conversion steps for soot particle growth as it already has a benzene ring which is an intermediate step in case of paraffinic hydrocarbon fuel conversion to soot. The jet fuels with some considerable amount of aromatics show a very small gap which implies that by increasing the aromatic content in the fuel, the gap between the primary flame and the soot streak is reduced. This hypothesis is ascertained from the in – house fuel blend tests of HRJ tallow and mesitylene in varying proportions. On comparing the sooting flames for pure mesitylene, pure HRJ tallow and the two blends (see **Figure 5.4**) it is observed that the gap tends to reduce as the concentration of mesitylene increases in HRJ tallow.

Aromatics are also found responsible for increasing the sooting propensity of a hydrocarbon fuel which was also observed from the $\phi_{incipient}$ values computed and observed in the previous chapter and in the literature. This statement can be verified by referring again to **Figure 5.4** where the intensity of the soot radiation can be observed to vary with being higher for pure mesitylene and lowest for pure HRJ tallow. This observation though qualitative is in accordance to the literature.

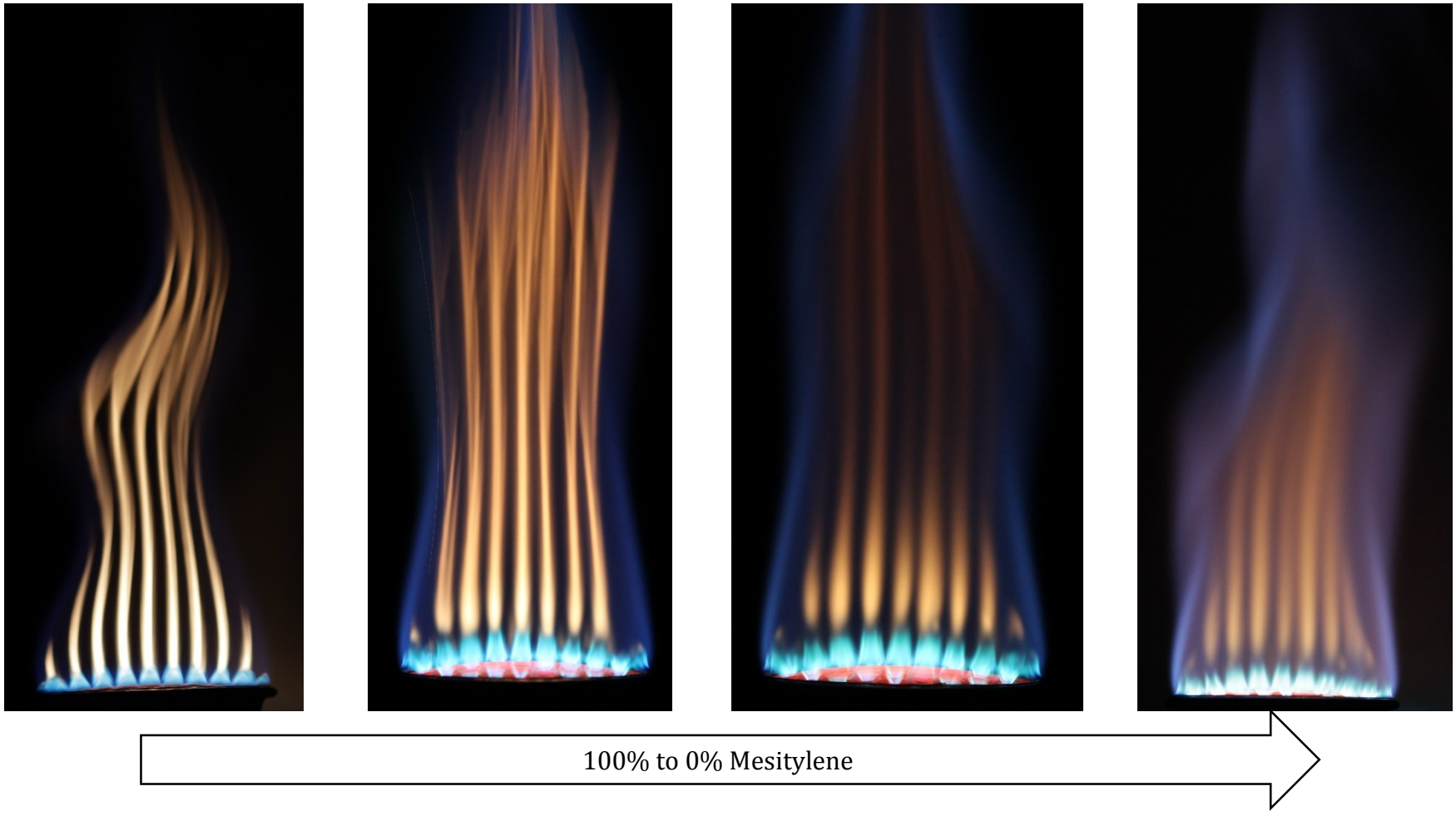

Figure 5.4: Variation in gap size between the primary blue flame and soot streak and soot radiation intensity with the addition of Mesitylene to HRJ Tallow

The key results deduced from the study of different hydrocarbon fuels on the Meker burner setup are validated and found to be consistent with prior studies and theories.

***

6. CONCLUSIONS

6.1. Summary of Work

The primary motive of this study was to understand the reasons the various fuels produced differing sooting behavior. The results support the following conclusions:

1. Fuels containing aromatic, alkyne or alkene hydrocarbons are susceptible to produce more soot upon combustion due to their rate of forming soot precursors is much higher in comparison to alkane, iso – alkane and cyclo – alkane groups.
2. Among the conventional jet fuels tested JP – 8 has the lowest sooting propensity due to its low aromatic content in comparison to JP – 5. Aromatic hydrocarbons are a necessity in transportation fuels due to the advantages to the fuel system and the fuel flow itself but there is a scope for further improvements in the fuel quality in terms of particulate emissions.
3. The synthetic fuels obtained from Fischer Tropsch process and renewable fuels from hydro treatment process or from fermentation process show a higher sooting thresholds in comparison to the other fuels tested. These fuels have less than 1% by weight of aromatic which is one of the primary reasons. Such a behavior makes these fuels as prime candidates for making jet fuel blends with higher sooting thresholds.
4. In reference to the comparison chart in **Figure 6.1** for all the 18 fuels tested, HRJ tallow shows the highest sooting threshold. Upon blending HRJ tallow with 10% and 20% vol. mesitylene, the sooting threshold was still the highest among the other test fuels. Such a characteristic of HRJ tallow can be accounted for due to high concentration of iso – paraffins and low amounts of heavy dicyclic paraffins and aromatic compounds.

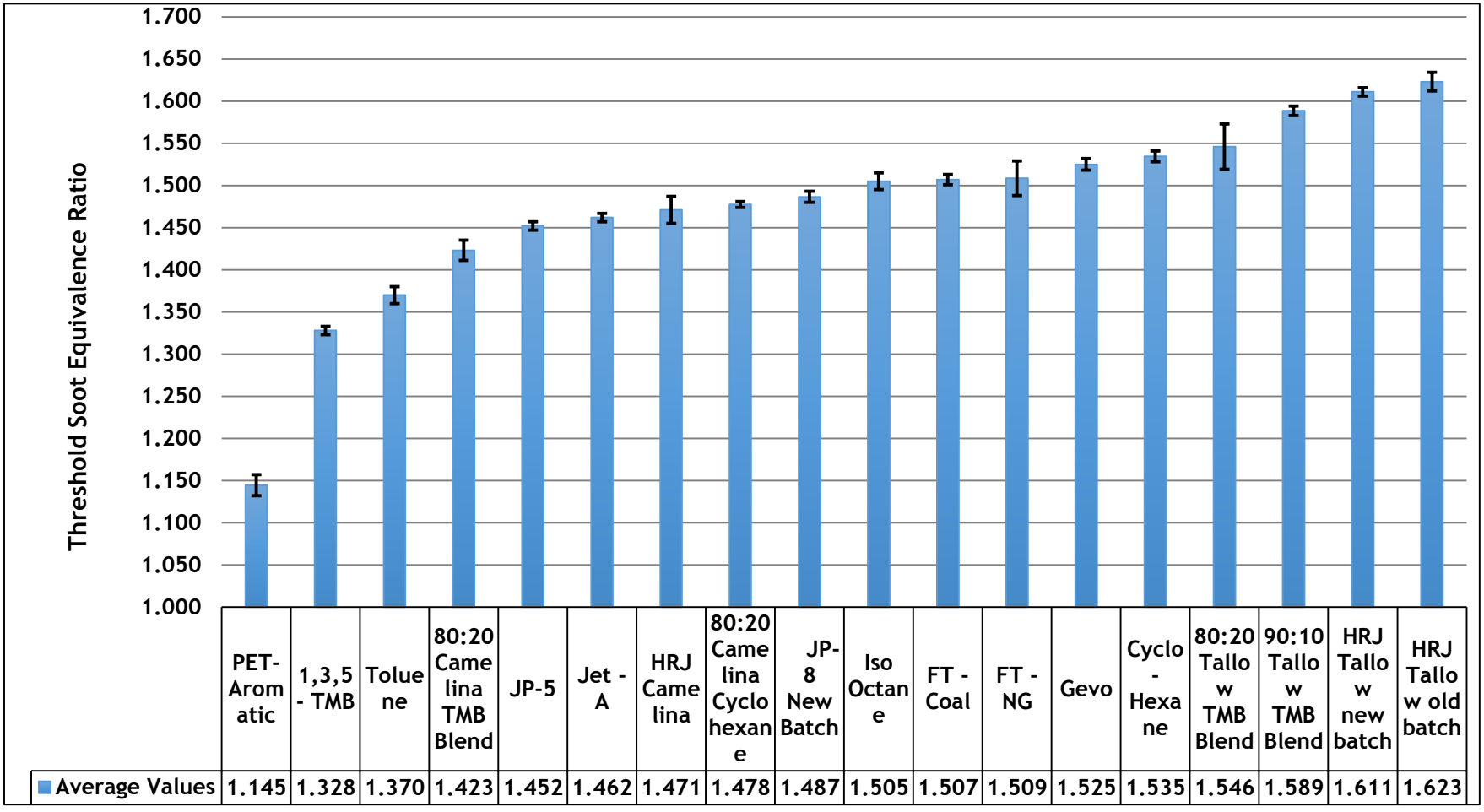

Figure 6.1: Incipient Soot points for 18 test fuels obtained from the Meker burner study.

6.2. Future Work

This study has been a qualitative approach to determine the behavior of fuels with varying compositions on production of soot particles. The results from the study provide an understanding of which hydrocarbon compounds increase or decrease a fuel's tendency to soot and also put these fuels on a scale of highly sooting to least sooting, relative to one another. This research on the whole has formed a strong base for conducting more in – depth study of these fuels by taking a quantitative approach.

One of the methods is to use a particle counting instrument such as a Differential

Flat Flame Burner

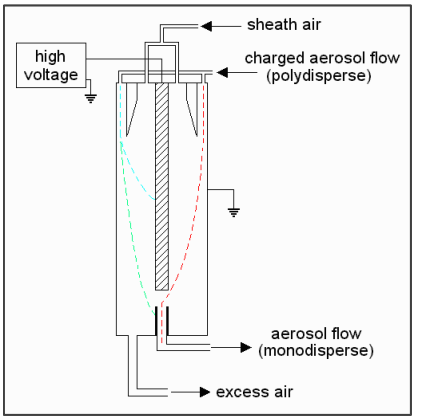

Differential Mobility Analyzer

Mobility Analyzer in conjunction with an aerosol collection probe to sample the products of combustion from the test fuels at varying fuel – air ratios and recording the variation in particle density. This approach will allow us to determine the variation in production of soot with change in fuel – air ratio and other parameters. This approach of particle counting is found to be more effective with a flat flame burner such as a McKenna burner which provides the ability to assess the flame properly so as to obtain profiles for soot emissions both axially and radially.

Other baseline experiments with fuels like decalin and benzene, both pure and in a blend should be conducted to provide a better idea of their sooting thresholds and simultaneous validation of the claim that decalin reduces sooting threshold whereas benzene raises it if mixed with an n – paraffin.

***

BIBLIOGRAPHY

[1] EPA, "Report to Congress on Black Carbon," 2012. [Online]. Available: http://www.epa.gov/blackcarbon/2012report/fullreport.pdf. [Accessed: 01-Jan-2015].

[2] IPCC, "Summary for Policymakers," in *Climate Change 2013: The Physical Science Basis. Contribution of Working Group I to the Fifth Assessment Report of the Intergovernmental Panel on Climate Change*, 2013, p. 33.

[3] National Research Council, Washington, DC and National Aeronautics and Space Administration, Washington, DC, "Aviation Turbine Fuels: An Assessment of Alternatives," 1982.

[4] N. Hudda, T. Gould, K. Hartin, T. V. Larson, and S. A. Fruin, "Emissions from an international airport increase particle number concentrations 4-fold at 10 km downwind," *Environ. Sci. Technol.*, vol. 48, no. 12, pp. 6628–6635, 2014.

[5] I. Glassman and R. Yetter, *Combustion, Fourth Edition*, vol. 79, no. 3. 2008.

[6] M. Hertzberg, "The Theory of Flammability Limits: Flow Gradient Effects and Flame Stretch," 1984.

[7] F. TAKAHASHI and I. GLASSMAN, "Sooting Correlations for Premixed Flames," *Combustion Science and Technology*, vol. 37, no. 1–2. pp. 1–19, 1984.

[8] K. H. Homann and H. G. Wagner, "No Title," *Proc. Combust. Insitute*, no. 11, p. 371, 1967.

[9] H. F. Calcote, "No Title," *Combust. Flame*, no. 42, p. 215, 1981.

[10] B. S. Haynes and H. G. Wagner, "No Title," *Prog. Energy Combust. Sci.*, no. 7, p. 229, 1981.

[11] M. Frenklach, "Reaction mechanism of soot formation in flames," *Physical Chemistry Chemical Physics*, vol. 4, no. 11. pp. 2028–2037, 2002.

[12] M. Frenklach and H. Wang, "Detailed modeling of soot particle nucleation and growth," *Symp. Combust.*, vol. 23, no. 1, pp. 1559–1566, 1991.

[13] M. Frenklach, D. W. Clary, W. C. Gardiner, and S. E. Stein, "Effect of fuel structure on pathways to soot," *Symp. Combust.*, vol. 21, no. 1, pp. 1067–1076, 1988.

[14] I. GLASSMAN, “Princeton University Mechanical and Aerospace Engineering Report No. 1450,” 1979.

[15] C. F. Melius, M. E. Colvin, N. M. Marinov, W. J. Pitz, and S. M. Senkan, “No Title,” in *Combustion Institute*, 1996, p. 685.

[16] M. J. Castaldi, N. M. Marinov, C. F. Melius, J. Huang, S. M. Senkan, W. J. Pitz, and C. K. Westbrook, “No Title,” in *Combustion Institute*, 1996, p. 693.

[17] M. B. Colket and D. J. Seery, “No Title,” in *Combustion Institute*, 1994, p. 425.

[18] H. Wang, “Formation of nascent soot and other condensed-phase materials in flames,” *Proc. Combust. Inst.*, vol. 33, no. 1, pp. 41–67, 2011.

[19] S. J. Harris and A. M. Weiner, “No Title,” in *Combustion Science and Technology*, 1983, pp. 267–275.

[20] J. C. Street and A. Thomas, “Carbon formation in Pre - Mixed flames,” *Fuel. Lond.*, no. 34, pp. 4 – 36, 1955.

[21] M. Frenklach and H. Wang, “Detailed mechanism and modeling of soot particle formation.,” *Springer Ser. Chem. Phys.*, vol. 59, no. Soot Formation in Combustion, pp. 165–192, 1994.

[22] R. C. Millikan, “No Title,” *J. Phys. Chem.*, no. 66, p. 794, 1962.

[23] H. F. CALCOTE and D. B. OLSON, “Importance of Temperature on Soot Formation in Premixed Flames,” *Combustion Science and Technology*, vol. 28, no. 5–6. pp. 315–317, 1982.

[24] K. Ono, Y. Matsukawa, K. Dewa, A. Watanabe, K. Takahashi, Y. Saito, Y. Matsushita, H. Aoki, K. Era, T. Aoki, and T. Yamaguchi, “Formation mechanisms of soot from high-molecular-weight polycyclic aromatic hydrocarbons,” *Combust. Flame*, no. 162, pp. 2670–2678, 2015.

[25] Y. Yang, A. L. Boehman, and R. J. Santoro, “A study of jet fuel sooting tendency using the threshold sooting index (TSI) model,” *Combust. Flame*, vol. 149, no. 1–2, pp. 191–205, 2007.

[26] D. B. Olson, J. C. Pickens, and R. J. Gill, “The effects of molecular structure on soot formation II. Diffusion flames,” *Combustion and Flame*, vol. 62, no. 1. pp. 43–60, 1985.

[27] A. Mensch, R. J. Santoro, T. A. Litzinger, and S. Y. Lee, “Sooting characteristics of surrogates for jet fuels,” *Combust. Flame*, vol. 157, no. 6, pp. 1097–1105, 2010.

[28] M. Saffaripour, P. Zabeti, M. Kholghy, and M. J. Thomson, "An experimental comparison of the sooting behavior of synthetic jet fuels," *Energy and Fuels*, vol. 25, no. 12, pp. 5584–5593, 2011.

[29] Y. C. Liu, A. J. Savas, and C. T. Avedisian, "The spherically symmetric droplet burning characteristics of Jet-A and biofuels derived from camelina and tallow," *Fuel*, vol. 108, pp. 824–832, 2013.

[30] A. G. Gaydon, *The Spectroscopy of Flames*. Wiley, 1974.

[31] P. F. Jessen and A. G. Gaydon, "Study of the absorption spectra of free radicals in flames," *Combustion and Flame*, vol. 11, no. 1. pp. 11–16, 1967.

[32] L. C. Haber and U. Vandsburger, "A global reaction model for oh* chemiluminescence applied to a laminar flat-flame burner," *Combustion Science and Technology*, vol. 175, no. 10. pp. 1859–1891, 2003.

[33] M. A. Fahim, T. A. Alsahhaf, and A. Elkilani, *Fundamentals of Petroleum Refining*. 2010.

[34] J. Speight, *Synthetic Fuels Handbook: Properties, Process and Performance*. McGraw Hill, 2008.

[35] B. Jager, "Development of Fischer Tropsch Reactors," in *2003 AIChE Spring Meeting*, 2003.

[36] E. Dahlquist, *Biomass as Energy Source: Resources, Systems and Applications*. CRC Press, 2013.

[37] A. C. Lee, "Experimental Investigation of Liquid Fuel Vaporization and Mixing in Steam and Air," University of Washington, Seattle, 2003.

[38] EIA, "Crude oil distillation and the definition of refinery capacity - Today in Energy - U.S. Energy Information Administration (EIA)." [Online]. Available: http://www.eia.gov/todayinenergy/detail.cfm?id=6970. [Accessed: 04-Sep-2015].

APPENDIX A

DETAILED FUEL PROPERTIES

Additional required information pertaining to the different Liquid Fuels mentioned in Chapter 2 concerning the identification, composition and properties is provided.

A.1 Fuel Identification

The fuel samples obtained from the Air Force Research Lab carry a unique identification number which varies with fuel type, manufacturer and composition. Table provides the common names of these fuels and their identification number as specified on the containers and other reference publications.

Fuel	POSF #	Manufacturer
Petroleum Aromatic Blend	6871/10240	Exxon Mobil
Mesitylene (1,3,5 -trimethylbenzene)	6898	Swift
JP – 5	10289	Valero
Jet – A	10325	Shell Chemicals
JP – 8	10264	NuStar
FT – Coal	7629	Sasol Oil
FT – Natural Gas	5018	Syntroleum Corp.
HRJ – Camelina	10301	UOP
HRJ – Tallow	6308	UOP
Gevo Jet Blend Stock	8092	GEVO Inc.

Table A. 1: List of fuels with identification number obtained from AFRL.

A.2 Fuel Composition

	JP - 8	Jet - A	JP - 5	FT Coal	FT Natural Gas	HRJ Camelina	HRJ Tallow	Gevo Jet Blend Stock	Petroleum Aromatic Blend
Aromatics	**13.41**	**18.66**	**20.59**	**0.64**	**0.20**	**0.18**	**0.08**	**0.06**	**99.27**
Total Alkylbenzenes	**10.86**	**12.90**	**10.37**	**0.47**	**0.16**	**0.14**	**0.05**	**0.02**	**76.56**
benzene (C06)	<0.01	<0.01	<0.01	<0.01	<0.01	<0.01	<0.01	<0.01	0.00
toluene (C07)	0.25	0.16	0.04	<0.01	<0.01	<0.01	<0.01	<0.01	0.00
C2-benzene (C08)	2.00	1.11	0.44	0.02	0.02	0.02	0.01	<0.01	0.54
C3-benzene (C09)	4.20	3.03	1.36	0.11	0.03	0.04	0.01	<0.01	28.14
C4-benzene (C10)	2.27	3.33	2.10	0.16	0.03	0.03	<0.01	<0.01	36.85
C5-benzene (C11)	1.15	2.23	1.95	0.09	0.03	0.02	<0.01	<0.01	9.97
C6-benzene (C12)	0.56	1.32	1.79	0.06	0.02	0.01	<0.01	<0.01	1.07
C7-benzene (C13)	0.24	0.76	1.21	0.02	0.02	0.01	<0.01	0.01	
C8-benzene (C14)	0.12	0.52	0.99	<0.01	0.01	<0.01	<0.01	<0.01	
C9-benzene (C15)	0.05	0.30	0.45	<0.01	<0.01	<0.01	<0.01	<0.01	
C10+-benzene (C16+)	0.01	0.14	0.04	<0.01	<0.01	<0.01	<0.01	<0.01	
Total Alkylnaphthalenes	**1.06**	**2.33**	**1.34**	**0.02**	**<0.01**	**<0.01**	**<0.01**	**0.02**	**15.55**
diaromatic-C10	0.10	0.22	0.09	<0.01	<0.01	<0.01	<0.01	<0.01	7.02

diaromatic-C11	0.32	0.66	0.33	<0.01	<0.01	<0.01	<0.01	<0.01	3.76
diaromatic-C12	0.40	0.86	0.56	0.01	<0.01	<0.01	<0.01	0.01	
diaromatic-C13	0.18	0.41	0.29	<0.01	<0.01	<0.01	<0.01	<0.01	4.77
diaromatic-C14+	0.06	0.18	0.06	<0.01	<0.01	<0.01	<0.01	<0.01	
Total Cycloaromatics	**1.49**	**3.43**	**8.88**	**0.15**	**0.03**	**0.03**	**0.02**	**0.02**	**7.16**
cycloaromatic-C09	0.02	0.03	0.03	<0.01	<0.01	<0.01	<0.01	<0.01	
cycloaromatic-C10	0.18	0.28	0.59	0.01	<0.01	<0.01	<0.01	<0.01	
cycloaromatic-C11	0.36	0.67	1.84	0.01	<0.01	<0.01	<0.01	<0.01	
cycloaromatic-C12	0.37	0.93	2.71	0.08	<0.01	<0.01	<0.01	0.01	7.16
cycloaromatic-C13	0.36	0.86	2.42	0.04	<0.01	<0.01	<0.01	<0.01	
cycloaromatic-C14	0.16	0.45	1.11	<0.01	<0.01	<0.01	<0.01	<0.01	
cycloaromatics-C15+	0.04	0.22	0.17	<0.01	<0.01	<0.01	<0.01	<0.01	
Paraffins	**66.51**	**49.48**	**32.03**	**98.75**	**99.25**	**97.66**	**99.03**	**99.14**	**0.54**
Total iso - Paraffins	**39.69**	**29.45**	**18.14**	**98.43**	**75.88**	**86.70**	**88.34**	**99.14**	**0.48**
C07 and lower-iso	0.23	0.18	0.04	0.04	0.01	0.02	<0.01	0.09	0.01
C08-isoparaffins	0.95	0.55	0.17	0.49	1.48	1.39	2.10	0.36	0.01
C09-isoparaffins	2.88	1.20	0.50	10.69	6.28	10.87	9.40	0.08	0.00
C10-isoparaffins	8.53	4.07	1.69	22.07	8.29	11.67	9.69	0.18	0.27
C11-isoparaffins	9.18	5.68	2.60	34.28	9.89	10.24	9.69	0.32	0.11

C12-isoparaffins	6.05	5.41	3.06	21.56	10.93	8.54	9.25	79.74	0.07
C13-isoparaffins	4.41	4.27	3.18	7.16	11.50	8.48	9.53	0.60	0.01
C14-isoparaffins	4.22	4.16	3.48	1.72	11.16	6.41	7.84	0.60	0.00
C15-isoparaffins	2.31	2.41	2.60	0.29	9.92	5.75	11.75	0.00	0.00
C16-isoparaffins	0.73	0.98	0.73	0.07	5.84	10.95	12.83	15.99	0.00
C17-isoparaffins	0.18	0.38	0.08	0.02	0.56	11.56	5.92	0.00	0.00
C18-isoparaffins	0.02	0.11	<0.01	0.01	0.02	0.81	0.34	0.00	0.00
C19-isoparaffins	<0.01	0.05	<0.01	<0.01	<0.01	<0.01	<0.01	0.00	0.00
C20-isoparaffins	<0.01	0.01	<0.01	<0.01	<0.01	<0.01	<0.01	1.20	0.00
C21-isoparaffins	<0.01	<0.01	<0.01	<0.01	<0.01	<0.01	<0.01	0.00	0.00
C22-isoparaffins	<0.01	<0.01	<0.01	<0.01	<0.01	<0.01	<0.01	0.00	0.00
C23-isoparaffins	<0.01	<0.01	<0.01	<0.01	<0.01	<0.01	<0.01	0.00	0.00
C24-isoparaffins	<0.01	<0.01	<0.01	<0.01	<0.01	<0.01	<0.01	0.00	0.00
Total n - Paraffins	**26.82**	**20.03**	**13.89**	**0.32**	**23.37**	**10.96**	**10.69**	**<0.01**	**0.06**
n-C07	0.20	0.14	0.02	0.00	0.03	0.02	0.00	<0.01	0.00
n-C08	1.14	0.56	0.22	0.01	1.37	1.31	1.49	<0.01	0.00
n-C09	3.05	1.45	0.67	0.04	3.04	1.89	1.45	<0.01	0.01
n-C10	6.77	3.29	1.50	0.05	4.00	1.54	1.23	<0.01	0.04
n-C11	5.29	4.31	2.75	0.05	4.24	1.14	1.18	<0.01	0.01

n-C12	4.14	3.74	3.01	0.05	3.87	1.01	1.09	<0.01	0.00
n-C13	2.99	2.80	2.43	0.04	3.10	0.89	1.04	<0.01	0.00
n-C14	2.07	2.03	2.14	0.03	2.26	0.77	0.88	<0.01	0.00
n-C15	0.88	1.02	0.98	0.02	1.32	0.99	1.57	<0.01	0.00
n-C16	0.24	0.42	0.14	0.01	0.14	1.22	0.68	<0.01	0.00
n-C17	0.06	0.20	0.01	<0.01	<0.01	0.17	0.07	<0.01	0.00
n-C18	<0.01	0.04	<0.01	<0.01	<0.01	<0.01	<0.01	<0.01	0.00
n-C19	<0.01	0.01	<0.01	<0.01	<0.01	<0.01	<0.01	<0.01	0.00
n-C20	<0.01	<0.01	<0.01	<0.01	<0.01	<0.01	<0.01	<0.01	0.00
n-C21	<0.01	<0.01	<0.01	<0.01	<0.01	<0.01	<0.01	0.00	0.00
n-C22	<0.01	<0.01	<0.01	<0.01	<0.01	<0.01	<0.01	0.00	0.00
n-C23	<0.01	<0.01	<0.01	<0.01	<0.01	<0.01	<0.01	0.00	0.00
Cycloparaffins	**20.08**	**31.86**	**47.38**	**0.61**	**0.55**	**2.16**	**0.89**	**0.80**	**0.19**
Total Monocycloparaffins	**17.01**	**24.87**	**31.33**	**0.57**	**0.50**	**1.92**	**0.77**	**0.64**	**0.12**
C07-monocyclocycloparaffins	0.49	0.33	0.08	<0.01	<0.01	<0.01	<0.01	<0.01	0.12
C08-monocyclocycloparaffins	0.98	0.80	0.44	<0.01	0.12	0.37	0.26	0.05	

C09-monocyclocycloparaffins	2.86	2.27	1.50	<0.01	0.16	0.86	0.25	0.02	
C10-monocyclocycloparaffins	3.83	4.57	3.59	0.26	0.12	0.38	0.13	0.02	
C11-monocyclocycloparaffins	2.92	5.42	5.91	0.26	0.07	0.14	0.07	0.27	
C12-monocyclocycloparaffins	1.99	3.77	6.70	<0.01	0.02	0.07	0.02	0.06	
C13-monocyclocycloparaffins	2.06	3.73	6.43	<0.01	<0.01	0.09	0.04	<0.01	
C14-monocyclocycloparaffins	1.16	2.06	4.07	0.02	<0.01	0.01	<0.01	<0.01	
C15-monocyclocycloparaffins	0.59	1.27	2.35	0.02	<0.01	<0.01	<0.01	<0.01	
C16-monocyclocycloparaffins	0.12	0.43	0.25	<0.01	<0.01	<0.01	<0.01	<0.01	
C17-monocyclocycloparaffins	0.02	0.18	0.02	<0.01	<0.01	<0.01	<0.01	0.17	
C18-monocyclocycloparaffins	<0.01	0.04	<0.01	<0.01	<0.01	<0.01	<0.01	<0.01	
C19+-monocyclocycloparaffins	<0.01	0.02	<0.01	<0.01	<0.01	<0.01	<0.01	0.04	
Total Dicycloparaffins	**2.95**	**6.78**	**15.97**	**0.04**	**0.05**	**0.23**	**0.12**	**0.16**	**0.07**

C08-dicycloparaffins	0.03	0.04	0.03	<0.01	<0.01	<0.01	<0.01	<0.01	0.07
C09-dicycloparaffins	0.24	0.45	0.45	<0.01	<0.01	0.02	<0.01	<0.01	
C10-dicycloparaffins	0.26	0.46	0.71	<0.01	0.01	0.03	0.01	0.13	
C11-dicycloparaffins	0.72	1.63	2.72	<0.01	0.01	0.06	0.03	<0.01	
C12-dicycloparaffins	0.66	1.72	3.44	<0.01	0.01	0.06	0.04	<0.01	
C13-dicycloparaffins	0.54	1.50	4.94	<0.01	<0.01	0.03	0.02	0.01	
C14-dicycloparaffins	0.42	0.79	3.01	0.02	<0.01	0.01	<0.01	<0.01	
C15-dicycloparaffins	0.07	0.14	0.64	<0.01	<0.01	<0.01	<0.01	<0.01	
C16-dicycloparaffins	<0.01	0.02	0.03	<0.01	<0.01	<0.01	<0.01	<0.01	
C17+-dicycloparaffins	<0.01	0.02	<0.01	<0.01	<0.01	<0.01	<0.01	<0.01	
Total Trcicycloparaffins	**0.12**	**0.21**	**0.08**	**<0.01**	**<0.01**	**<0.01**	**<0.01**	**<0.01**	**<0.01**
C10-tricycloparaffins	0.02	0.02	<0.01	<0.01	<0.01	<0.01	<0.01	<0.01	<0.01
C11-tricycloparaffins	0.05	0.07	0.08	<0.01	<0.01	<0.01	<0.01	<0.01	<0.01
C12-tricycloparaffins	0.06	0.11	<0.01	<0.01	<0.01	<0.01	<0.01	<0.01	<0.01
TOTAL	**100.00**	**100.00**	**100.00**	**100.00**	**100.00**	**100.00**	**100.00**	**100.00**	**100.00**

Table A. 2: Gas chromatography data for the synthetic and renewable jet fuels provided by Air Force Research Laboratory.

APPENDIX B

ROTAMETER CALIBRATION CURVES

The Rotameter flow devices used in the experiment are calibrated for every fuel sample tested so as to relate the rotameter reading with flow rate and eventually ϕ. The procedure of calibration is discussed in Chapter 3 while the calibration charts of the fuels are provided here for reference. The ϕ value of importance in the study is once the fuel and air form a mixture near the end of the Meker burner tube. Thus, the change in air density has to be accounted for the final calibrated value.

The calibration conditions which remain similar for all the fuels are provided in **Table B. 1**.

Fuel Flow Condition		
Pressure:	**65**	**psig**
Air Properties [Calibration]:		
Pressure:	**62**	**psig**
Temperature:	**25**	**^{o}C**
Density:	**1.2**	**Kg/m^{3}**
Air Properties [Actual]:		
Temperature :	**110**	**^{o}C**
Density :	**0.91**	**Kg/m^{3}**

Table B. 1: Fuel and Air flow properties for rotameter calibration and calculation.

The calculations for determining the liquid flow rate and mass flow rate from the calibration steps and relating rotameter graduations with corresponding ϕ values are presented in a tabular form along with a ϕ vs. Rotameter reading plot with a linear curve fit to determine a relation between the two values.

B.1 Iso - Octane

RM Reading	Fuel (ml)	Time (s)			Avg. time (s)	Q (ml/s)	m_dot (Kg/s)
		T1	T2	T3			
20	1	32.5	33	32.7	32.73	0.0305	2.11E-05
30	1	22	22	22	22.00	0.0455	3.14E-05
40	1	16	16	16.4	16.13	0.0620	4.28E-05
50	2	27	26	26.5	26.50	0.0755	5.21E-05
60	2	21	21	21	21.00	0.0952	6.57E-05
RM Reading	**Air meter (cu. ft)**	**Time (s)**			**Avg. time (s)**	**Q (m^3/s)**	**m_dot (Kg/s)**
		T1	**T2**	**T3**			
55	0.1	7.8	8	7.8	7.87	3.60E-04	**4.32E-04**
Fuel Air Ratio							
RM Reading	**FAR**	**phi**					
20	**4.88E-02**	**0.74**					
30	**7.26E-02**	**1.10**					
40	**9.90E-02**	**1.50**					
50	**1.21E-01**	**1.83**					
60	**1.52E-01**	**2.30**					

Table B. 2: Iso – Octane calibration recorded data.

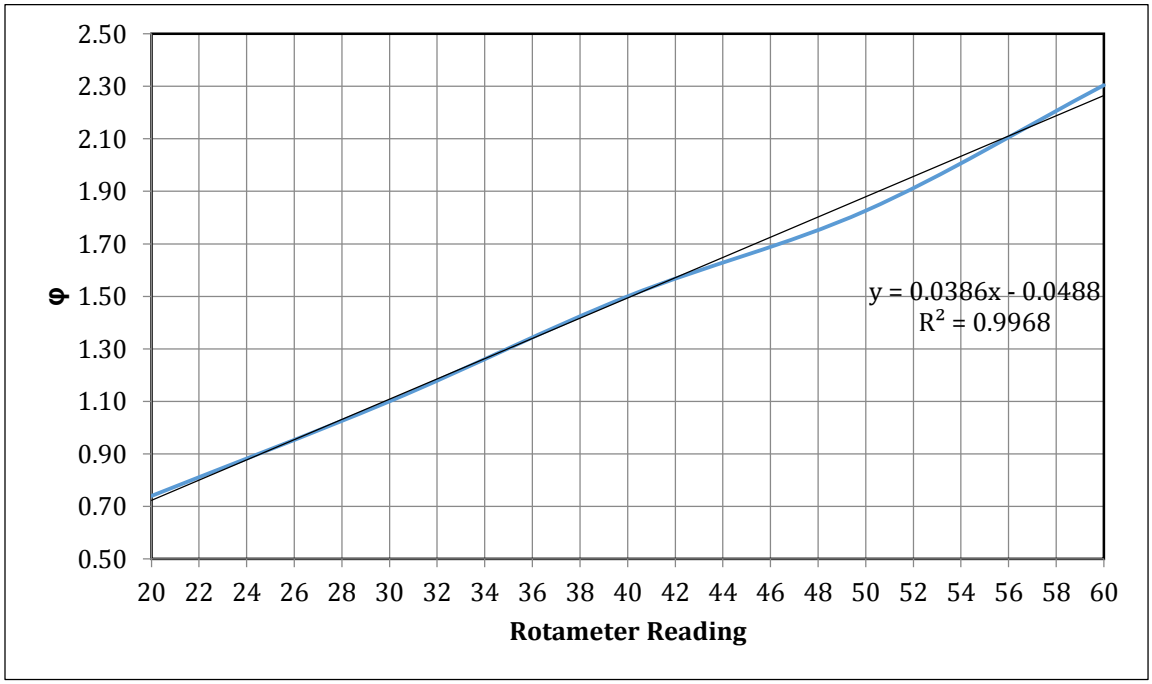

Figure B. 1: Calibration curve and Linear fit for Iso – Octane.

B.2 Cyclohexane

RM Reading	Fuel (ml)	Time (s)				Avg. time (s)	Q (ml/s)	m_dot (Kg/s)
		T1	T2	T3	T4			
40	1	29.5	29	29.3	29.4	29.30	0.0341	2.63E-05
50	1	22	23	21.9	22.2	22.28	0.0449	3.46E-05
60	1	19	18.3	19	18.2	18.63	0.0537	4.13E-05
70	1	15.8	15.1	15.7	15.1	15.43	0.0648	4.99E-05
RM Reading	**Air meter (cu. ft)**	**Time (s)**			**Avg. time (s)**	**Q (m^3/s)**	**m_dot (Kg/s)**	
		T1	**T2**	**T3**				
55	0.1	7.8	8	7.8	7.87	3.60E-04	**4.32E-04**	
Fuel Air Ratio								
RM Reading	**FAR**	**phi**						
40	**6.08E-02**	**0.90**						
50	**8.00E-02**	**1.19**						
60	**9.57E-02**	**1.42**						
70	**1.16E-01**	**1.71**						

Table B. 3: Cyclohexane calibration recorded data.

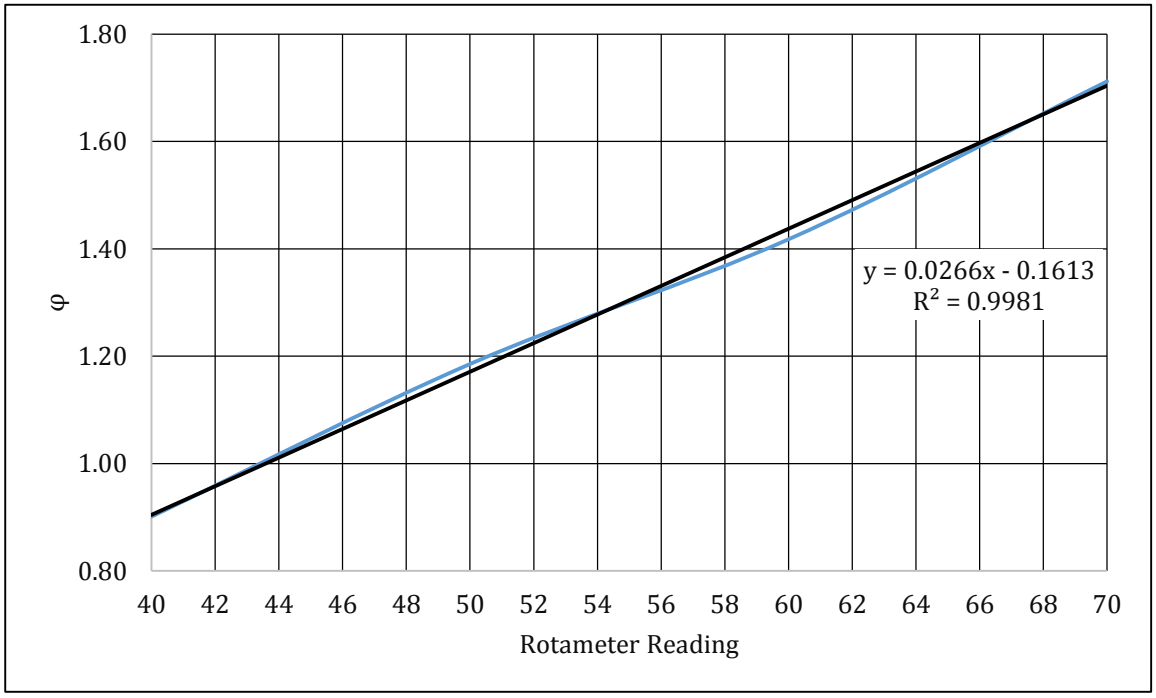

Figure B. 2: Calibration curve and Linear fit for Cyclohexane.

B.3 Petroleum Aromatic Blend

RM Reading	Fuel (ml)	Time (s) T1	T2	T3	T4	Avg. time (s)	Q (ml/s)	m_dot (Kg/s)
40	1	34.7	31.7	34.6	31.3	33.08	0.0302	2.80E-05
50	1	25.7	27.1	25.4	26.4	26.15	0.0382	3.54E-05
60	1	21	22.2	21.1	22.1	21.60	0.0463	4.28E-05
70	1	18.5	17.5	18.8	17.8	18.15	0.0551	5.10E-05

RM Reading	Air meter (cu. ft)	Time (s) T1	T2	T3	Avg. time (s)	Q (m^3/s)	m_dot (Kg/s)
55	0.1	7.8	8	7.8	7.87	3.60E-04	**4.32E-04**

Fuel Air Ratio

RM Reading	FAR	phi
50	**6.47E-02**	**0.89**
60	**8.19E-02**	**1.13**
70	**9.91E-02**	**1.37**
80	**1.18E-01**	**1.63**

Table B. 4: Petroleum Aromatic Blend calibration recorded data.

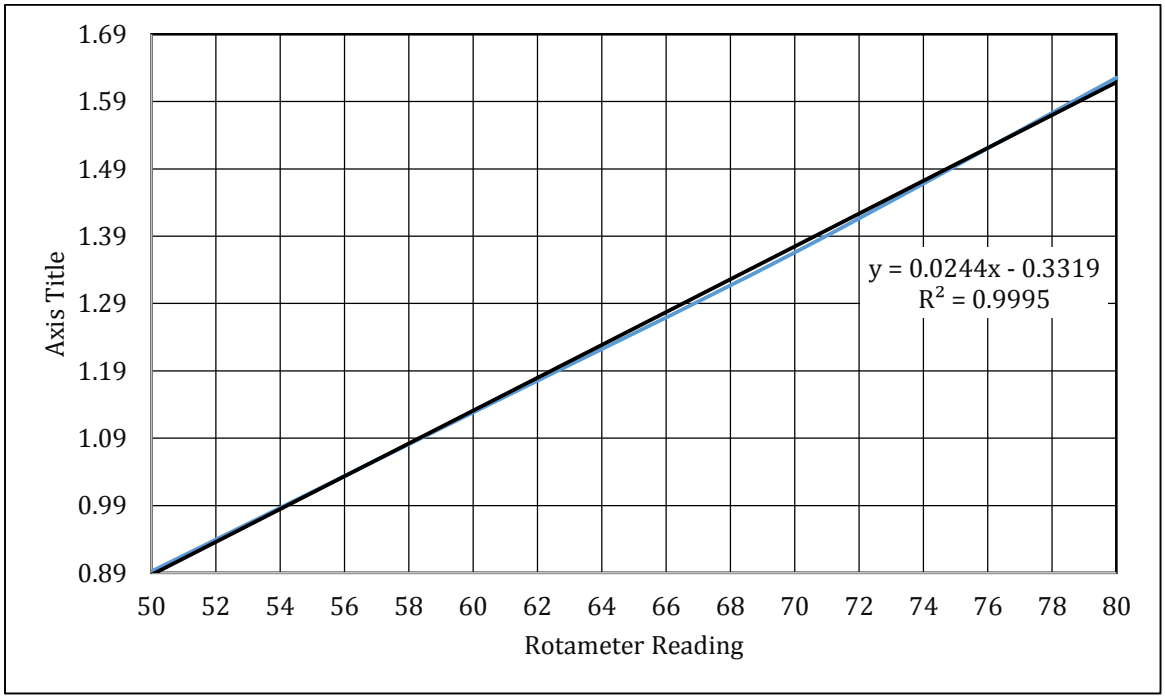

Figure B. 3: Calibration curve with linear fit for Petroleum Aromatic Blend.

B.4 Mesitylene

RM Reading	Fuel (ml)	Time (s) T1	T2	T3	T4	Avg. time (s)	Q (ml/s)	m_dot (Kg/s)
20	1	43.3	42.6	42.8	44.2	43.23	0.0231	2.00E-05
30	1	28.7	28.5	29	26.8	28.73	0.0348	3.01E-05
40	1	20.7	22.4	19.4	23.3	21.45	0.0466	4.03E-05
50	1	16	17.6	15.1	18.6	16.83	0.0594	5.13E-05

RM Reading	Air meter (cu. ft)	Time (s) T1	T2	T3	Avg. time (s)	Q (m^3/s)	m_dot (Kg/s)
55	0.1	7.8	8	7.8	7.87	3.60E-04	**4.32E-04**

Fuel Air Ratio		
RM Reading	**FAR**	**phi**
20	**4.63E-02**	**0.63**
30	**6.96E-02**	**0.95**
40	**9.32E-02**	**1.28**
50	**1.19E-01**	**1.63**

Table B. 5: Mesitylene calibration recorded data.

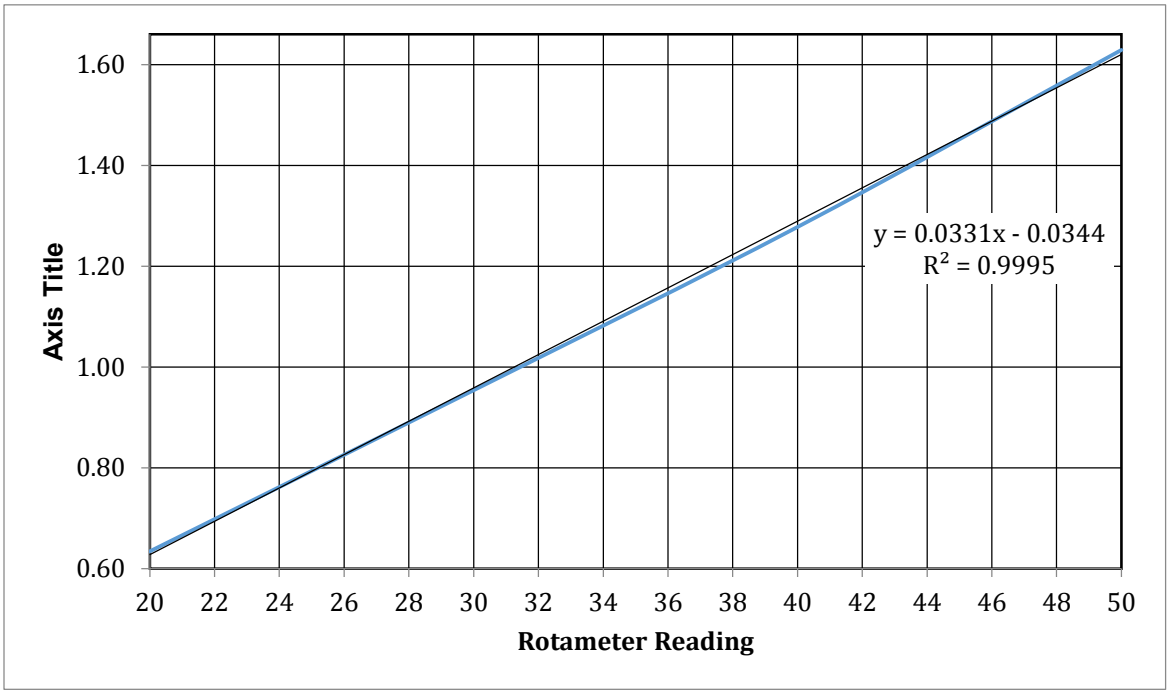

Figure B. 4: Calibration curve with linear fit for Mesitylene.

B.5 Toluene

RM Reading	Fuel (ml)	Time (s) T1	T2	T3	T4	Avg. time (s)	Q (ml/s)	m_dot (Kg/s)
20	1	35.2	36.3	36.7	35.5	36.07	0.0277	2.40E-05
30	1	22.8	24.9	22.4	26.8	23.37	0.0428	3.71E-05
40	1	19	20.2	18.4	20.3	19.20	0.0521	4.52E-05
50	1	14.5	16.4	15.4	14.6	15.43	0.0648	5.62E-05

RM Reading	Air meter (cu. ft)	Time (s) T1	T2	T3	Avg. time (s)	Q (m^3/s)	m_dot (Kg/s)
55	0.1	7.8	8	7.8	7.87	3.60E-04	**4.32E-04**

Fuel Air Ratio		
RM Reading	**FAR**	**phi**
20	**5.57E-02**	**0.75**
30	**8.59E-02**	**1.15**
40	**1.05E-01**	**1.40**
50	**1.30E-01**	**1.75**

Table B. 6: Toluene calibration recorded data.

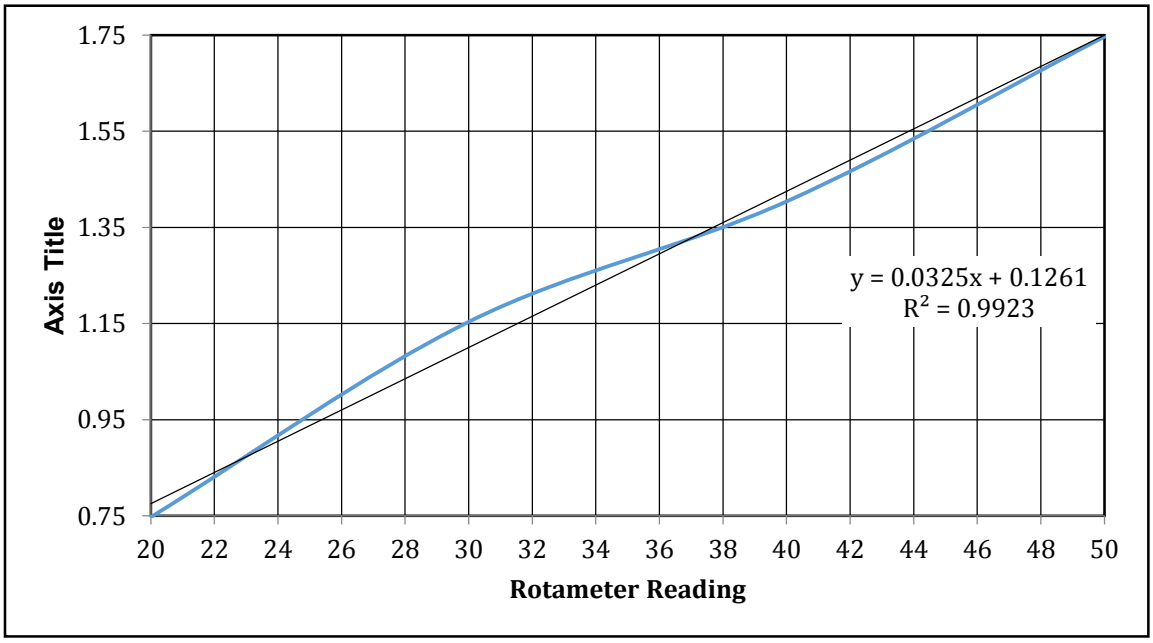

Figure B. 5: Calibration curve with linear fit for Toluene.

B.6 JP – 5

RM Reading	Fuel (ml)	Time (s)				Avg. time (s)	Q (ml/s)	m_dot (Kg/s)
		T1	T2	T3	T4			
50	1	40.2	38.3	40.4	37.9	39.20	0.0255	2.066E-05
60	1	31.4	31.9	32.3	30.6	31.55	0.0317	2.567E-05
70	1	26.4	25.5	26.3	26.2	26.10	0.0383	3.103E-05
80	1	22.5	22.3	22.2	22.7	22.43	0.0446	3.612E-05
90	1	18.4	19.4	19.1	18.9	18.95	0.0528	4.274E-05
100	1	16.1	17.2	16.6	16.1	16.50	0.0606	4.909E-05

RM Reading	Air meter (cu. ft)	Time (s)			Avg. time (s)	Q (m^3/s)	m_dot (Kg/s)
		T1	T2	T3			
55	0.1	7.8	8	7.8	7.87	3.60E-04	**4.32E-04**

Fuel Air Ratio		
RM Reading	FAR	phi
50	**4.78E-02**	**0.70**
60	**5.94E-02**	**0.87**
70	**7.18E-02**	**1.05**
80	**8.36E-02**	**1.22**
90	**9.90E-02**	**1.45**
100	**1.14E-01**	**1.66**

Table B. 7: JP – 5 calibration recorded data.

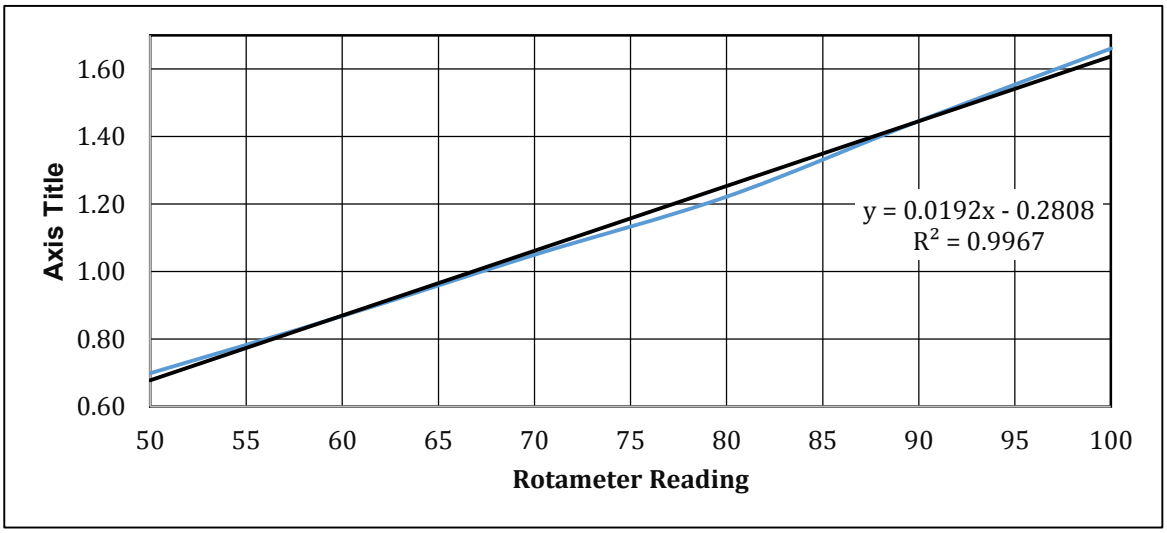

Figure B. 6: Calibration curve with linear fit for JP - 5.

B.7 Jet – A

RM Reading	Fuel (ml)	Time (s) T1	T2	T3	T4	Avg. time (s)	Q (ml/s)	m_dot (Kg/s)
40	1	42.7	41.6	43.6	43.4	42.83	0.0234	1.915E-05
50	1	31.7	32.8	32.5	33.6	32.65	0.0306	2.511E-05
60	1	27.7	25.6	27.8	26.3	26.85	0.0372	3.054E-05
70	1	21.9	22.3	22.2	22.7	22.28	0.0449	3.681E-05
80	1	18.7	19.1	19.5	18.8	19.03	0.0526	4.310E-05
90	1	17.1	15.2	17	15.9	16.30	0.0613	5.031E-05

RM Reading	Air meter (cu. ft)	Time (s) T1	T2	T3	Avg. time (s)	Q (m^3/s)	m_dot (Kg/s)
55	0.1	7.8	8	7.8	7.87	3.60E-04	**4.32E-04**

Fuel Air Ratio

RM Reading	FAR	phi
40	**4.43E-02**	**0.65**
50	**5.81E-02**	**0.85**
60	**7.07E-02**	**1.04**
70	**8.52E-02**	**1.25**
80	**9.98E-02**	**1.46**
90	**1.16E-01**	**1.71**

Table B. 8: Jet – A calibration recorded data.

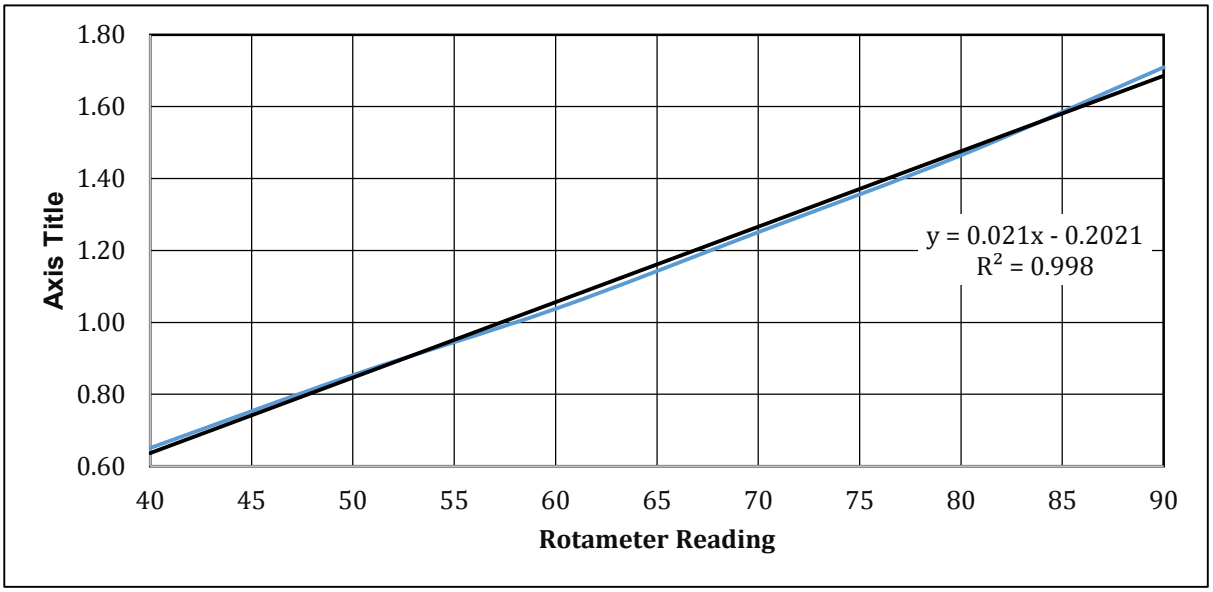

Figure B. 7: Calibration curve with linear fit for Jet – A.

B.8 JP – 8

RM Reading	Fuel (ml)	Time (s)				Avg. time (s)	Q (ml/s)	m_dot (Kg/s)
		T1	T2	T3	T4			
50	1	27.8	27.3	28.6	27.3	27.75	0.0360	2.85E-05
60	1	21.9	22.6	21.7	22.4	22.15	0.0451	3.57E-05
70	1	19	17.3	20.2	17.7	18.55	0.0539	4.26E-05
80	1	15.5	15.5	15.3	15.3	15.40	0.0649	5.13E-05
RM Reading	**Air meter (cu. ft)**	**Time (s)**				**Avg. time (s)**	**Q (m^3/s)**	**m_dot (Kg/s)**
		T1	**T2**	**T3**				
55	0.1	7.8	8	7.8		7.87	3.60E-04	**4.32E-04**
Fuel Air Ratio								
RM Reading	**FAR**	**phi**						
50	**6.59E-02**	**0.98**						
60	**8.26E-02**	**1.22**						
70	**9.86E-02**	**1.46**						
80	**1.19E-01**	**1.76**						

Table B. 9: JP – 8 calibration recorded data.

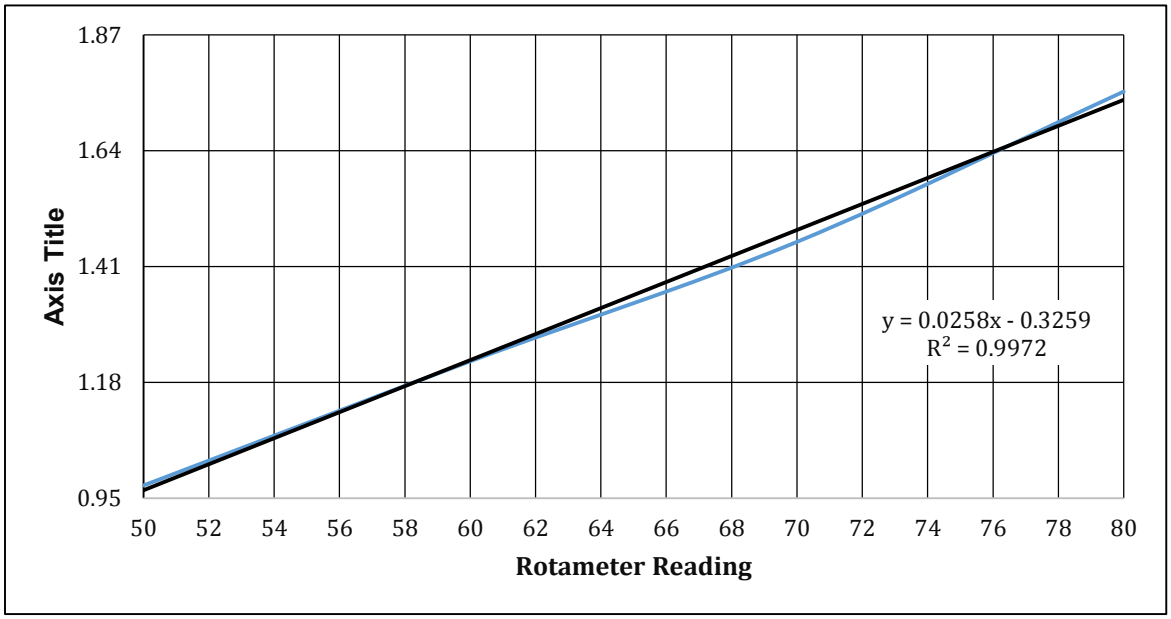

Figure B. 8: Calibration curve with linear fit for JP – 8.

B.9 FT – Coal

RM Reading	Fuel (ml)	Time (s) T1	T2	T3	T4	Avg. time (s)	Q (ml/s)	m_dot (Kg/s)
40	1	34.5	31.1	35.3	32.8	33.43	0.0299	2.27E-05
50	1	24.9	26.2	24.4	26.4	25.48	0.0393	2.98E-05
60	1	19.5	21.4	19.6	22.2	20.68	0.0484	3.68E-05
70	1	17.2	18.7	16.5	17.7	17.53	0.0571	4.34E-05
80	1	15.1	15.6	15.5	15.8	15.50	0.0645	4.90E-05

RM Reading	Air meter (cu. ft)	Time (s) T1	T2	T3	Avg. time (s)	Q (m^3/s)	m_dot (Kg/s)
55	0.1	7.8	8	7.8	7.87	3.60E-04	**4.32E-04**

Fuel Air Ratio

RM Reading	FAR	phi
40	**5.26E-02**	**0.79**
50	**6.91E-02**	**1.04**
60	**8.51E-02**	**1.28**
70	**1.00E-01**	**1.51**
80	**1.14E-01**	**1.71**

Table B. 10: FT - Coal calibration recorded data.

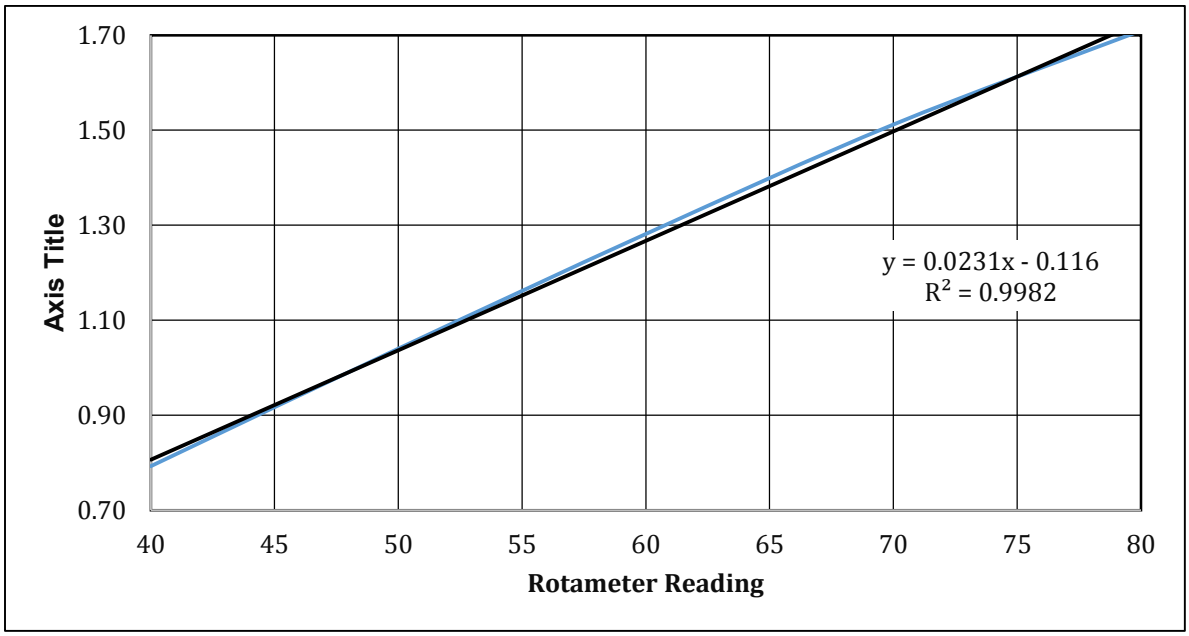

Figure B. 9: Calibration curve with linear fit for FT - Coal.

B.10 FT – Natural Gas

RM Reading	Fuel (ml)	Time (s) T1	T2	T3	T4	Avg. time (s)	Q (ml/s)	m_dot (Kg/s)
40	1	41.2	41.5	41.1	40.8	41.15	0.0243	1.847E-05
50	1	32.8	32.8	33.8	31	32.60	0.0307	2.331E-05
60	1	26.8	26.1	27.2	26.5	26.65	0.0375	2.852E-05
70	1	22.5	21.3	22.6	21.5	21.98	0.0455	3.458E-05
80	1	19.2	18.1	19.5	18.2	18.75	0.0533	4.053E-05
90	1	15.6	17.1	15.7	17.2	16.40	0.0610	4.634E-05
100	1	13.3	14.6	13.8	14	13.93	0.0718	5.458E-05

RM Reading	Air meter (cu. ft)	Time (s) T1	T2	T3	Avg. time (s)	Q (m^3/s)	m_dot (Kg/s)
55	0.1	7.8	8	7.8	7.87	3.60E-04	**4.32E-04**

Fuel Air Ratio		
RM Reading	**FAR**	**phi**
40	**4.28E-02**	**0.64**
50	**5.40E-02**	**0.81**
60	**6.60E-02**	**0.99**
70	**8.01E-02**	**1.20**
80	**9.38E-02**	**1.40**
90	**1.07E-01**	**1.60**
100	**1.26E-01**	**1.89**

Table B. 11: 90:10 HRJ tallow – mesitylene calibration recorded data.

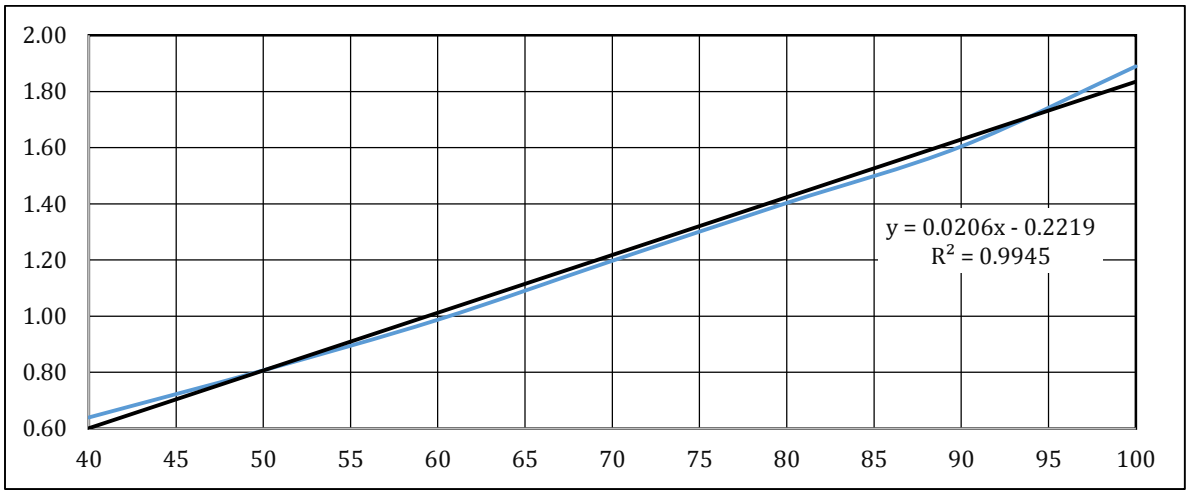

Figure B. 10: Calibration curve with linear fit for 90:10 HRJ tallow – mesitylene blend.

B.11 HRJ – Camelina

RM Reading	Fuel (ml)	Time (s) T1	T2	T3	T4	Avg. time (s)	Q (ml/s)	m_dot (Kg/s)
40	1	34.6	34.6	34.9	34.4	34.63	0.0289	2.17E-05
50	1	26.4	26.3	28.2	26.6	26.88	0.0372	2.79E-05
60	1	22.6	21	21.9	21	21.63	0.0462	3.47E-05
70	1	17.8	18.6	17.6	17.8	17.95	0.0557	4.18E-05
80	1	15	14.8	14.9	15.1	14.95	0.0669	5.02E-05
90	1	13	13	13.2	13.1	13.08	0.0765	5.74E-05

RM Reading	Air meter (cu. ft)	Time (s) T1	T2	T3	Avg. time (s)	Q (m^3/s)	m_dot (Kg/s)
55	0.1	7.8	8	7.8	7.87	3.60E-04	**4.32E-04**

Fuel Air Ratio		
RM Reading	**FAR**	**phi**
40	**5.01E-02**	**0.75**
50	**6.46E-02**	**0.97**
60	**8.03E-02**	**1.21**
70	**9.67E-02**	**1.45**
80	**1.16E-01**	**1.74**
90	**1.33E-01**	**1.99**

Table B. 12: 90:10 HRJ tallow – mesitylene calibration recorded data.

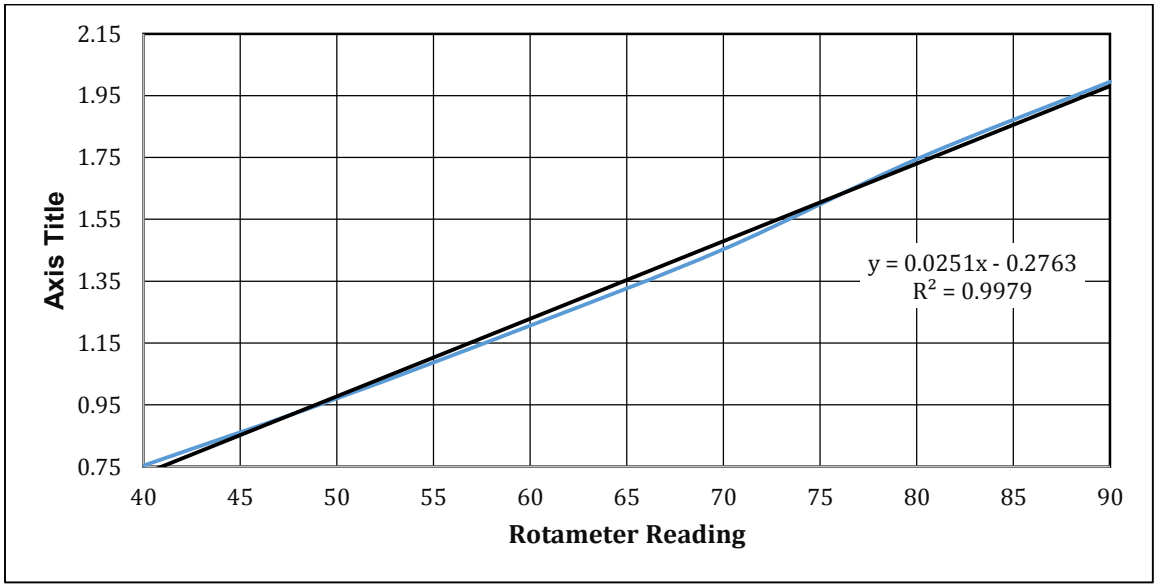

Figure B. 11: Calibration curve with linear fit for 90:10 HRJ tallow – mesitylene blend.

B.12 HRJ – Tallow (Old Batch)

RM Reading	Fuel (ml)	Time (s) T1	T2	T3	T4	Avg. time (s)	Q (ml/s)	m_dot (Kg/s)
50	1	33.6	33.8	32.9	33.8	33.53	0.0298	2.34E-05
60	1	26.1	29	26.1	27.7	27.23	0.0367	2.88E-05
70	1	22	22.6	23.7	22.3	22.65	0.0442	3.47E-05
80	1	19.1	19	18.8	19.5	19.10	0.0524	4.11E-05
90	1	16.5	16.3	16.6	16.4	16.45	0.0608	4.77E-05
100	1	14	14.2	14	14.4	14.15	0.0707	5.55E-05

RM Reading	Air meter (cu. ft)	Time (s) T1	T2	T3	Avg. time (s)	Q (m^3/s)	m_dot (Kg/s)
55	0.1	7.8	8	7.8	7.87	3.60E-04	**4.32E-04**

Fuel Air Ratio		
RM Reading	**FAR**	**phi**
50	**5.42E-02**	**0.81**
60	**6.68E-02**	**1.00**
70	**8.02E-02**	**1.21**
80	**9.51E-02**	**1.43**
90	**1.10E-01**	**1.66**
100	**1.28E-01**	**1.93**

Table B. 13: 90:10 HRJ tallow – mesitylene calibration recorded data.

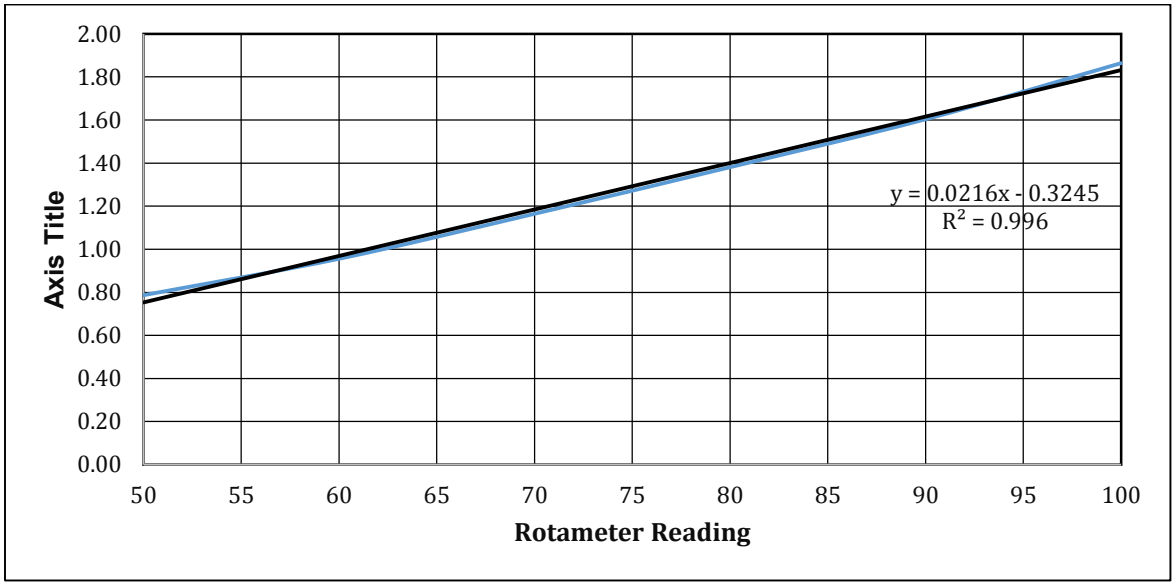

Figure B. 12: Calibration curve with linear fit for 90:10 HRJ tallow – mesitylene blend.

B.13 HRJ – Tallow (New Batch)

RM Reading	Fuel (ml)	Time (s) T1	T2	T3	T4	Avg. time (s)	Q (ml/s)	m_dot (Kg/s)
50	1	35.4	35.7	36.2	33.9	35.30	0.0283	2.25E-05
60	1	28.1	29.2	28.1	28.7	28.53	0.0351	2.78E-05
70	1	23.8	24.1	23.3	24.9	24.03	0.0416	3.30E-05
80	1	21.6	19.2	21.2	20.5	20.63	0.0485	3.84E-05
90	1	17.3	17.6	18	18	17.73	0.0564	4.47E-05
100	1	15.1	15.2	15.2	15.1	15.15	0.0660	5.23E-05

RM Reading	Air meter (cu. ft)	Time (s) T1	T2	T3	Avg. time (s)	Q (m^3/s)	m_dot (Kg/s)
55	0.1	7.8	8	7.8	7.87	3.60E-04	**4.32E-04**

Fuel Air Ratio

RM Reading	FAR	phi
50	**5.20E-02**	**0.78**
60	**6.44E-02**	**0.97**
70	**7.64E-02**	**1.15**
80	**8.90E-02**	**1.34**
90	**1.04E-01**	**1.56**
100	**1.21E-01**	**1.82**

Table B. 14: 90:10 HRJ tallow – mesitylene calibration recorded data.

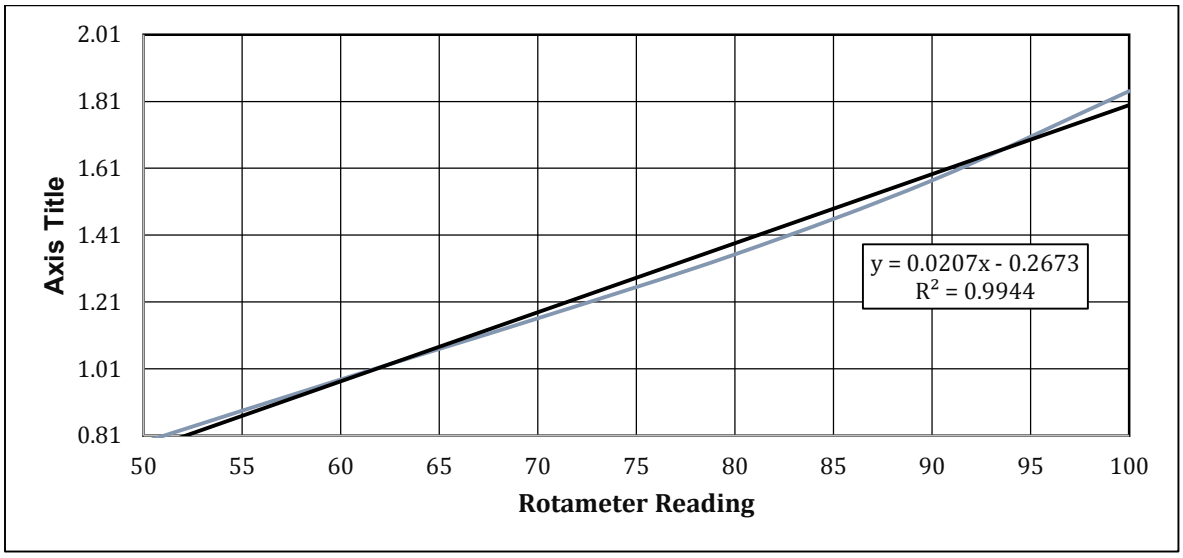

Figure B. 13: Calibration curve with linear fit for 90:10 HRJ tallow – mesitylene blend.

B.14 80:20 HRJ – Tallow and Mesitylene

RM Reading	Fuel (ml)	Time (s) T1	T2	T3	T4	Avg. time (s)	Q (ml/s)	m_dot (Kg/s)
60	1	25.6	22.7	24.2	22.4	23.73	0.0421	3.29E-05
70	1	18.9	19.3	20	19.3	19.38	0.0516	4.03E-05
80	1	16.3	16.3	15.9	16.8	16.33	0.0613	4.78E-05
90	1	14	14.1	13.9	14.3	14.08	0.0710	5.54E-05

RM Reading	Air meter (cu. ft)	Time (s) T1	T2	T3	Avg. time (s)	Q (m^3/s)	m_dot (Kg/s)
55	0.1	7.8	8	7.8	7.87	3.60E-04	**4.32E-04**

Fuel Air Ratio		
RM Reading	**FAR**	**phi**
60	**7.61E-02**	**1.12**
70	**9.32E-02**	**1.37**
80	**1.11E-01**	**1.63**
90	**1.28E-01**	**1.89**

Table B. 15: 90:10 HRJ tallow – mesitylene calibration recorded data.

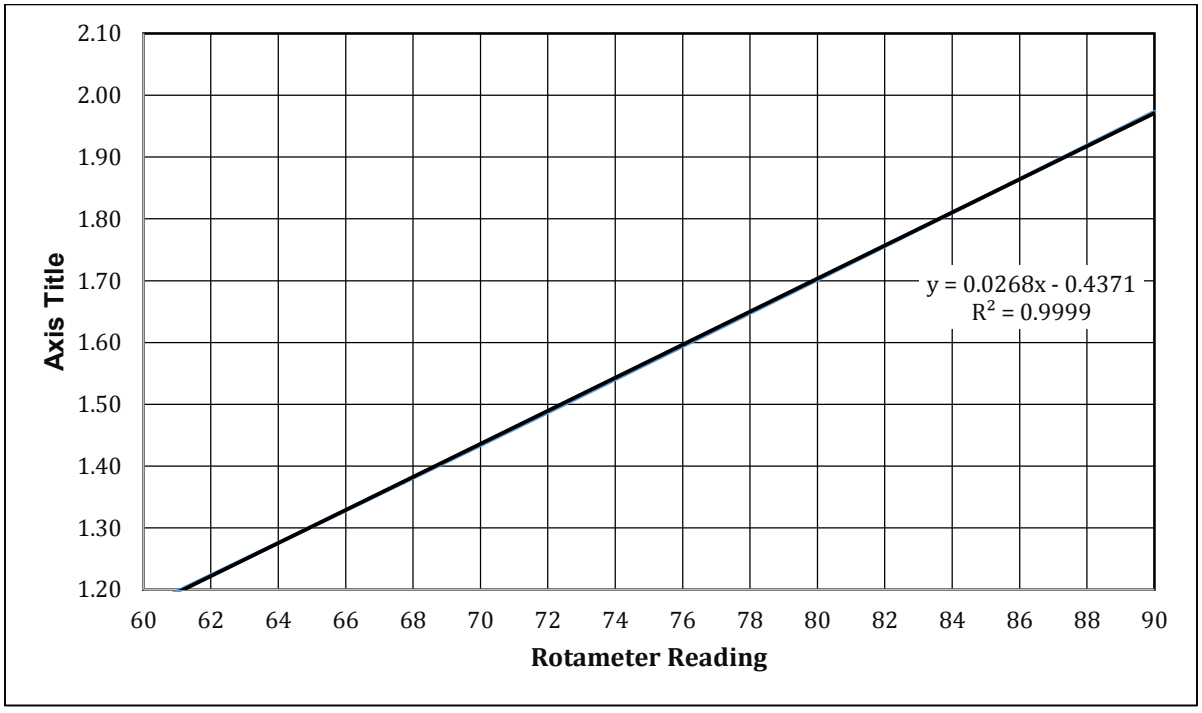

Figure B. 14: Calibration curve with linear fit for 90:10 HRJ tallow – mesitylene blend.

B.15 90:10 HRJ – Tallow and Mesitylene

RM Reading	Fuel (ml)	Time (s) T1	T2	T3	T4	Avg. time (s)	Q (ml/s)	m_dot (Kg/s)
50	1	29.4	31.7	32.7	33.3	31.78	0.0315	2.42E-05
60	1	26.1	25.7	27.1	23.3	25.55	0.0391	3.01E-05
70	1	21.4	20.4	22.1	19.8	20.93	0.0478	3.68E-05
80	1	18.3	17.1	18.7	17.4	17.88	0.0559	4.30E-05
90	1	16.2	15.9	16.7	16.5	16.33	0.0613	4.71E-05

RM Reading	Air meter (cu. ft)	Time (s) T1	T2	T3	Avg. time (s)	Q (m^3/s)	m_dot (Kg/s)
55	0.1	7.8	8	7.8	7.87	3.60E-04	**4.32E-04**

Fuel Air Ratio

RM Reading	FAR	phi
50	**5.60E-02**	**0.83**
60	**6.97E-02**	**1.04**
70	**8.51E-02**	**1.27**
80	**9.96E-02**	**1.48**
90	**1.09E-01**	**1.62**

Table B. 16: 90:10 HRJ tallow – mesitylene calibration recorded data.

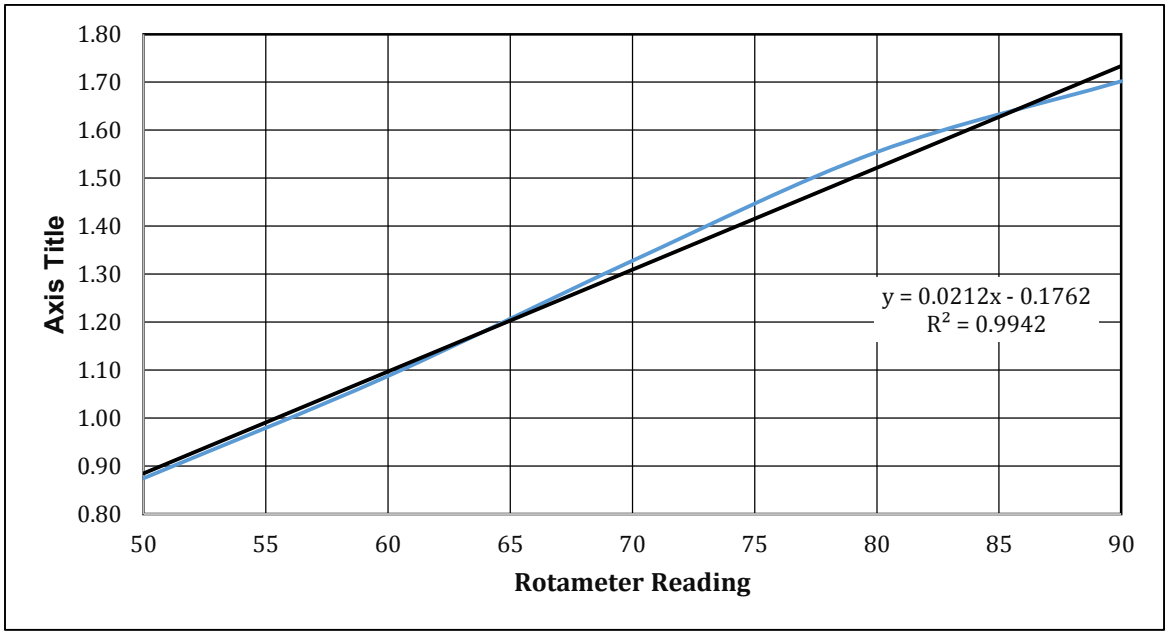

Figure B. 15: Calibration curve with linear fit for 90:10 HRJ tallow – mesitylene blend.

B.16 80:20 HRJ – Camelina and Mesitylene

RM Reading	Fuel (ml)	Time (s) T1	T2	T3	T4	Avg. time (s)	Q (ml/s)	m_dot (Kg/s)
40	1	30.4	29	31.3	30.1	30.20	0.0331	2.56E-05
50	1	23.6	22.7	23.7	22.5	23.13	0.0432	3.34E-05
60	1	20.3	20.5	19.1	19	19.73	0.0507	3.92E-05
70	1	16.6	15.9	16.7	16.5	16.43	0.0609	4.71E-05

RM Reading	Air meter (cu. ft)	Time (s) T1	T2	T3	Avg. time (s)	Q (m^3/s)	m_dot (Kg/s)
55	0.1	7.8	8	7.8	7.87	3.60E-04	**4.32E-04**

Fuel Air Ratio		
RM Reading	FAR	phi
40	**5.93E-02**	**0.87**
50	**7.74E-02**	**1.14**
60	**9.07E-02**	**1.34**
70	**1.09E-01**	**1.61**

Table B. 17: 80:20 HRJ camelina – mesitylene calibration recorded data.

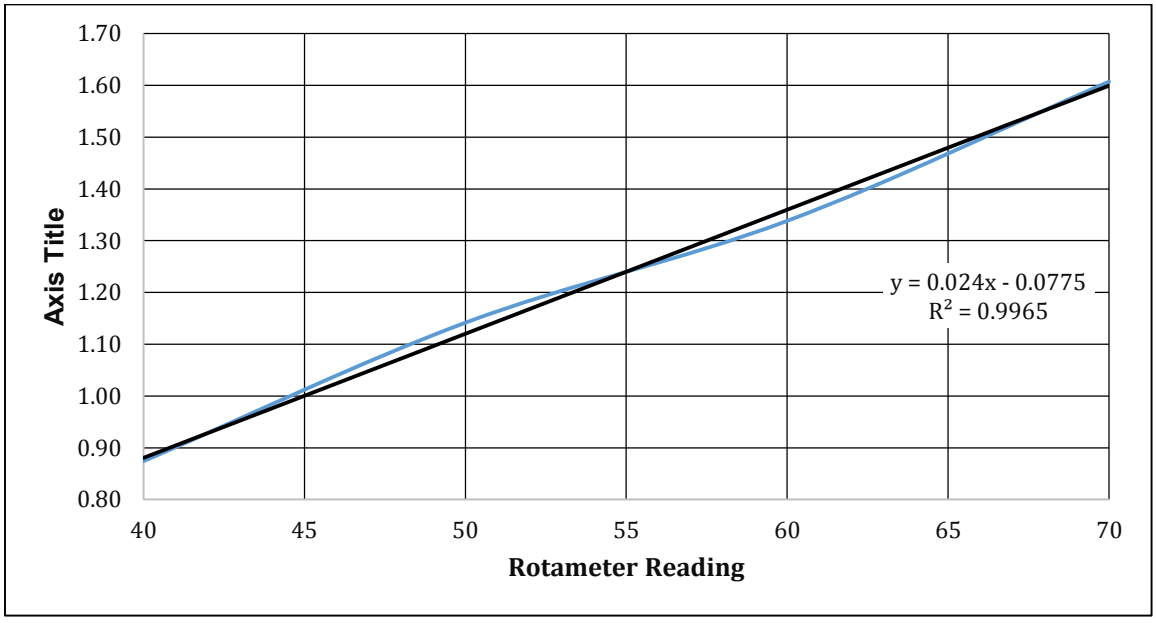

Figure B. 16: Calibration curve with linear fit for 80:20 HRJ camelina – mesitylene blend.

B.17 80:20 HRJ – Camelina and Cyclohexane

RM Reading	Fuel (ml)	Time (s) T1	T2	T3	T4	Avg. time (s)	Q (ml/s)	m_dot (Kg/s)
40	1	31.8	31.5	31.8	31.5	31.65	0.0316	2.38E-05
50	1	22.7	25.1	23.8	23.9	23.88	0.0419	3.16E-05
60	1	20.1	18.9	19.5	20.4	19.73	0.0507	3.82E-05
70	1	15.8	17.5	15.7	17.2	16.55	0.0604	4.56E-05
80	1	14.4	13.9	14.9	14.2	14.35	0.0697	5.25E-05

RM Reading	Air meter (cu. ft)	Time (s) T1	T2	T3	Avg. time (s)	Q (m^3/s)	m_dot (Kg/s)
55	0.1	7.8	8	7.8	7.87	3.60E-04	**4.32E-04**

Fuel Air Ratio

RM Reading	FAR	phi
40	**5.52E-02**	**0.83**
50	**7.31E-02**	**1.09**
60	**8.85E-02**	**1.33**
70	**1.05E-01**	**1.58**
80	**1.22E-01**	**1.82**

Table B. 18: 80:20 HRJ camelina – cyclohexane calibration recorded data.

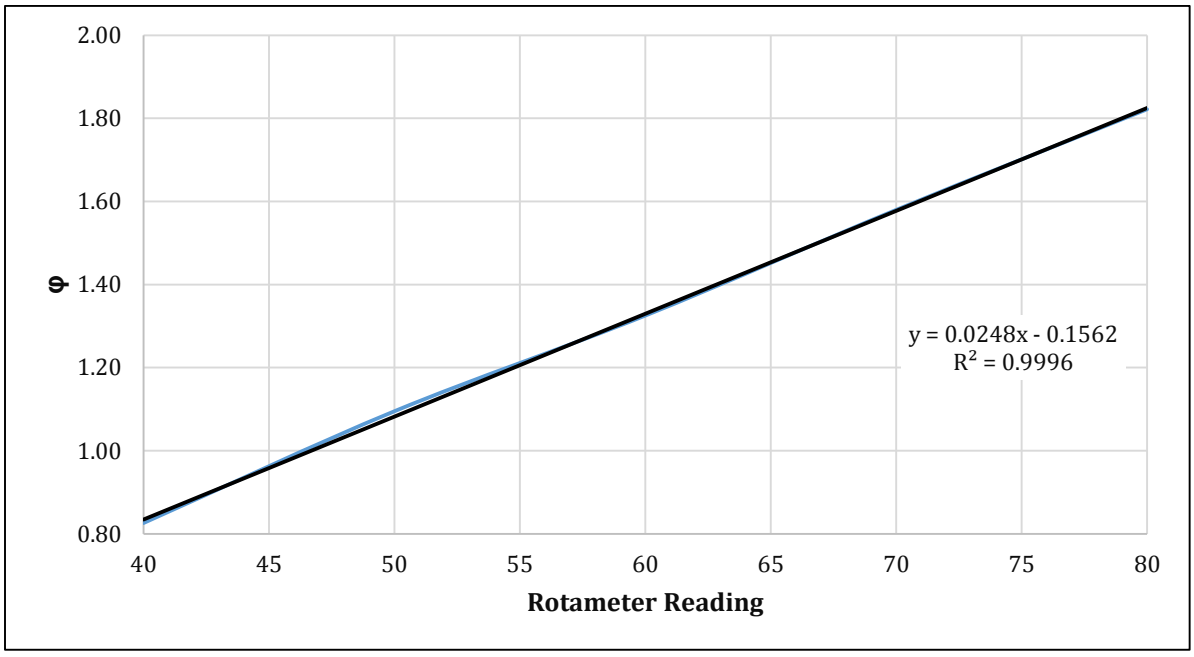

Figure B. 17: Calibration curve with linear fit for 80:20 HRJ camelina – cyclohexane blend.

APPENDIX C

SETUP COMPONENTS DESIGN

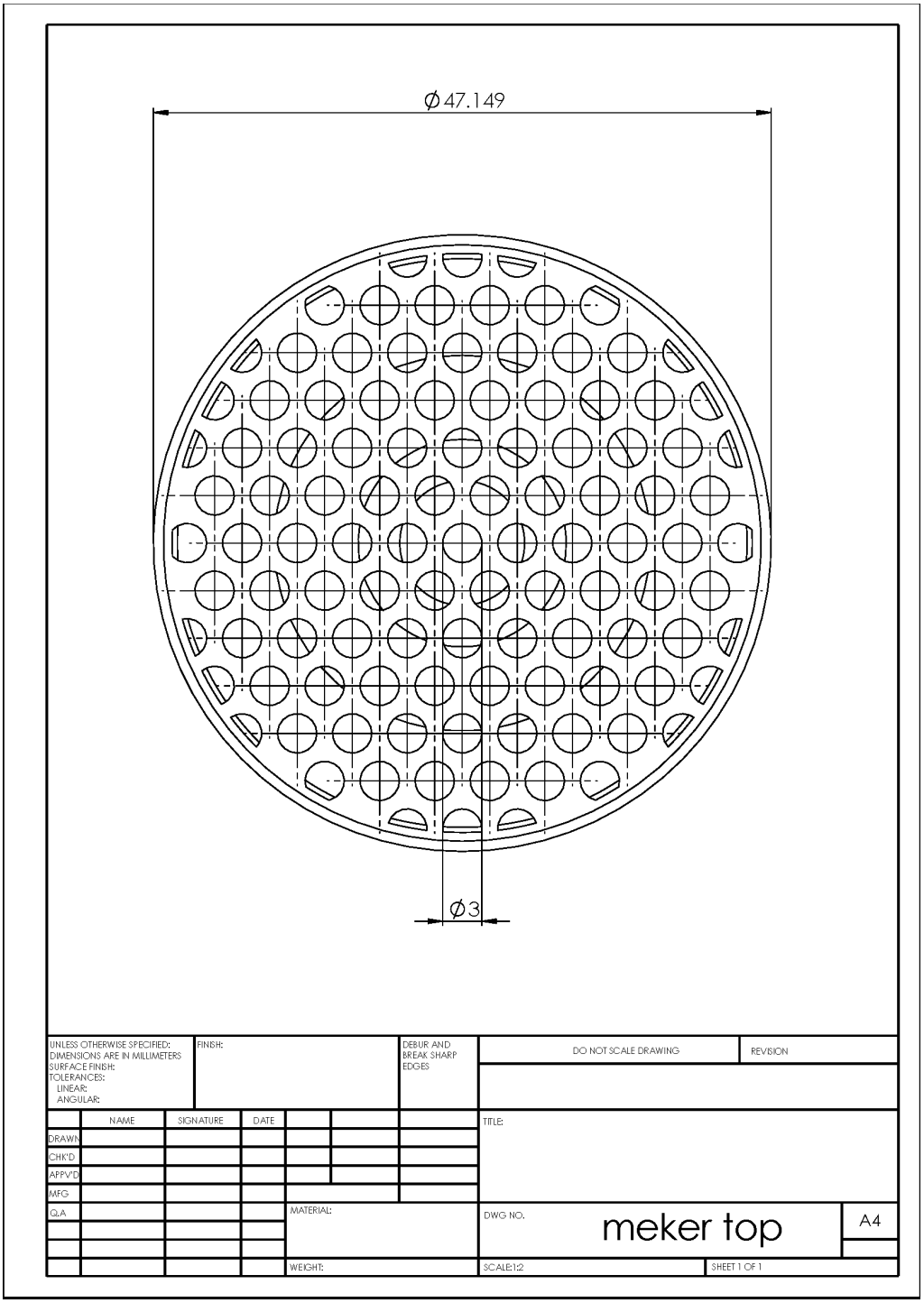

Figure C. 1: CAD design of the top view of meker burner.

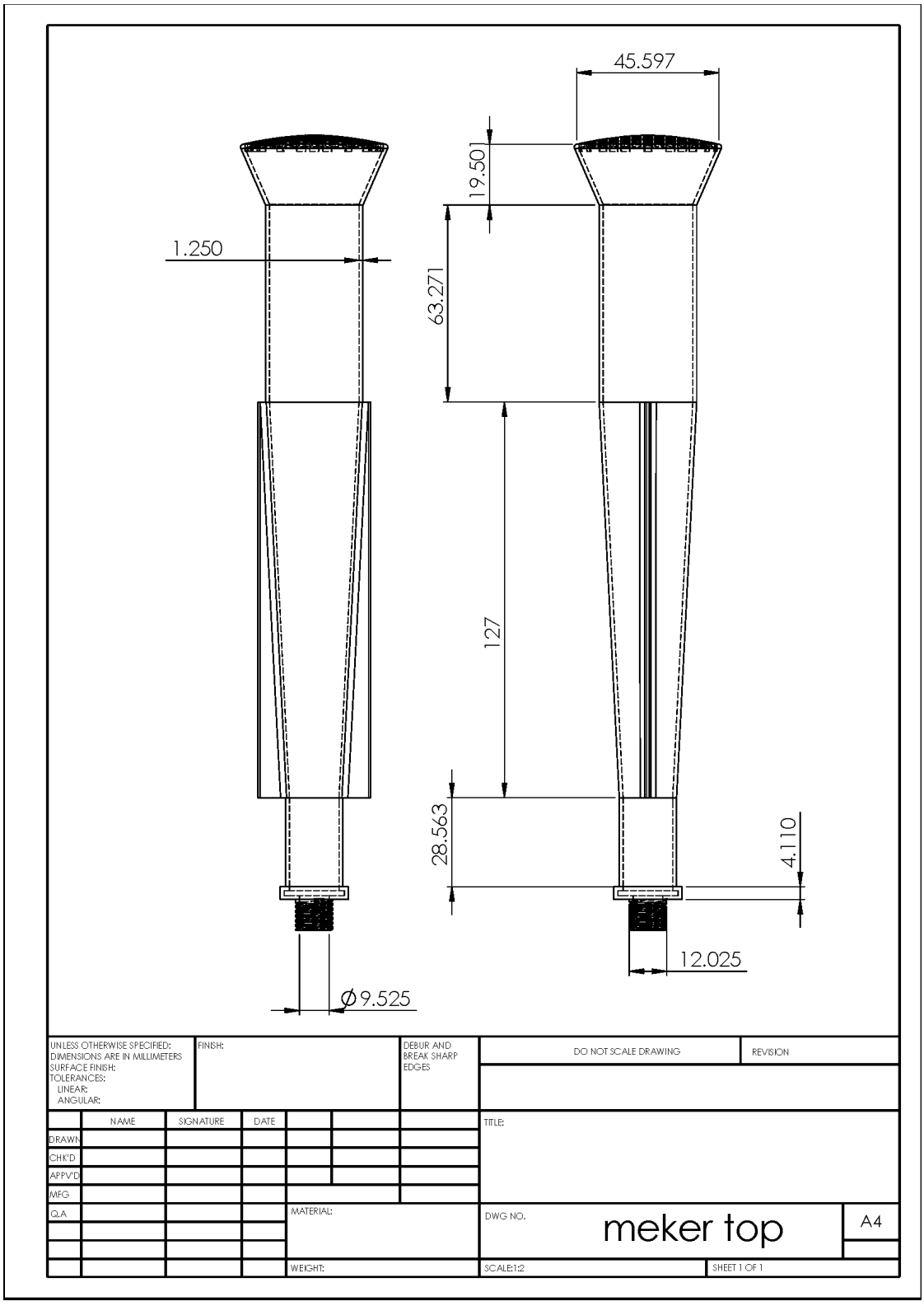

Figure C. 2: CAD design of side views of meker burner.

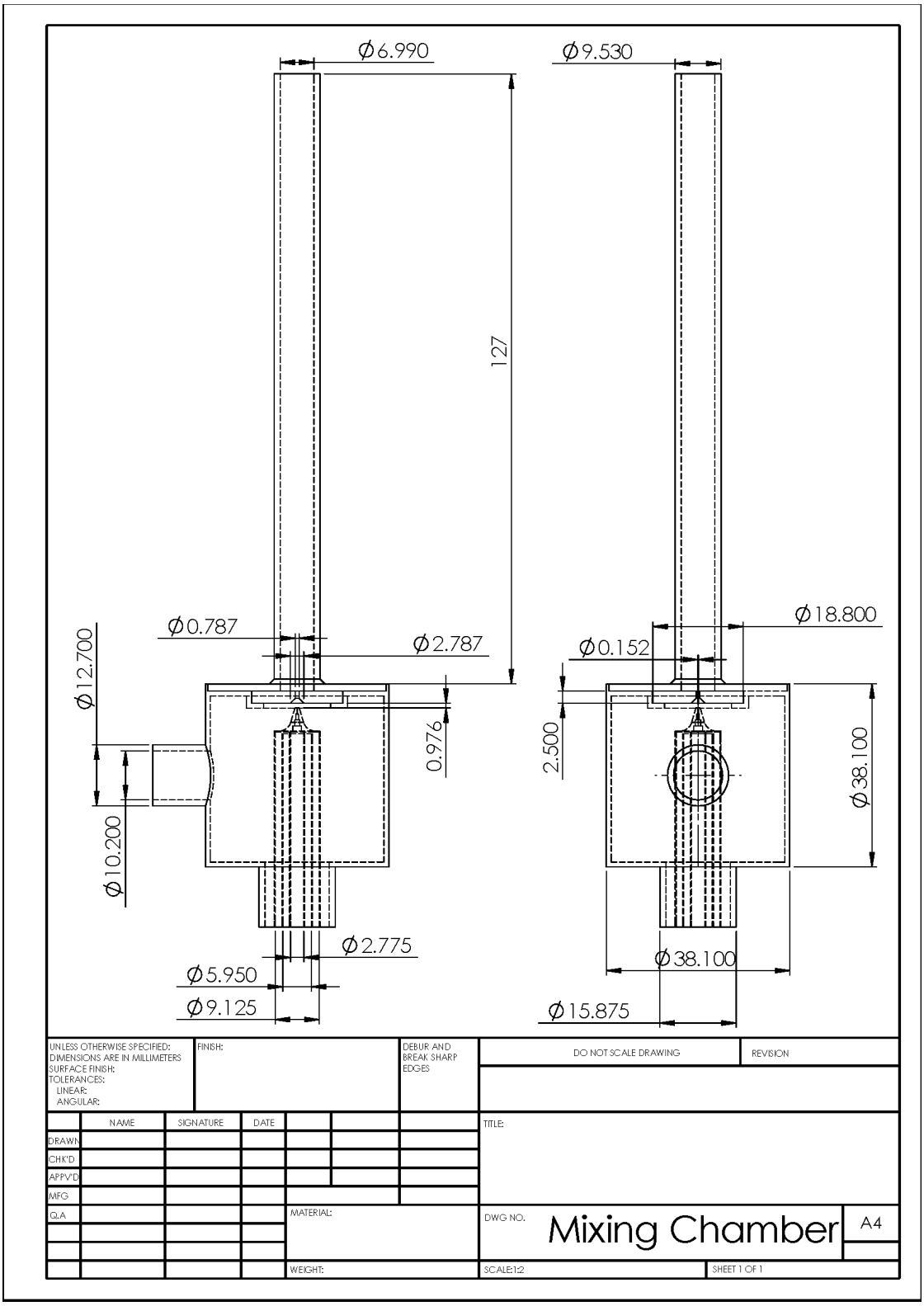

Figure C. 3: CAD design of Plane Jet Atomizer Assembly.